Performance Evaluation of Uplink Cell-free Massive MIMO Network under Weichselberger Rician Fading Channel

Birhau Dessie Ayalew

A Thesis Submitted to

the Department of Electronics and Communication Engineering

School of Electrical Engineering and Computing

Presented in Partial Fulfillment of the Requirement for the Degree of

Master's in Electronics and Communication Engineering

Office of Post Graduate Studies

Adama Science and Technology University

June 2023

Adama Ethiopia

Performance Evaluation of Uplink Cell-free Massive MIMO Network under Weichselberger Rician Fading Channel

Birhanu Dessie Ayalew

Major Advisor: - Dr. Shaikh Javed Rasheed (PhD)

Co-Advisor:- Mr. Bayisa Taye (MSc)

A Thesis Submitted to

The Department of Electronics and Communication Engineering

School of Electrical Engineering and Computing

Presented in Partial Fulfillment of the Requirement for the Degree of Master's in Electronics and Communication Engineering

Office of Post Graduate Studies

Adama Science and Technology University

June 2023

Adama, Ethiopia

APPROVAL PAGE of M.SC. THESIS

We, the advisors of the thesis entitled "**Performance Evaluation of Uplink Cell-free Massive MIMO Network under Weichselberger Rician Fading Channel**" and developed by **Birhanu Dessie Ayalew**, hereby certify that the recommendation and suggestions made by the board of examiners are appropriately incorporated into the final version of the thesis.

<u>Dr. Shaikh Javed Rasheed</u>	____________________	______________
Major Advisor	Signature	Date
<u>Mr. Bayisa Taye</u>	____________________	______________
Co-Advisor	Signature	Date

We, the undersigned members of the board of Examiners of the thesis by **Birhanu Dessie Ayalw** have read and evaluated the thesis entitled "**Performance Evaluation of Uplink Cell-free Massive MIMO Network under Weichselberger Rician Fading Channel**" and examined the candidate during the open defense. This is, therefore, to certify that the thesis is accepted for partial fulfillment of the requirement of the degree of Master of Science in Electronics and Communication Engineering.

________________________	__________________	____________
Chairperson	Signature	Date
________________________	__________________	____________
Internal Examiner	Signature	Date
________________________	__________________	____________
External Examiner	Signature	Date

Finally, approval and acceptance of the thesis are contingent upon submission of its final copy to the Office of Postgraduate Studies (OPGS) through the Department Graduate Council (DGC) and School Graduate Committee (SGC).

________________________	__________________	____________
Department Head	Signature	Date
________________________	__________________	____________
School Dean	Signature	Date
________________________	__________________	____________
Office of Postgraduate Studies, Dean	Signature	Date

DECLARATION

I hereby declare that this Master's Thesis entitled "**Performance Evaluation of Uplink Cell-free Massive MIMO Network under Weichselberger Rician Fading Channel"** is my own work and has not been submitted to any university for the award of any academic degree, diploma, or certificate. The references used in this thesis are duly recognized by proper citations.

Birhanu Dessie Ayalew	_________________	_______________
Name of Student	Signature	Date

RECOMMENDATION

We, the advisors of this thesis, hereby certify that we have read the revised version of the thesis entitled "**Performance Evaluation of Uplink Cell-free Massive MIMO Network under Weichselberger Rician Fading Channel**'' prepared under our guidance by **Birhanu Dessie Ayalew** submitted in partial fulfillment of the requirements for the degree of Mater's of Science in Electronics and Communication Engineering. Therefore, we recommend the submission of revised version of the thesis to the department following the applicable procedures.

______________________	______________	______________
Major Advisor	Signature	Date
______________________	______________	______________
Co-advisor	Signature	Date

ACKNOWLEDGEMENT

First and foremost, praise and thanks to the Almighty God for his mercies in allowing me to finish this thesis successfully.

I would like to express my thanks to my advisor, Dr. Shaikh Javed Rasheed (Ph.D.), for his encouragement and sacrifice of valuable time to encourage me to work on my way and for giving me the freedom to explore this thesis deeply. Without his assistance, it would not have been possible to achieve the ultimate goal of this thesis. He was a great help whenever I had a problem with my thesis.

I would like to express my sincere gratitude to my co-advisor, Mr. Bayisa Taye (MSC), for his continuous support of my M.Sc. research and his patience, motivation, and enthusiasm. His guidance helped me in all the research and writing of this thesis.

In addition, I would like to thank Adama Science and Technology University (ASTU) and all members of the School of Electrical Engineering and Computing (SoEEC), particularly the program of Electronics and communication engineering, for providing such an excellent educational and research environment. I am grateful to all of the students in the Communication Engineering division who have shared their knowledge with me.

Finally, I am grateful to my family for always allowing me to go my own way and making me feel as if I could do whatever I wanted without feeling pressed.

TABLE OF CONTENTS

LIST OF TABLES

LIST OF FIGURES

LIST OF ACRONYMS AND ABBREVIATIONS

5G	5 Generation
AI	Artificial Intelligent
AP	Access Point
B5G	Beyond 5 generation
BSs	Base Stations
CBDNet	Convolutional Blind Denoising Network
CE	Channel Estimation
CF	Cell-Free
CF M-MIMO	Cell-Free Massive Multiple Input Multiple Output
COMP-JP	Coordinated Multipoint Joint Processing
CPU	Central Processing Unit
C-RAN	Cloud Radio Access Network
CSI	Channel State Information
DAS	Distributed Antenna System
DL	Downlink
DCC	Dynamic Coopration Clustering
EE	Energy Efficiency
FCP	Fully Centralizing Processing
FFDNet	Fast and Flexible Denoising Convolutional Neural Network
IEEE	Institute of Electrical and Electronics Engineering
IRS	Intelligent Reflecting Surface
I-WMMSE	Iterative Weight Minimum Mean Square Error

LIS	Large Intelligent Surface
LIS	Large Intelligent Surface
LMMSE	Linear Minimum Mean Square Error
LoS	Line of Sight
LS	Least Square
LSFD	Large Scale Fading Decoding
MIMO	Multiple Input Multiple Output
M-MIMO	Multiple Input Multiple Output
MMSE SIC	Minimum Mean Square Error Successive Interference Cancellation
MRC	Maximum Ratio Combining
MSE	Mean Square Error
NLoS	Non Line of Sight
PA-EW-MMSE	Phase Aware Element Wise Minimum Mean Square Error
PA-MMSE	Phase Aware Minimum Mean Square Error
PEW-MMSE	Partial Element Wise Minimum Mean Square Error
PMMSE	Partial Minimum Mean Square Error
RIS	Reconfigurable Intelligent Surface
RS	Radio Stripes
SE	Spectral Efficiency
TDD	Time Duplex Mode
UDN	Ultra Dense Network
UE	User Equipment

UL	Uplink
ULA	Uniform Linear Array
UPA	Uniform Planner Array

ABSTRACT

Cell-Free Massive Multiple Input Multiple Output (CF M-MIMO) is one of the promising technologies for future wireless communication such as (5G) and beyond fifth-generation (B5G) networks. It is a type of network technology that uses a massive number of distributed antennas to serve a large number of users at the same time. There are no predefined cells in this network, and users are not assigned to a specific base station or cell. Its ability to provide high spectral efficiency (SE) and energy efficiency (EE), as well as improved coverage and interference management, compared to traditional cellular networks. However, estimating the channel with high performance and low computational methods is still a problem. Different algorithms have been developed to address these challenges in channel estimation. One of the high-performance channel estimators is a phase-aware minimum mean square error (MMSE). This channel estimator has high computational complexity. To address the shortcomings of the existing estimator, this thesis proposed an efficient channel estimator that is a phase-aware element-wise minimum mean square error (PA-EW-MMSE) with QR decomposition and precoding matrix at the user side. The focus of this thesis is on the uplink (UL) phase of CF M-MIMO, where both the access point (AP) and user equipment (UE) has multiple antennas, and the communication channel is subject to Weichselberger Rician fading. The investigated channel model consists of a line of sight (LoS) and non-line of sight (NLoS) components. To account for the effects of mobility and phase noise on the phase shifts, the phase of the LoS component is modeled as a random variable that is uniformly distributed. The closed form uplink SE with phase MMSE and proposed estimator are evaluated for MMSE combining. The EE and area throughput are also calculated from the SE. The complexity of the MMSE and the proposed channel estimator are compared. The simulation results show that the proposed estimator achieved the best SE, EE, and area throughput performance with a substantial reduction in the complexity of the computation.

Keywords: *Access point, spectral efficiency, energy efficiency, throughput, phase aware element-wise minimum mean square error, cell-free massive MIMO, phase aware minimum mean square error, line of sight, and non-line of sight.*

CHAPTER ONE

1. INTRODUCTION

1.1 Background of the Study

Future wireless networks will need to manage billions of devices simultaneously, and each one will require high throughput to serve a variety of applications including speech, real-time video, high-definition movies, etc. Cellular networks cannot handle such high connection volumes due to the high levels of interference and poor performance of user terminals located at the cell boundary. Additionally, traditional cellular systems are primarily built for human users. The Internet of Things, the Internet of Everything, smart X, and other machine-type communication systems are anticipated to be crucial in the development of future wireless networks. Expandable and effective connectivity for billions of units is the primary difficulty in machine-type communications. Since each cell can only serve a certain number of UE, centralized architecture with cellular topology does not appear to be effective in these situations. Therefore, why not build a cell-free structure with distributed technology? Which is called the CF M-MIMO system, created by combining M-MIMO technology with cell-free structures (Foschini et al., 2006),(Björnson et al., 2010),(Ngo et al., 2017).

In the future of wireless communication, CF M-MIMO is considered a promising technology (Ngo et al., 2017). To implement CF M-MIMO, APs must be set up throughout the coverage area, spread geographically, and linked to the central processing unit (CPU) using front haul connections. Numerous distributed APs are present in a CF M-MIMO network, which is simultaneously serving fewer UEs. The CPU manages data processing and coordination, and it is connected to all APs. With the aid of their cooperation and the CPU's assistance by spatially multiplexing on the same time-frequency resource, all APs effectively service all UEs. CF M-MIMO can be seen as a particular application of the principles underlying network MIMO, virtual MIMO, and distributed MIMO, as well as distributed antenna systems (DAS) and cooperative multipoint joint processing (Interdonato, Frenger, et al., 2019).

A comparison of traditional and CF M-MIMO technology is shown in Figure 1.1 (Abdul Kadir et al., 2021). In cellular M-MIMO, the base station has a lot of antennas installed, allowing for the spatial multiplexing of large user signals in the identical frequency range. Both the system's capacity and the communication links' dependability can be greatly increased as a result. Cellular M-MIMO's performance is, however, constrained by several issues, such as pilot contamination, inter-cell interference, and the requirement for precise channel state data. CF M-MIMO, on the other hand, is not dependent on the conventional cellular network architecture. The transmission and reception of signals are instead coordinated across the antennas by the use of signal processing algorithms, which are widely dispersed over the coverage area. By using this strategy, inter-cell interference may be reduced and the communication lines' durability can be increased. The CF M-MIMO approach is an excellent fit for indoor and hot-spot coverage situations in the next generation of wireless communication, including locations such as subways, smart factories, shopping malls, railway stations, small towns, hospitals stadiums, community centers, and college campuses.

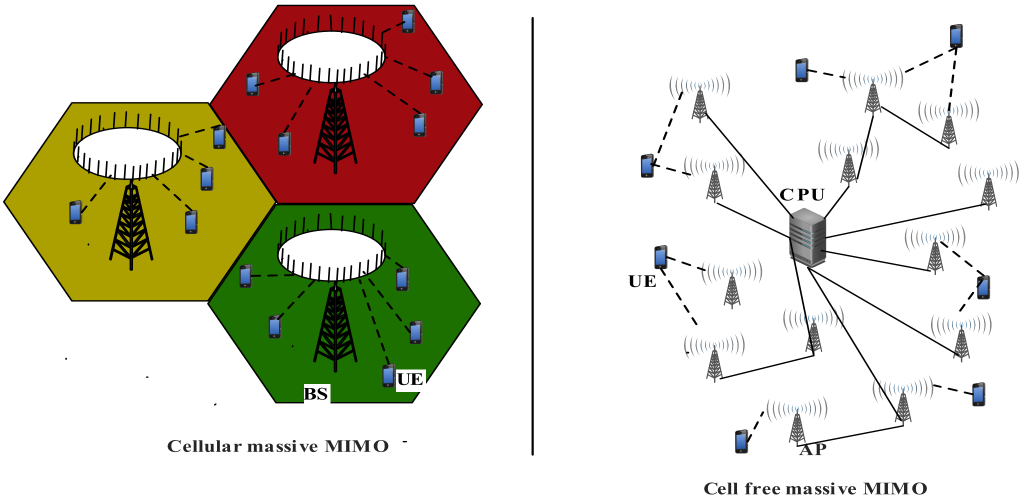

Figure 1.1: Comparison of CF M-MIMO and cellular M-MIMO systems (Abdul Kadir et al., 2021).

Cell-free refers to a situation in which there are no cell borders during uplink (UL) and downlink (DL) transmission, as seen by the UE since every AP that has an impact on the UE will actively participate in the connection (Demir et al., 2021). For instance, all APs that receive an uplink data signal from a UE will work together to decode the signal. Even though not all APs may serve every UE, the network is collectively serving all K active UEs within its coverage region.

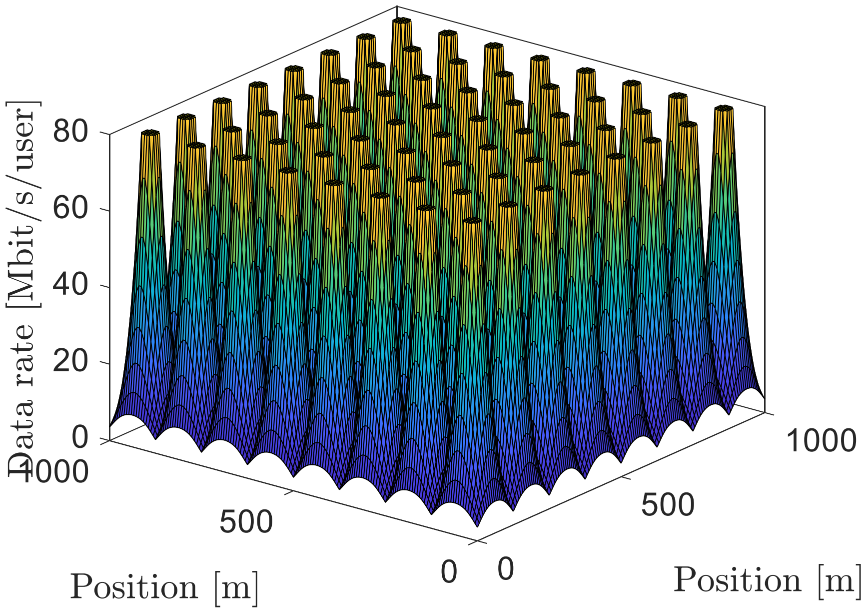

(a)

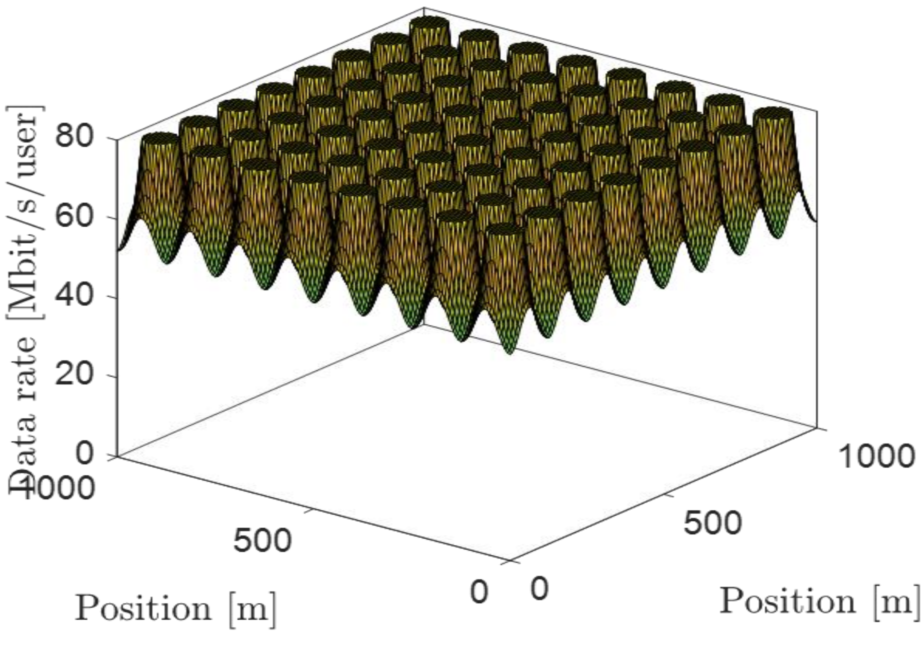

(b)

Figure 1.2 (a) Cellular M-MIMO and (b) CF M-MIMO demonstrates the downstream data rate attained by a UE with 64 APs at various locations (Interdonato, Björnson, et al., 2019).

Figure 1.2 (a) provides an example of this behavior by displaying the DL data rate attained by the user equipment at different places where each AP uses an ordinary fixed-gain antenna and transmits at its highest strength. The system's maximum rate, which in this case is 80 Mbit/s, is reached by the UE when it is near one of the APs. In comparison, UEs in cell boundaries only manage rates of less than 1 Mbit/s. There is data rate variation between cell edge and cell center users. The figure1.2 (b) demonstrates the downstream data rate attained by a UE with 64 APs at various locations. In this case, the user gets a uniform data rate compared to (a). The throughput achieved by Figure (b) is greater than that of Figure (a).

In a cellular system, the coverage area is divided into cells, and each cell has a limited coverage range. As users move away from the base station, the received signal strength decreases, leading to variations in the data rate across different locations. In CF M-MIMO, with a large number of distributed APs, the coverage area can be effectively divided into smaller regions, reducing the signal strength variations and enabling a more uniform data rate across the entire coverage area. CF M-MIMO enables spatial multiplexing, which means that multiple users can be served simultaneously using the same time and frequency resources. The distributed APs, in collaboration with advanced signal processing techniques, can separate the signals from different users spatially and transmit them concurrently. This spatial multiplexing capability allows for more efficient utilization of the available resources, leading to a more uniform data rate allocation (Björnson & Sanguinetti, 2019a).

1.1.1 Motivation

The CF M-MIMO technology idea has advanced every year since it was first introduced only a few years ago. Due to its enormous advantages in 5G and beyond standardization, it has become one of the most recent study subjects in wireless communication networks. The current cellular M-MIMO network is not enough to manage the huge increase in wireless network data traffic and demand for user equipment. The 5G and beyond network is considering the CF M-MIMO system as a possible remedy for the issue brought on by extremely high levels of data traffic and users. The worldwide bandwidth shortage in the wireless communication industry has served as a driving force behind the research and study of CF M-MIMO wireless access technology.

1.2 Statement of Problem

Even though CF M-MIMO is one of the potential networks for 5G and beyond, it has its problems. It requires perfect channel state information (CSI) between the access point and user equipment. Additionally, a better combining algorithm at the access points should be deployed to mitigate interference. Researchers have previously attempted to address this challenge by using various methods such as minimum mean square error (MMSE) channel estimator followed by MMSE combining which resulted in better performance. There are other estimators such as least square (LS) and linear MMSE estimators which have less performance than MMSE estimators. But the MMSE estimator has high computational complexity due to matrix inversion as well as all elements participating in the channel estimation. And also MMSE estimator considers the correlation between different antennas. The channel may be highly correlated across antennas, and the MMSE estimator may be more effective in capturing this correlation. However, there is a chance of channel correlation is low in CF M-MIMO with multi-antenna user equipment that reduces the performance without a high reduction of computational complexity. To solve this problem, an equivalent or better performance and low-complexity algorithm is required. In this study, a phase-aware element-wise minimal mean square error (PA-EW-MMSE) channel estimator with QR matrix decomposition and user precoding matrix are proposed to obtain a better performance and low computational complexity channel estimator method.

1.3 Objectives

1.3.1 General Objective

The primary aim of this thesis is to examine uplink CF M-MIMO systems over rician fading channels, using channel estimators that offer both high performance and low computational complexity.

1.3.2 Specific Objectives

- To assess the effectiveness of uplink CF M-MIMO based on SE with the number of antenna per UE and number of AP over the rician fading channel.
- To analyse the uplink's performance CF M-MIMO based on EE with the number of antenna per UE and the number of AP over the rician fading channel.
- To evaluate the uplink's performance CF M-MIMO based on area throughput with the number of antenna per UE and number of AP over the rician fading channel.
- To improve the performance of CF M-MIMO by using PA-EW-MMSE channel estimator with QR decomposition and user-side precoding matrix.
- To examine the proposed estimator with the existing estimator based on computational complexity.

1.4 Scope of the Study

This thesis emphasizes finding the channel estimator for UL CF M-MIMO systems that are efficient in performance and low in computational complexity. The complexity and performance of the existing channel estimator i.e. MMSE estimator are compared with the proposed channel estimator. The rician fading channel i.e. both the line of sight path and non-line of sight path is considered. The performance parameters such as SE, EE, and area throughput are obtained based on the existing estimator and proposed estimator with MMSE and MR combiner. The simulation result is based on SE, EE, and area throughput versus the number of antenna per AP and the number of antennae per UE. The simulation includes information about the computational complexity of both the proposed method and the existing method. The channel estimation was improved by PA-EW-MMSE with QR decomposition and user-side precoding matrix which enhance the effectiveness of the UL CF M-MIMO system.

1.5 Significance of the Study

The complexity of the channel estimation process and signal processing schemes in the CF M-MIMO system increases proportionally with the number of users. This thesis provides a low-complexity, high-performance channel estimator technique that is a PA-EW-MMSE with QR decomposition followed by a precoding matrix at the user side under rician fading channels.

1.6 Thesis Contribution

CF M-MIMO shows potential as a technology for networks 5G and beyond 5G. However, during deployment, it faces the challenges of UL channel estimation. The primary contribution of this thesis is to propose a low-complexity and high-performance channel estimator to address this challenge. In addition to that, enhancing and analyzing the upstream SE of a CF M-MIMO system with a UE having more than one antenna under a rician fading channel. This thesis analyses the performance of the developed estimator with the existing channel estimator based on parameters such as SE, EE, and area throughput. The complexity of the proposed and existing channel predictor is also analyzed th the number of multiplications required in the algorithm. Our investigation centers on a completely centralized processing approach that employs global MMSE combining techniques for CF M-MIMO systems. These systems operate over Weichselberger Rician fading channels, which exhibit random phase changes in the LoS component.

1.7 Limitation of the Thesis

The investigation for the thesis is limited to simulations.

1.8 Outline of the Thesis

The rest of the thesis is structured in the following manner:

Chapter 2: This chapter presents the basic introduction, working principle, characteristics, limitations, channel estimation, data transmission, UL, and DL, and technologies of the CF M-MIMO network. A review of different related works on the CF M-MIMO UL system under the rician fading channel is also included in this chapter.

Chapter 3: System model, mathematical models of phase aware MMSE and EW-MMSE channel estimator, MMSE combiner, proposed method, and performance metrics are included in this chapter. The formulation of the SE for CF M-MIMO network in a multi-antenna user equipment scenario over a rician fading environment with fully centralized implementation is what this chapter touches on.

Chapter 4: This chapter mainly focuses on simulation parameter EE, SE, and area throughput with the number of antenna per UE and number of AP. The complex multiplication of the proposed estimator and existing estimator versus the number of users, number of antenna per UE, number of antenna per AP, and number of AP are discussed.

Finally, the thesis ends with a conclusion and recommendation for future works on the CF M-MIMO network.

CHAPTER TWO

2. LITERATURE REVIEW

2.1 Introduction to Cell-Free Massive MIMO

CF M-MIMO is a wireless communication technological advancement that has a possible answer to address the rising need for high-capacity and high-performance wireless networks. In conventional cellular networks, a base station serves a predetermined geographic region or cell. In contrast, CF M-MIMO networks use a lot of scattered antennas to create a virtual cell with no set boundaries. The main concept behind CF M-MIMO is to simultaneously service a lot of user devices with a lot of scattered antennas. It can achieve great SE, low latency, and vast connectivity by utilizing innovative signal processing methods and efficient resource allocation approaches. Advanced signal processing techniques, like beam formation and precoding, is used to combine the signals received from the various antennas, improving the signal quality and reducing interference (Kassam et al., 2023),(Obakhena et al., 2021).

2.2 Physical Layer Aspects of Cell-Free Massive MIMO

In the CF M-MIMO system, many antennas are dispersed beyond the coverage area to create a virtual cell with no set boundaries. The signals collected by several antennas are processed using advanced signal processing techniques to coherently combine the signals and reduce interference, allowing one antenna to serve numerous users at once (Demir et al., 2021). It is made up of a network of user devices, a central processing unit, and dispersed antennas. The distributed antennas are usually tiny, inexpensive, and arranged in a tight grid throughout the coverage region. The distributed antennas are connected to the CPU, which manages resource allocation and performs signal processing, through high-capacity backhaul lines. The dispersed antennae are used for user device communication, while the CPU is used for data reception.

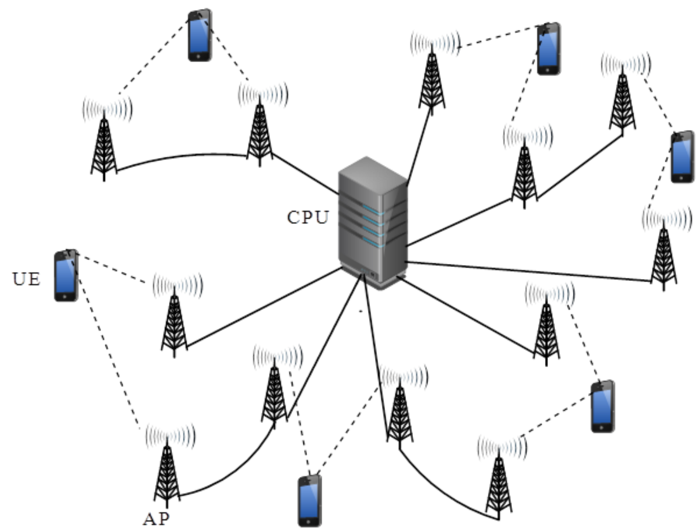

Figure 2.1: Physical layer of CF M-MIMO system (Bashar et al., 2018).

CF M-MIMO is not a novel idea conceptually, but it combines the following most effective currently used methods (Shaik, 2022).

1. **Physical layer aspects of cellular M-MIMO:** It is an advanced technology used in wireless communication systems, particularly in cellular networks, to improve SE and overall system performance. The physical layer aspects of cellular M-MIMO involve various considerations related to antenna arrays, beamforming, channel estimation, and interference management. These aspects work together to enable high-capacity, efficient, and reliable wireless communication in cellular networks.
2. **Coordinated multipoint joint processing (CoMP-JP):** It is a technique used in cellular networks to enhance system performance by coordinating the transmission and reception of signals across multiple base stations (BSs). It is an advanced form of cooperative communication that aims to mitigate interference, improve coverage, and increase overall capacity. CoMP-JP involves joint signal processing and coordination among neighboring BSs to achieve these objectives. By enabling cooperation and joint processing among neighboring BSs, CoMP-JP can improve system capacity, coverage, and overall user experience in cellular networks.
3. **Ultra-Dense Networks (UDNs):** refer to wireless communication networks characterized by an extremely high density of base stations (BSs) or access points. UDNs are designed to meet the growing demands for higher capacity, improved coverage, and enhanced quality of service in crowded urban areas or hotspots with high user concentrations. By leveraging the high BS density and advanced

interference management techniques, UDNs can address the challenges associated with growing wireless communication demands in urban environments.

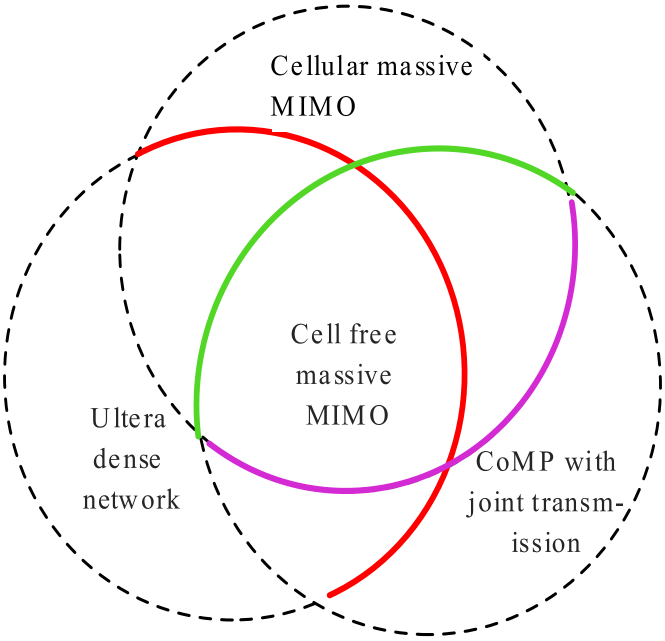

Figure 2.2: Describing CF M-MIMO as a blend of three technologies (Shaik, 2022).

2.3 Key Feature of Cell-Free Massive MIMO System

CF M-MIMO system has the potential to revolutionize wireless communication networks by enhancing capacity and SE, improving user experience, and enabling new applications such as smart cities and autonomous vehicles. The key features of CF M-MIMO technology include (J. Zhang, Chen, et al., 2019b):

- Distributed antennas: Multiple user devices can transmit and receive signals simultaneously because of the extensive deployment of dispersed antennas throughout the service area.
- The CPU: The dispensed antennas are linked to a CPU, which utilizes sophisticated resource allocation and signal processing techniques to enhance network performance.
- Interference mitigation: By reducing interference between various user devices, the cutting-edge signal processing algorithms employed in CF M-MIMO networks increase the network's overall SE and capacity.
- High spatial reuse: High spatial reuse is made possible by the employment of numerous distributed antennas and sophisticated signal processing techniques,

allowing various user devices to share the same frequency and temporal resources at once.

- Massive connectivity: In CF M-MIMO networks, the abundance of scattered antennas enables vast connectivity and the concurrent service of a huge number of UE.
- Low latency: In CF M-MIMO networks, low latency is made possible by high spatial reuse and cutting-edge signal processing algorithms. This allows for real-time applications and communication.

2.4 Advantage of Cell-Free Massive MIMO

CF M-MIMO networks offer several advantages over traditional cellular networks. Here are some of the key advantages (J. Zhang et al., 2019):

i. **High capacity:** Due to the numerous antennas and dispersed access points, CF M-MIMO networks can accommodate numerous users concurrently. As a result, the network can manage large amounts of data traffic and offer high capacity.

ii. **Improved spectral efficiency:** In the CF M-MIMO system, cooperative signal processing and beam formation techniques improve SE, enabling more data to be carried over the same bandwidth.

iii. **Better coverage and connectivity:** Users are more likely to be near at least one access point because of the randomly dispersed AP used in CF M-MIMO networks, which enhances coverage and connectivity.

iv. **Lower latency:** In CF M-MIMO networks, the user-centric strategy decreases latency, guaranteeing that users receive the optimum service and minimizing data transmission delays.

v. **Enhanced reliability:** In CF M-MIMO networks, the distributed access points and cooperative signal processing techniques boost network dependability, making sure that consumers encounter few pauses or interrupted connections.

vi. **Lower power consumption:** CF M-MIMO networks employ interference management strategies like power regulation, resource allocation, and scheduling to cut power consumption and associated operational expenses.

vii. **Flexibility:** M-MIMO networks operating without cell service are very adaptable and can change to satisfy the requirements of both the users and the network.

viii. **Scalability:** Because CF M-MIMO networks are highly scalable, they can expand and change to accommodate more users and faster data rates.

2.5 Limitation of Cell-Free Massive MIMO System

M-MIMO without cells has a lot of benefits, but the technology has significant drawbacks as well. M-MIMO systems without cells have some drawbacks, such as:

- High implementation complexity: M-MIMO systems without cells require a lot of coordination and processing resources to control the signals coming from numerous scattered antennas. The system's implementation could become complicated and expensive due to this.
- High power usage: M-MIMO systems without cell service demand a lot of antennas and sophisticated signal processing, which can use a lot of power. For applications that need minimal power consumption, like IoT devices, this can be difficult.
- Limited coverage area: M-MIMO systems without cells are often used in crowded cities where it is possible to disperse the antennas across the coverage area. However, in rural or distant regions where it may be challenging to disperse the antennas, the system's coverage area may be constrained.

2.6 Working Principle of Cell-Free Massive MIMO System

A network without cell boundaries is comprised of L Aps that are distributed throughout a geographic area and collaborate to provide service to nearby UEs (Demir et al., 2021). Each AP has a fronthaul connection to the CPU, which manages AP collaboration. The link between the AP and CPU can be cable or wireless. Like cellular networks, a CF system can be partitioned into an edge and a core. The communication links between the APs and CPUs at the edge are referred to as fronthaul links, whereas the links between the edge and the core are known as backhaul links. To support a range of data services, the CPUs are connected to the core network through backhaul links, which are responsible for transmitting and receiving data from the internet and other sources. On the other hand, fronthaul links are used for transmitting CSI and physical-layer signals related to the physical channels, as well as forwarding received UL data signals that have not yet been decoded.

The CPUs can be composed of a collection of local processors that are distributed across multiple APs or other physical locations and connected via fronthaul links. This aligns with the ongoing trend of wireless network cloudification, which is also known as Cloud Radio Access Network (C-RAN) (Interdonato, Frenger, et al., 2019b). In this network deployment design, multiple APs are connected to a single CPU, which handles the majority of baseband processing for the APs. The CPU is linked to the C-RAN. Figure 2.3, presented below, illustrates the operation of the CF M-MIMO system.

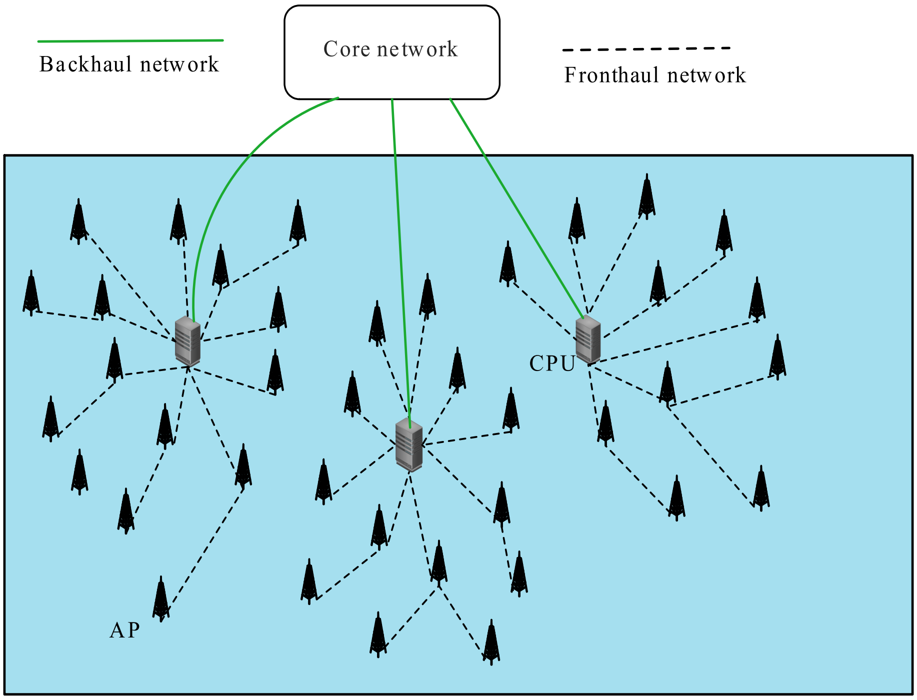

Figure 2.3: Depicts a representation of a CF network that consists of numerous geographically dispersed APs (Demir et al., 2021).

2.6.1 Cell-free massive MIMO uplink system

The UL channel is used to send message signals from the user equipment to AP (Chen et al., 2022a). Numerous APs are distributed throughout the coverage area. These APs are equipped with multiple antennas, forming an M-MIMO system. The distributed APs facilitate spatial multiplexing and beamforming techniques to simultaneously serve multiple users. In a fully centralized implementation, all the processing tasks, including channel estimation, signal detection, user scheduling, beamforming, and resource allocation, are performed at a central processor. This central processor has a global view of the network and access to the CSI from all APs and users. Figure 2.4 illustrates CF M-MIMO UL transmission with centralized implementation.

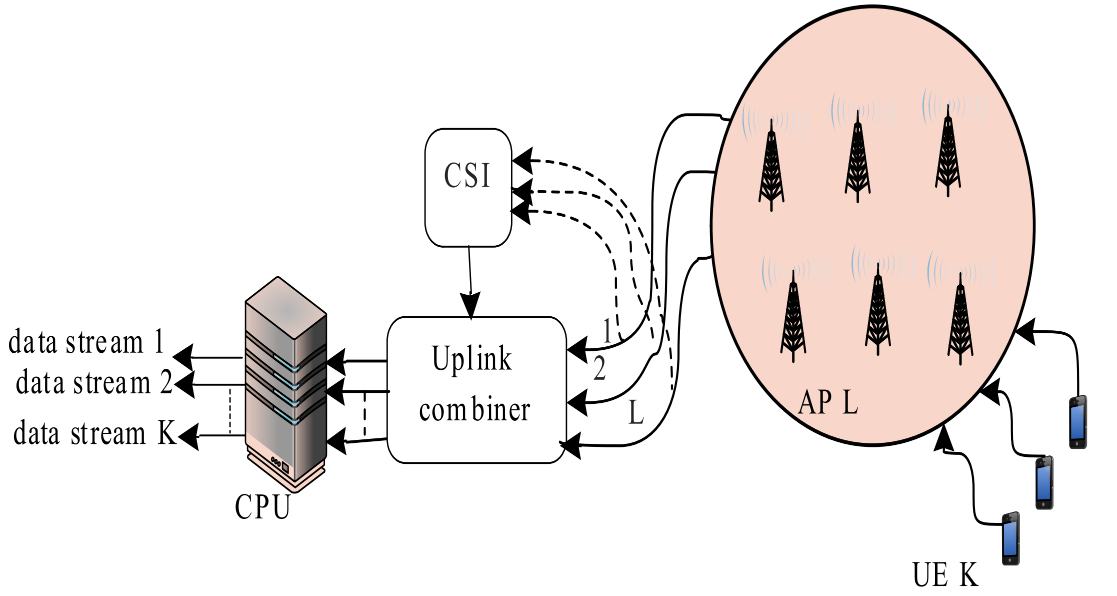

Figure 2.4: CF M-MIMO UL transmission (Chataut & Akl, 2020a).

2.6.2 Channel estimation

In CF M-MIMO systems, channel estimation is crucial since it entails estimating the CSI between the APs and the UE. To optimize signal transmission and reception, reduce interference, and enhance network performance, an accurate channel estimate is required. The difficulty of channel estimate is made more difficult in CF M-MIMO networks by the abundance of antennas and dispersed APs. In addition to being computationally difficult, estimating the CSI for each antenna and AP necessitates efficient coordination and synchronization across the AP. A CF M-MIMO system can employ a variety of approaches to estimate the channel (Chen et al., 2022a). These consist of:

1. **Pilot-based channel estimation:** In this method, pilot signals that are needed to calculate the channel state information occupy a specific portion of the broadcast. At each antenna and access point, the channel is estimated using the pilot signals that were received.
2. **Compressed sensing-based channel estimation:** A signal processing method called compressed sensing makes it possible to recover a sparse signal from a limited set of samples. With fewer pilot symbols, this method can be utilized to estimate the medium in a M-MIMO network without any cells.
3. **Machine learning-based channel estimation:** A CF M-MIMO system can use machine learning methods like deep learning and neural networks to estimate the channel. The more precise channel estimate is made possible by these techniques

because they can learn the intricate link between the broadcast signal and the received signal. But, this thesis focuses on only pilot-based channel estimation techniques.

2.6.3 Uplink data transmission

During Time Division Duplexing (TDD) mode, a portion of the coherence interval is assigned for UL data transmission. In the UL transmission, all users use the same time-frequency resources to transmit their data to the AP. As shown in Figure 2.4, the AP employs a channel estimator with linear combining techniques to detect the signals transmitted by all users. The specifics of the UL data transmission will be covered in Chapter Three.

2.6.4 Cell-free massive MIMO downlink system

The downstream transmission medium is used to send data from the APs to the UE. The DL process is the same as the UL process except the data flow is sent from the AP to UE. The AP sends signals to all K users downstream from the same time-frequency resource (Ammar et al., 2022). Consider a DL CF M-MIMO system that consists of multi-antenna AP and multi-antenna user equipment under the fading channel. Figure 2.5 shows CF M-MIMO DL transmission.

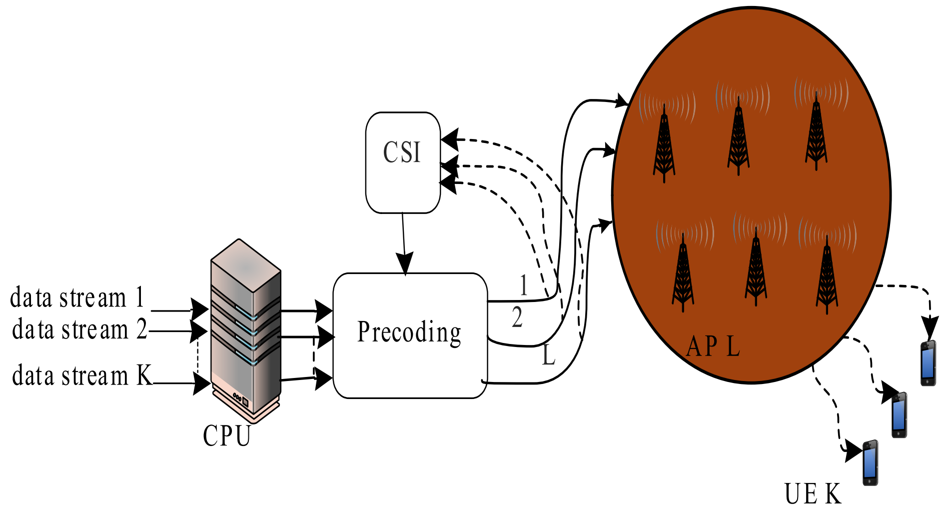

Figure 2.5: CF M-MIMO DL transmission (Chataut & Akl, 2020b).

2.7 Cell-Free Promising Technologies

This section outlines some of the current research directions looking at CF M-MIMO in conjunction with possible 5G and beyond network enablers. These include radio stripes (RS), reconfigurable intelligent surfaces (RIS), unmanned aerial vehicles (UAV), large intelligent surfaces (LIS), and artificial intelligence (AI) methods, as shown in Figure 2.6. In this thesis, unmanned aerial vehicle (UAV) is not considered.

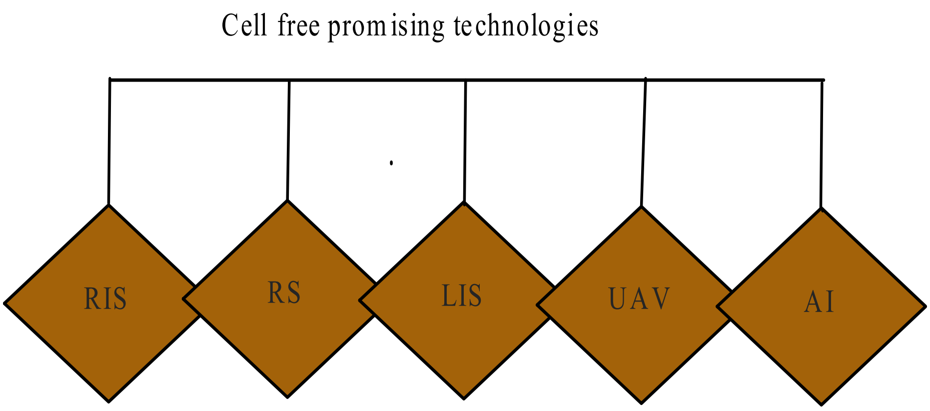

Figure 2.6: Cell-free promising enabling technologies (Kassam et al., 2023).

2.7.1 Reconfigurable intelligent surface

RIS often referred to as an intelligent reflecting surface (IRS), is an emerging technology that may be used to address the high costs of CF systems' hardware and electricity sources (Huang et al., 2021). RIS is a flat surface with lots of inexpensive, inactive reflecting parts. These parts can separately change the incident signals' amplitude and/or phase and reflect them in a controllable manner (Liu et al., 2021). Based on the wavefront control principle which involves using mathematical algorithms, the intelligent transmission technique of RIS optimizes the configuration of the RIS's components in real time under environmental factors and intended gearbox requirements factors. These algorithms frequently rely on techniques for optimization, using techniques to discover candidates, such as gradient-based optimization or reinforcement learning the best component configuration that can be used to accomplish the desired transmission objectives (Liu et al., 2021). RIS-aided CF, in contrast to conventional CF systems, does not require any additional gear, such as sophisticated digital phase shift circuits, which greatly lowers energy consumption and signal processing complexity. As a result, with RIS, less power is required to attain an equal level of QoS as with traditional CF systems. Additionally, RIS-aided wireless systems have some advantages and disadvantages (Pereira et al., 2022),(Huang et al., 2021) such as:

- Since RIS serves as an antenna array, it can boost network capacity and data rates in an economical and energy-efficient way by calibrating various passive reflecting elements.

- Because RIS is passive, it is impossible to calculate the reflected medium for wireless communication systems with RIS assistance using conventional channel estimation methods.

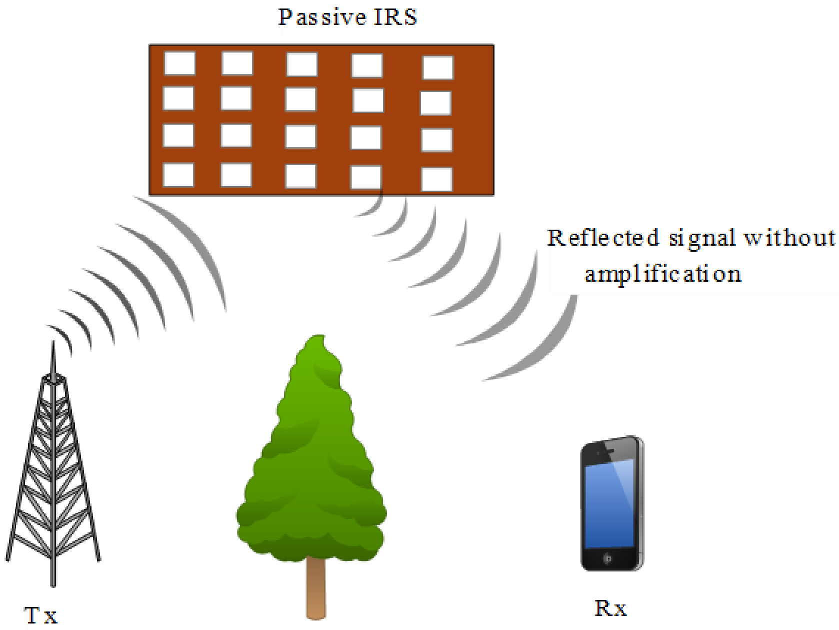

Figure 2.7: Block diagram of an IRS-enhanced wireless system (Gashtasbi et al., 2022).

2.7.2 Radio strips

One of the potential technologies for CF networks is radio strips (RSs), which can help them deal with the expensive deployment costs and complexity as well as the constrained fronthaul and backhaul link capacities. RSs have active antenna components as compared to RIS. To implement the CF M-MIMO network in crowded spaces and indoor locations like stadiums, train stations, factories, and shopping malls with numerous APs and UEs in such areas, they use a sequential topology, which is thought to be quite an interesting method (Elhoushy et al., 2022). To link the APs and the CPU, separate fronthaul cables are required in the traditional CF M-MIMO network, which should be noticed. As a result, the system performance is not scalable and implementation costs are exorbitant(Interdonato, Björnson, et al., 2019). However, in CF systems with RSs, a large number of APs are combined into a single cable to more efficiently carry out synchronization, data transmission, and power supply activities than in a typical CF system design (Elhoushy et al., 2022). The followings are some benefits and drawbacks of such CF networks with RSs (Shaik et al., 2020);

- Flexible deployment and cable routing in real-world applications to create more useful and scalable systems.

- By implementing routing methods that might mitigate the effects of node failures, the network can be fault-tolerant.
- RSs increase durability and resilience, which lowers upkeep costs.
- Low heat dissipation makes cooling devices easier to use and less expensive.
- Precise synchronization and coordination between antennas and antenna processing units is a critical prerequisite for CF networks with RSs.

2.7.3 Large intelligent surface

LIS is a novel idea in the field of wireless communication. It is similar to RSs since it implies active elements and functions as a sizable active antenna array, which is a development of massive MIMO technology (Hu et al., 2018). LIS is composed of a continuous surface that radiates and communicates with and receives data from neighboring users. It serves as a radio entry point and promotes one-on-one user interaction. LIS takes a portion of the channel and acts as a movable reflector between the AP and the users (Liu et al., 2021). When the user and the LIS are near one another, the LIS reduces route loss while increasing antenna gain. As a result, it is anticipated that both sides of the communication will have minimal transmit power (Liu et al., 2021).

The advantage of LIS-assisted wireless communication systems are:

- LIS offers the highest data rates with a conventional big antenna array for a specific surface area.
- LIS can reduce interference and work well as the number of terminals rises.

2.7.4 Artificial intelligence

Since it enables connectivity for millions of mobile devices with internet access, AI is one of the technologies that have the potential to enhance the performance of 5G and beyond networks (Yadav et al., 2022). The primary objective of AI is to enable machines and systems to function at levels of intelligence comparable to those of humans. Despite the extensive study of AI learning techniques, it still faces challenges and has room for improvement, particularly in light of the rapid advancements in contemporary computing and data storage technologies in recent years (C. Zhang et al., 2020). These days, both academia and industry are very interested in studying the fusion of AI with 5G and beyond networks. As a result, there has been a recent convergence of a lot of new research on AI-based communication systems, promising better data rates, improved QoS, and low implementation costs (Yadav et al., 2022). Applying machine/deep learning techniques to CF wireless communication systems has several benefits, including the ability to identify previously unidentified patterns, reduce complexity, improve sustainability and reliability, and produce performance results on par with or better than those of conventional methods (Yetis et al., 2021).

2.8 Related Work

Finding a low-complexity, high-performance channel estimator for CF M-MIMO UL systems is the subject of numerous research. Among them are some of the following:

The author takes into consideration a real-world M-MIMO system with multiple APs and spatially correlated rician fading channels (Wang et al., 2021a). The UL SE with maximum ratio (MR) and local minimum mean squared error (L-MMSE) combining techniques, as well as optimal large-scale fading decoding (LSFD), have been explored in the literature. To achieve these techniques, the received signal at the AP is first estimated using channel estimation techniques such as PA-MMSE and PA EW-MMSE estimators. To account for phase shifts brought on by mobility and phase noise, LoS path's phase is represented as a random variable with a constant distribution. The SE with MR combining is derived. The EE and area throughput are not addressed. The author only considers single antenna UE which has a high significance change in SE.

In (Wang et al., 2022), a CF M-MIMO with a multi-antenna AP and UE under a Rayleigh fading channel is investigated. The closed-form SE expression with MMSE SIC and MR combiner are derived. Additionally, MMSE combiner schemes are derived at both AP and CPU, which can maximize the achievable SE for the fully centralized and distributed implementations, respectively. The two-layer decoding implementation is studied with a first layer (AP) that uses an arbitrary combining algorithm and a second layer (CPU) that uses the best LSFD. Also calculated is the closed-form expression SE for the two-layer decoding scheme with MR combining. The author showed the SE performance of different implementations such as fully centralized, distributed, and two-layer decoding with MMSE and MR combining under fading channels that only consider the NLOS path. The author does not address the signal that came in the LOS path, and also the user mobility that leads to phase shift is not considered. The EE and area throughput are not addressed. The channel estimation in this work is estimated by the MMSE estimator, which does not consider the phase shift or mobility of user equipment. In addition to that, this estimator has high computational complexity.

In (zdogan et al., 2019), the UL and DL SE of CF M-MIMO under a rician fading channel are studied. Due to the mobility of the user and phase noise, the LoS phase is considered a random variable with a constant distribution. The LS, non-aware linear MMSE (LMMSE), and phase-aware MMSE estimators are derived taking into consideration the accessibility to earlier data at the APs. To reduce both coherent and non-coherent interference in the UL, a two-layer decoding approach is explored. Additionally, the closed-form expression SE with aware MMSE, non-aware MMSE, and the LS estimator combined with MR combining are driven. To reduce the disturbance from both coherent and noncoherent sources, a two-layer decoding technique was investigated. Coherent and non-coherent propagation were examined in the DL section. The author showed that coherent transmission is significantly superior to DL transmission that is not coherent and the LSFD enhances the UL SE performance. The author only considered single antenna APs and user equipment. This paper is limited to SE analysis, area throughput, and EE not addressed. Also the author not considered other combining like MMSE with less computational complexity combining.

In (Amadid, Belhabib, & Zeroual, 2022), in this work, the channel estimation of UL CF M-MIMO under the rician fading channel is analyzed. The channel consists of both the LOS and NLOS path. The dynamic cooperative cluster is illustrated, where only APs with the optimal channel conditions with the intended user are permitted to serve it. The author proposed a partial channel estimator in which a set of APs with the best channel condition can evaluate the channel estimates. The normalized MSE and the computational complexity for the partial MMSE and partial EW-MMSE are derived. In addition, the author showed the PEW-MMSE almost the same result as the PMMSE in terms of normalized MSE. However, the computational complexity of PEW-MMSE is low compared to that of the PMMSE channel estimator. The author demonstrated, when the number of users increases, the channel estimation reduced. Moreover, when the number of antennae per access point increases, the channel estimation is more beneficial. In this paper the analysis is limited to channel estimations only, the EE, area throughput, and SE of the paper are not addressed. The author did not show the channel estimation when the number of antennas per user equipment is more than one.

In (Amadid, Belhabib, Khabba, et al., 2022), this work examines the UL phase channel estimation (CE) process and the SE under correlated Rayleigh channel. This work tackles the linked and uncorrelated channels where the correlated channel is demonstrated using the uniform linear array (ULA) and a uniform planar array. The MMSE channel estimator with MMSE combiner is investigated. The author proposed a UPA configuration for an M-MIMO system based on the equivalent ULA configuration's Kronecker product. The comparison of CF M-MIMO with the conventional M-IMO is being considered. The author showed in the simulation result, the MMSE estimator and MMSE aggregating vector perform better in the correlated channel case than they do in the uncorrelated channel case. The EE and area throughput are not addressed. The analysis was not addressed when the number of antennas per user equipment was more than one. The channel estimator used in this work has high computational complexity and also the signal propagation in the LoS is not addressed.

CF M-MIMO with multiple antennas on both the AP and user devices under Rayleigh fading channels is analyzed (Wang et al., 2023). The author investigated the SE for the LSFD scheme and fully centralized processing schemes. The iteratively weighted sum-minimum mean square error (I-WMMSE) algorithms have been proposed for two processing schemes in the literature, to improve the UL SE in CF M-MIMO systems. The closed form SE expression is derived. The I-WMMSE precoding scheme has been shown to achieve outstanding performance in CF M-MIMO systems, even with a large number of UE antennas. Importantly, the scheme has been shown to become even more effective with a larger number of UE antennas. The author didn't consider the LoS path. The EE and area throughput are not addressed. The MMSE channel estimator used in this work has high computational complexity.

The UL SEs for different CF M-MIMO implementations with an MME combiner are studied (Björnson & Sanguinetti, 2019b). The level 4 or fully centralized implementation in which the medium estimation and detection perform at the CPU. Level 3, operates in two stages. In the first stage, the channel estimated and applied the combiner at the APs to mitigate interference. In the second stage, the LSFD coefficient is applied to further mitigate the interference, gathering, and detection performed at the CPU. Level two is the simplification of level 3. Level 1, the estimation and detection performed at the APs. The author showed that CF M-MIMO outperforms that of cellular and small-cell M-MIMO networks. The closed-form SE expression for cellular M-MIMO, small cell, and CF M-MIMO networks are derived. Both the centralized and distributed implementation of CF M-MIMO is analyzed. The SE for cellular, small cell, and CF M-MIMO is compared. The MMSE and MR combiner are deployed for all three networks with different implementations. The author has not addressed the other performance parameter such as EE and area throughput. The line-of-sight path not consider during the channel estimation and the estimator used in this work has high computational complexity.

In (Ueoka et al., 2022), this study examines how various channel fades affect the SE channel hardening and advantageous propagation of CF M-MIMO) systems. The LoS and NLoS channel for the indoor and outdoor environment is analyzed. The findings suggested that cell-free systems may exhibit higher SE and hardening when the channel exhibits rician fading, whereas they may gain an advantage from more favorable transmission in Rayleigh fading channels. Due to the predictable LoS component that exists in the rician channel, it has a higher channel hardening than the Rayleigh channel. The author also showed that in outdoor situations, the statistical CSI is unreliable and low levels of channel hardening in outdoor settings result in subpar SE for CF systems.

In (Ye et al., 2022), the effect of an imperfect channel covariance matrix on the SE of CF M-MIMO systems is examined. The expression for the UL SE with maximum ratio combining (MRC) and zero forcing (ZF) receivers is derived. The impact of the covariance matrix with a different number of coherent blocks is analyzed. The author proposed a method to estimate the covariance matrix by changing the pilot in an adjacent coherence block. The proposed method in this work improves the channel estimation accuracy without requiring additional pilot overhead, which can lead to better system performance in terms of UL SE. The simulation findings demonstrate that the channel estimation algorithm can achieve good estimation accuracy even when the channel covariance information is not perfect. Additionally, improved system efficiency results from a more accurate estimation of the covariance matrix of the received signal.

In (Li et al., 2022), the multi-antenna AP and multi-antenna UE under Weichselberger rician fading channel with random phase shift is studied. The UL SE for two practical processing strategies i.e., the fully centralized processing (FCP) approach with global MMSE or MR combining and the LSFD technique with local MMSE or MR combining are examined. To improve the SE effectiveness of the system, the author proposed an effective UL precoding method that relies only on the UE-side correlation matrices' eigenvalues. Additionally, the closed-form SE equations for the LSFD scheme with MR combining have been developed. The channel estimation used in this work has high computational complexity. The analysis is only based on the SE, the EE and area throughput is not addressed.

Table 2.1: Contribution and gap of different related works.

Author/year	Title	Contribution	Gap
(Li et al., 2022)	Cell-Free Massive MIMO with Multi-Antenna Users over Weichselberger rician Channels	The average UL SE for FCP and LFSD with MMSE and MR combining is analyzed.	The channel estimator has a high computational complexity

(Wang et al., 2021a)	Uplink performance of cell-free massive MIMO over spatially correlated rician fading channels	The UL SE is analyzed based on MR/MMSE combined with EW-MMSE, L-MMSE, and MMSE channel estimator.	The number of antenna per UE is one, the EE and area throughput is not addressed.
(Wang et al., 2022)	Uplink performance of cell-free massive MIMO with multi-antenna users over jointly-correlated Rayleigh fading channels	The UL SE for four implementations with MMSE-SIC detectors and MMSE and L-MMSE combining is investigated.	The channel estimator has high computational complexity. The EE and area throughput are not addressed. The LoS path is not considered.
(Amadid et al., 2022)	On channel estimation in cell-free massive MIMO for spatially correlated channels with correlated shadowing	The normalized MSE of P-MMSE and P-EW_MMSE is studied. The estimation is only for the set APs.	The number of antennae per UE is not practical. The SE, EE, and area throughput were not addressed.
(zdogan et al.,2019)	Performance of cell-free massive MIMO with rician fading and phase shift	The UL and DL SE for the MMSE, L-MMSE, and LS channel estimator with MR combining is studied.	The number of antennas per APs and UE is one. EE and area throughput not addressed.

(Wang et al., 2023)	Uplink precoding design for cell-free massive MIMO with iteratively weighted MMSE	The UL SE is analyzed based on the I-WMMSE precoding scheme.	The channel estimator has high computational complexity. The LoS path is not considered. The EE and area throughput are not addressed.

CHAPTER THREE

3. MATERIALS AND METHODS

3.1 Introduction

This thesis includes a literature review of secondary sources related to the performance evaluation of CF M-MIMO with multi-antenna UE over rician fading for UL systems. The review encompasses previous researchers' works, various articles from the Institute of Electrical and Electronics Engineers (IEEE), and journals. The researchers developed their techniques to achieve high-performance and low-complexity channel estimation methods in CF M-MIMO UL systems. The following methodology was employed in this study: a review of related literature was conducted to gather relevant information, a problem statement was formulated, and the limitations of existing channel estimation techniques were taken into account.

3.2 Materials

Software like MATLAB/R2022 and ConceptDraw DIAGRAM are used in this thesis work. Engineers and scientists can analyze and construct systems and technologies that will alter the world using the programming tool called MATLAB. ConceptDraw DIAGRAM is a comprehensive drawing software that provides users with a professional set of drawing tools, pre-designed templates, a vast object library, and a variety of custom printing and file export options. With this software, users can easily create diagrams, flowcharts, technical drawings, and other visual representations of information in a visually appealing and professional manner. Additionally, ConceptDraw DIAGRAM allows for collaboration and sharing of created content with other users.

3.3 Methods

3.3.1 System design

- Analyzing the mathematical model two channel estimators to calculate the SE, EE, and area throughput.
- Making CF M-MIMO uplink systems more performant and computationally simple.

3.3.2 Simulation methods

- Perform the SE, EE, and area throughput versus the number of antennas per user equipment’s simulation to compare the proposed channel estimation method’s performance to that of the existing estimator.

- Assess the proposed estimator's effectiveness with the existing estimator based on SE, EE, and area throughput versus the number of AP simulations.
- Compare the computational complexity of the proposed method with that of existing methods based on the simulation of the real number of multiplications vs the number of users, number of antenna per APs, and the number of antenna per UE and number of AP.

3.4 System Model

In the CF M-MIMO system, M APs and K UEs are randomly dispersed over a sizable region, with L and N denoting the number of antennas per AP and UE, respectively. The system operates based on the standard block fading model, where the coherence time-frequency block size has no impact on the channel responses (Björnson et al., 2017). The system operates in TDD mode, each block consists of a total of τ_{c} samples, with τ_p samples set for UL and the remaining $\tau_{\mathrm{u}} = \tau_{\mathrm{c}} - \tau_p$ samples used for data transmission. Let us denote the complex-valued channel between the k-th UE and the m-th AP $\mathrm{H}_{mk} \in \mathbb{C}^{L \times N}$. We assume that the channel coefficients H_{mk} are independent for different AP-UE pairs and independent and identically distributed (IID) across different blocks.

The system model for the CF M-MIMO system is shown in Figure 3.1. In this model, M APs and K UEs are randomly dispersed over a sizable region, with L and N denoting the number of antennas per AP and the number of antenna per UE, respectively. In a fully centralized implementation of CF M-MIMO channel estimation and data detection, all the processing tasks are performed at the CPU. The received signal from each UE is transmitted to the CPU through the help of AP. The channel estimation algorithm estimates the channel coefficients for each UE-AP pair using techniques such as the PA-MMSE or PA-EW-MMSE, which take into account the spatial correlation between the antennas and the noise statistics. The estimated channel coefficients are then used for data detection, which aims to recover the transmitted data from the received signal.

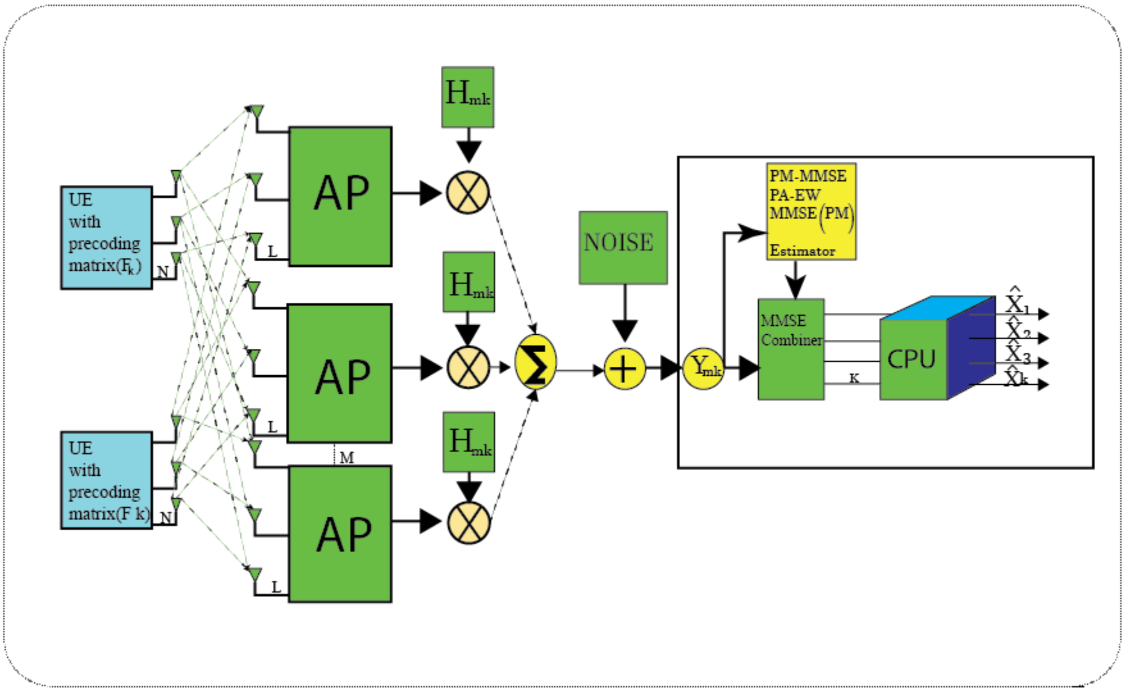

Figure 3.1: System model for M access point and K user equipment.

3.4.1 Time-division duplexing protocol

TDD is a method of transmitting and receiving wireless signals where the sender and receiver occur at identical frequencies at different times. Each coherence block in a TDD system is divided into three slots, as shown in Figure 3.2, where τ_p symbols are used for UL pilots to estimate the channel, τ_u symbols are dedicated to UL data, and τ_d symbols are assigned for DL data. A key benefit of TDD operation is that, because of channel reciprocity, an AP can use the channel information discovered during UL processing for DL transmission. The work described in this thesis is all predicated on TDD functioning (Shaik, 2022).

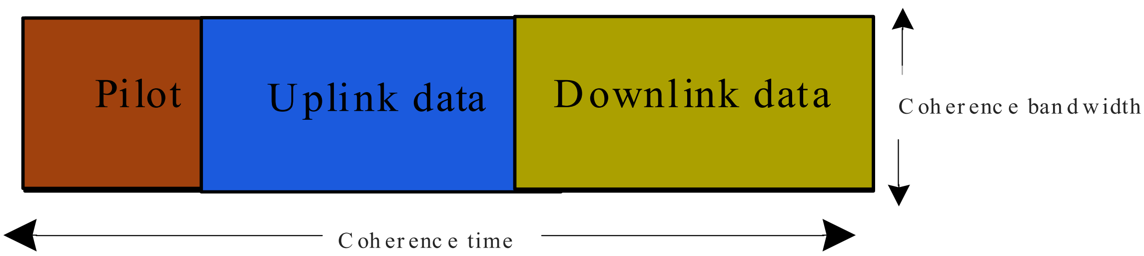

Figure 3.2: TDD protocol (Shaik, 2022)

The τ_c provides three different tasks in the CF M-MIMO system in TDD protocol.

$$\tau_c = B_c T_c = \tau_p + \tau_u + \tau_d \tag{3.1}$$

Where, τ_c the coherence block sample size, τ_p the samples for the ULpilot signal, τ_u the samples for UL data transmission, and τ_d the samples for DL data transmission.

3.4.2 Weichselberger rician fadig channnel

The Weichselberger approach is realistic and appropriate for real-world situations involving multiple UEs. Compared to the often researched Rayleigh fading channel model, the Weichselberger rician fading channel model, the channel impulse response is modeled as a sum of a deterministic LoS component and NLoS component, where the NLoS component is modeled as a complex Gaussian process with zero mean and variance proportional to the distance between the transmitter and receiver. The Weichselberger model, in particular, can represent the joint-correlation fluctuations between the AP and UE side (Wang et al., 2021b). More significantly, the model's eigenmode coupling matrix may describe how the scattering objects are arranged between each AP-UE pair in a real-world setting. Additionally, it was confirmed by the measurement studies in (Weichselberger et al., 2006) that the Weichselberger model exhibits much lower modeling error than other well-liked stochastic channel models. It belongs to the category of rician fading channels, which means that it has both a dominant LOS component and a scattered component. The jointly-correlated rician fading channel, which consists of a stochastic NLoS path component and a semi-deterministic LoS path component with a random phase shift, is taken into account. The Weichselberger model-based H_{mk} model (Wang et al., 2022),

$$\mathrm{H}_{mk} = \bar{\mathrm{H}}_{mk} e^{j\varphi_{mk}} + \underbrace{\mathrm{U}_{mk,r}\left(\tilde{\mathrm{W}}_{mk} \odot \mathrm{H}_{mk,\mathrm{iid}}\right)\mathrm{U}_{mk,t}^{H}}_{\tilde{\mathrm{H}}_{mk}} \tag{3.2}$$

First, the LoS component of the channel $\bar{\mathrm{H}}_{mk} = \left[\bar{\mathrm{h}}_{mk1}, \cdots, \bar{\mathrm{h}}_{mkN}\right]$ is modeled as a deterministic complex vector with L elements, where $\bar{\mathrm{h}}_{mkn} \in \mathbb{C}^{L}$ is the channel between the n-th antenna of UE k and AP m, and $\varphi_{mk} \sim \mathcal{U}[-\pi, \pi]$ is a uniformly distributed phase shift (Özdogan et al., 2019). Second, the NLoS component of the channel $\tilde{\mathrm{H}}_{mk}$is modeled as a complex random vector with L elements, where $\mathrm{H}_{mk,\,\mathrm{iid}} \in \mathbb{C}^{L\times N}$is a matrix of i.i.d. complex Gaussian entries with zero mean and unit variance.

Third, the unitary matrices $\mathrm{U}_{mk,r} \in \mathbb{C}^{L\times L}$ and $\mathrm{U}_{mk,t} \in \mathbb{C}^{N\times N}$ are the eigenbasis of the one-sided correlation matrices $\mathrm{R}_{mk,\mathrm{r}} \triangleq \mathbb{E}\{\tilde{\mathrm{H}}_{mk}\tilde{\mathrm{H}}_{mk}^{H}\}$ and $\mathrm{R}_{mk,\mathrm{t}} \triangleq \mathbb{E}\{\tilde{\mathrm{H}}_{mk}^{T}\tilde{\mathrm{H}}_{mk}^{*}\}$, respectively, which are defined as the expected values of the outer product of the NLoS component $\tilde{\mathrm{H}}_{mk}$ (Weichselberger et al., 2006). Fourth, the eigenmode coupling matrix $\mathrm{W}_{mk} \triangleq \tilde{\mathrm{W}}_{mk} \odot \tilde{\mathrm{W}}_{mk}$ is defined as the element-wise product of the matrix $\mathrm{U}_{mk,\mathrm{r}}$ and the conjugate transpose of the matrix $\mathrm{U}_{mk,\mathrm{t}}$ where the $(i,j)^{\mathrm{th}}$ element of $[\mathrm{W}_{mk}]_{ij}$ specifies the average amount of power coupling from the i^{th} column of $\mathrm{U}_{mk,\mathrm{r}}$ to the j^{th} column of $\mathrm{U}_{mk,\mathrm{t}}$.

Finally, the full correlation matrix R_{mk} is calculated by taking the Kronecker product of the conjugate transpose of $\mathrm{U}_{mk,\mathrm{t}}$ and $\mathrm{U}_{mk,\mathrm{r}}$, and then multiply it by a diagonal matrix formed by the vectorization of the matrix W_{mk}. The full correlation matrix is calculated as shown below by taking into consideration the channel between the UE and AP as $\mathrm{h}_{mk} = \mathrm{vec}(\mathrm{H}_{mk}) \in \mathbb{C}^{LN}$.

$$\mathrm{R}_{mk} \triangleq \mathbb{E}\left\{\mathrm{vec}\left(\tilde{\mathrm{H}}_{mk}\right)\mathrm{vec}\left(\tilde{\mathrm{H}}_{mk}\right)^{H}\right\} \in \mathbb{C}^{LN\times LN} \tag{3.3}$$

$$\mathrm{R}_{mk} = \left(\mathrm{U}^{*}_{mk,t} \otimes \mathrm{U}_{mk,r}\right)\mathrm{diag}\left(\mathrm{vec}(\mathrm{W}_{mk})\right)\left(\mathrm{U}^{*}_{mk,t} \otimes \mathrm{U}_{mk,r}\right)^{H} \tag{3.4}$$

3.4.3 Uplink transmission

3.4.3.1 Uplink pilot transmission

Pilot refers to a specific pattern or sequence of symbols that is transmitted by UE in the wireless communication system. The wireless medium between the UE and the various APs in the network is estimated using pilot signals. The APs estimate the medium between themselves and the UE using the pilot signals received. We use mutually τ_p normal pilot sequences every pilot matrix contains N mutually orthogonal pilot sequences and is used for channel estimation (Mai et al., 2020).

$$\mathrm{P}_k \mathrm{P}_{k'} = \begin{cases} \tau_p \mathrm{I}_N & k' = k \\ 0 & \text{otherwise} \end{cases} \tag{3.5}$$

Where, $\mathrm{P}_k \in \mathbb{C}^{N\times\tau_p}$ denote the pilot matrix of UE k.

In practical CF M-MIMO systems, due to limited system resources, multiple UEs may have to use the same pilot matrix (Björnson & Sanguinetti, 2019b). Let $\mathcal{P}_k$ denote the set of indices of UEs that use the same pilot matrix as UE k, including UE k itself. In this scheme, all UEs send their pilot signals to the AP, and the received signal at the AP can be expressed as $\mathrm{Y}^{p}_{m} \in \mathbb{C}^{L\times\tau_p}$ at AP m is obtained by in (3.6).

$$\mathrm{Y}^{p}_{m} = \sum_{k=1}^{K} \mathrm{H}_{mk}\mathrm{F}_k\mathrm{P}_k + \mathrm{N}_m \tag{3.6}$$

Where, $\mathrm{F}_k \in \mathbb{C}^{N\times N}$ is the UL precoding matrix of UE k designed to maximize the received signal power at the AP while satisfying the maximum transmit power constraint $\mathbb{E}\{\|\mathrm{F}_k\|^2_{\mathrm{F}}\} \leq$

p_k with p_k being the maximum transmit power of UE k and $\mathrm{N}_m \in \mathbb{C}^{L\times\tau_p}$ it represents the noise and interference at the AP, which is modeled as complex Gaussian noise with zero mean and variance with $\mathcal{N}_{\mathrm{C}}(0,\sigma^2)$ elements.

3.4.3.2 Uplink channel estimation

The goal of channel estimation is to determine the wireless medium between UE and the APs in the network. To maximize the efficiency of the entire system, this information is then used to jointly process the data that was received from the UE. Pilot signals are commonly used in this thesis to estimate the channel. All APs in the network receive the pilot signals that the UE transmits. According to the received pilot signals, individual AP determines the channel between itself and the UE. CPU then incorporates the channel estimations from each AP to get an overall estimate of the channel. Then, for collaborative data processing, this global estimate is utilized (Amadid, Belhabib, Khabba, et al., 2022).

To find an estimate of h_{mk}, AP m matches Y_m^p with P_k^H as in the following equation (3.7).

$$\mathrm{Y}_{mk}^p = \mathrm{Y}_m^p \mathrm{P}_k^H = \textstyle\sum_{l\in\mathcal{P}_k} \tau_p \mathrm{H}_{ml}\mathrm{F}_l + \mathrm{N}_m\mathrm{P}_k^H \tag{3.7}$$

Consider, $\hat{\mathrm{h}}_{mk}$, R_{mk} and φ_{mk} are available for AP m, then the PA-MMSE estimate of h_{mk} is obtained by (3.8).

$$\hat{\mathrm{h}}_{mk} = \mathrm{vec}(\hat{\mathrm{H}}_{mk}) = \bar{\mathrm{h}}_{mk}e^{j\varphi_{mk}} + \mathrm{R}_{mk}\tilde{\mathrm{F}}_k\Psi_{mk}^{-1}\mathrm{vec}(\mathrm{Y}_{mk}^p) \tag{3.8}$$

Where, $\bar{\mathrm{h}}_{mk} = \mathrm{vec}(\bar{\mathrm{H}}_{mk}), \tilde{\mathrm{F}}_k = \mathrm{F}_k^T \otimes \mathrm{I}_L$ and $\Psi_{mk} = \sum_{l\in\mathcal{P}_k}\tau_p\tilde{\mathrm{F}}_l\mathrm{R}_{ml}\tilde{\mathrm{F}}_l^H + \sigma^2\mathrm{I}_{LN}$.

3.4.3.2 Phase-aware MMSE channel estimator

To estimate the medium between the scattered antennas and the users, a PA-MMSE channel estimator is used (Wang et al., 2022). The fact that the estimator takes into consideration the received signal's phase information proves that it is phase-aware. In fading channels, it minimizes the mean squared error between the UE and AP to estimate the channel. Theoretically, by including the phase information of user mobility in the estimating process, the MMSE channel estimator can be made phase-aware. To be more precise, the channel phase can be estimated by the estimator using the received signal's phase, which can then be utilized to boost the medium estimation's precision. The goal of designing an MMSE channel estimator is to generate CSI at the receiver and to minimize the error due to interference. The MMSE estimator is complex since it needs both the calculation of the correlation function and the inversion of a matrix. The MMSE channel estimation is a highly sophisticated estimate method. The equation for phase-aware MMSE is defined in equation (3.8).

3.4.3.3 Uplink data transmission

UL data transmission in the thesis involves transmitting data from UE to the Aps in the network. The UE sends its data to multiple APs simultaneously, and the APs cooperate to jointly process the received signal. This joint processing is achieved through a process called channel estimation, where the APs estimate the CSI of the UE. Once the channel state information is estimated, the APs use it to jointly decode the UE's data. This joint decoding is made possible by the huge number of distributed antennas, which allows the APs to effectively cancel out the interference from other UEs in the network. The decoded data is then forwarded to the CPU for further processing (Ngo et al., 2017). During the data transmission phase in CF M-MIMO systems, all antennas of all UEs simultaneously transmit their data symbols to all APs. The received signal at AP m can be expressed as,

$$\mathrm{y}_m = \sum_{k=1}^{K} \mathrm{H}_{mk}\mathrm{s}_k + \mathrm{n}_m \tag{3.9}$$

Where, $\mathrm{s}_k = \mathrm{F}_k\mathrm{x}_k \in \mathbb{C}^N$ is the transmitted signal of UE k with $\mathrm{x}_k \sim \mathcal{N}_{\mathbb{C}}(\mathbf{0}, \mathrm{I}_N)$ being the data symbol vector of UE k and $\mathrm{n}_m \sim \mathcal{N}_{\mathbb{C}}(0, \sigma^2\mathrm{I}_L)$ is the additive noise vector.

3.4.4.4 Uplink receives combining

The coherent signal processing, also known as receive combining, the APs perform linear projection based on the CSI acquired by channel estimation. Receive combining converts the vector channel from each UE into a scalar channel that can support higher SE compared to assigning only one single-antenna AP to each UE (Parida & Dhillon, 2021). Receiving combining serves to increase the target signal's strength relative to the sum of interfering signals and noise, which calls for CSI. The choice of combining techniques can significantly impact the SE and computational complexity of the system. This thesis takes into account the MMSE combining technique only.

3.4.5.4.1 MMSE combining

MMSE combining is a signal processing technique used to combine the signals received from multiple antennas before decoding them. The goal of MMSE combining is to minimize the mean squared error between the sender and the received signal, subject to some constraints on the channel model and noise. It can be used to enhance the efficiency of the system by reducing the effects of interference and noise. MMSE combining has a higher complexity compared to other combining methods because it requires the computation of the M*L by M*L matrix inverse, which is a computationally intensive operation, and then a matrix-vector multiplication (Björnson & Sanguinetti, 2019b). The computational demands of the signal processing techniques used in CF M-MIMO systems can be substantial, but this is generally not a significant concern because the processing is performed at the CPU, which is presumed to possess significant computational power. The MMSE combining is defined as shown in equation (3.10).

$$\mathrm{V}_k = \left(\sum_{l=1}^{K} \left(\hat{\mathrm{H}}_l \hat{\mathrm{F}}_l \hat{\mathrm{H}}_l^H + \mathrm{C}_l'\right) + \sigma^2 \mathrm{I}_{ML}\right)^{-1} \hat{\mathrm{H}}_k \mathrm{F}_k \tag{3.10}$$

Where, C_l' is defined on equation (3.16).

3.5 Spectral Efficiency of the System

Depending on the needed efficiency and sophistication trade-off, CF M-MIMO can employ four different signal processing methods (Björnson & Sanguinetti, 2019b). The fully centralized processing implementation is specifically recognized as a competitive option for utilizing the promising of CF M-MIMO. In this thesis, we illustrate fully centralized processing and evaluate their SE effectiveness.

3.5.1 Fully centralized processing

Under the completely centralized processing setup, APs send all pilot signals from user equipment to the CPU to perform the channel estimation, combining, and data detection process. The APs are only responsible for interfacing the UE and CPU as shown in Figure 3.3 below.

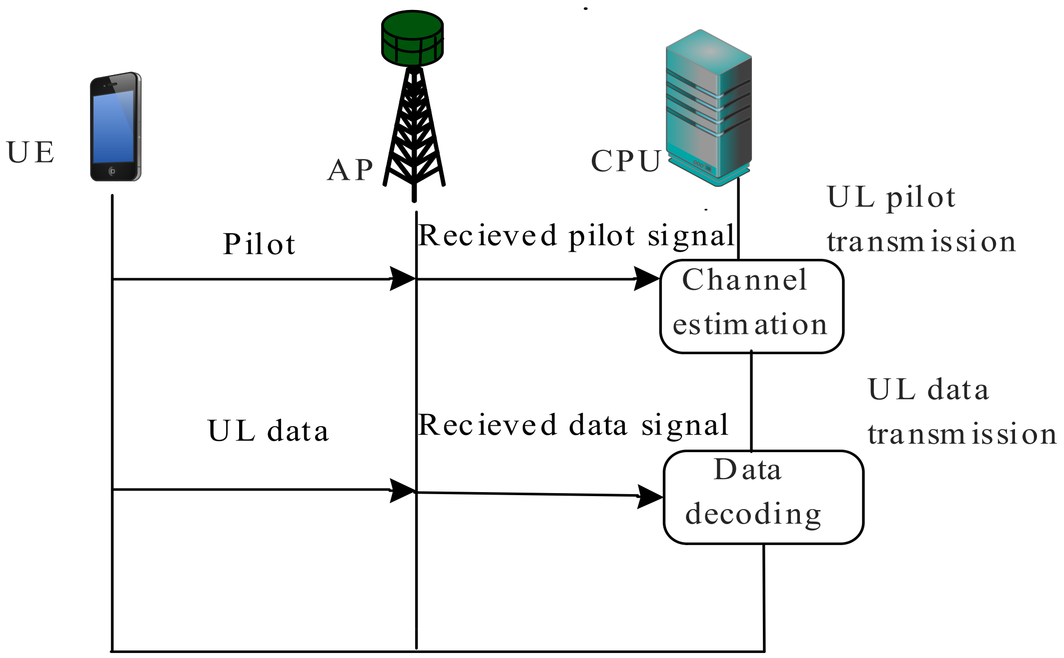

Figure 3.3: Full centralized processing schemes (Chen et al., 2022b).

The overall channel of UE k is represented as $\mathrm{h}_k = [\mathrm{h}_{1k}^T, \cdots, \mathrm{h}_{Mk}^T]^T \in \mathbb{C}^{MLN}$, where $\mathrm{h}_{MK} \in \mathbb{C}^{LN}$ is the channel matrix between AP M and UE K, with L and N denoting the number of antennas at the AP and UE, respectively. The mean of the collective channel estimate for

UE K is denoted as $\bar{\mathrm{h}}_k = \left[\bar{\mathrm{h}}_{1k}^T e^{j\varphi_{1k}}, \cdots, \bar{\mathrm{h}}_{Mk}^T e^{j\varphi_{Mk}}\right]^T$, where φ_{Mk} represents the phase shift in the LoS component of the wireless channel. The full covariance matrix of the collective channel estimate for UE K is denoted as $\mathrm{R}_k = \mathrm{diag}(\mathrm{R}_{1k}, \cdots, \mathrm{R}_{Mk})$. For fully centralized implementation, it is assumed that φ_{Mk} is available at the CPU, so channel estimates can be obtained by PA-MMSE estimators at the CPU. The collective channel estimate for UE k can be constructed as $\hat{\mathrm{h}}_k = \left[\hat{\mathrm{h}}_{1k}^T, \cdots, \hat{\mathrm{h}}_{Mk}^T\right]^T$, where the conditional mean and covariance matrix of the channel estimate given φ_{Mk} is given by,

$$\mathbb{E}\left\{\hat{\mathrm{h}}_k \mid e^{j\varphi_k}\right\} = \bar{\mathrm{h}}_k \tag{3.11}$$

$$\mathrm{Cov}\left\{\hat{\mathrm{h}}_k \mid e^{j\varphi_k}\right\} = \tau_p \mathrm{R}_k \bar{\mathrm{F}}_k \Psi_k^{-1} \bar{\mathrm{F}}_k^H \mathrm{R}_k \tag{3.12}$$

Here, τ_p represents the pilot length, $\bar{\mathrm{F}}_k = \mathrm{diag}(\underbrace{\tilde{\mathrm{F}}_k, \cdots, \tilde{\mathrm{F}}_k}_{M})$is a diagonal matrix where $\bar{\mathrm{F}}_k$is the precoding matrix for UE K, and $\Psi_k^{-1} = \mathrm{diag}(\Psi_{1k}^{-1}, \cdots, \Psi_{Mk}^{-1})$is a diagonal matrix where Ψ_{MK} is the variance of the estimation error of h_{MK}. The received signal available at the CPU can be expressed as,

$$\underbrace{\begin{bmatrix} \mathrm{y}_1 \\ \vdots \\ \mathrm{y}_M \end{bmatrix}}_{=\mathrm{y}} = \sum_{k=1}^{\mathrm{K}} \underbrace{\begin{bmatrix} \mathrm{H}_{1k} \\ \vdots \\ \mathrm{H}_{MK} \end{bmatrix}}_{=\mathrm{H}_\mathrm{k}} \mathrm{F}_k \mathrm{x}_k + \underbrace{\begin{bmatrix} \mathrm{n}_1 \\ \vdots \\ \mathrm{n}_M \end{bmatrix}}_{=\mathrm{n}} \tag{3.13}$$

The received signal at the AP can be expressed in (3.13) and can be rewritten as,

$$\mathrm{y} = \sum_{k=1}^{K} \mathrm{H}_k \mathrm{F}_k \mathrm{x}_k + \mathrm{n} \tag{3.14}$$

To decode the data symbol vector x_k for UE k, an arbitrary receive combining matrix $\mathrm{V}_k \in \mathbb{C}^{LM \times N}$can be designed by the CPU based on the collective channel estimates. The receive combining matrix V_k is a complex matrix of size LM x N, where LM is the number of antennas at the AP and N is the number of antennas at the UE k. The decoded signal x_k obtained as,

$$\hat{\mathrm{x}}_k = \mathrm{V}_k^H \mathrm{H}_k \mathrm{F}_k \mathrm{x}_k + \sum_{l \neq k}^{K} \mathrm{V}_k^H \mathrm{H}_l \mathrm{F}_l \mathrm{x}_l + \mathrm{V}_k^H \mathrm{n} \tag{3.15}$$

Based on $\hat{\mathrm{x}}_k$, it is possible to derive the achievable SE for UE k in a CF M-MIMO system using standard capacity lower bounds (Li et al., 2010). The feasible SE for UE k using the PA-MMSE estimator is given by equation (3.8) for the fully centralized processing with a given combining vector V_k defined in equation (3.10) for MMSE combining.

$$\mathrm{SE}_k^{(1)} = \left(1 - \frac{\tau_p}{\tau_c}\right) \mathbb{E}\left\{\log_2 \left|\mathrm{I}_N + \mathrm{D}_{k,(1)}^H \Sigma_{k,(1)}^{-1} \mathrm{D}_{k,(1)}\right|\right\} \tag{3.16}$$

Where, $\mathrm{D}_{k,(1)} \triangleq \mathrm{V}_k^H \hat{\mathrm{H}}_k \mathrm{F}_k$

$\Sigma_{k,(1)} \triangleq \mathrm{V}_k^H\left(\sum_{l=1}^{K} \hat{\mathrm{H}}_l \hat{\mathrm{F}}_l \hat{\mathrm{H}}_l^H + \sum_{l=1}^{K} \mathrm{C}_l' + \sigma^2 \mathrm{I}_{ML}\right)\mathrm{V}_k - \mathrm{D}_{k,(1)}\mathrm{D}_{k,(1)}^H$,

$\hat{\mathrm{F}}_l = \mathrm{F}_l \mathrm{F}_l^H$ and $\mathrm{C}_l' = \mathrm{diag}(\mathrm{C}_{1l}', \cdots, \mathrm{C}_{Ml}')$ and the (i,j)-th element of C_{ml}',

$[\mathrm{C}_{ml}']_{ij} = \sum_a^N \sum_b^N [\hat{\mathrm{F}}_l]_{ba} [\mathrm{C}_{ml}^{ba}]_{ij}$,defined on (Wang et al., 2022) collolary 1.

The MMSE combining stated in (3.10) can be further minimized as, $\mathrm{MSE}_k = \mathbb{E}\left\{\|\mathrm{x}_k - \mathrm{V}_k^H \mathrm{y}\|^2 \mid \hat{\mathrm{H}}_k\right\}$ and resulted in the maximization of SE defined in (3.16).

The maximized SE using the minimized MMSE combining can be evaluated as follows in (3.17).

$$\mathrm{SE}_k^{(1)} = \left(1 - \frac{\tau_p}{\tau_c}\right) \mathbb{E}\left\{\log_2 \left|\mathrm{I}_N + \left(\mathrm{D}_{k,(1)}'\right)^H \left(\Sigma_{k,(1)}'\right)^{-1} \mathrm{D}_{k,(1)}'\right|\right\} \tag{3.17}$$

Where, $\mathrm{D}_{k,(1)}' \triangleq \hat{\mathrm{H}}_k \mathrm{F}_k$, $\Sigma_{k,(1)}' \triangleq \sum_{l \neq k}^{K} \hat{\mathrm{H}}_l \hat{\mathrm{F}}_l \hat{\mathrm{H}}_l^H + \sum_{l=1}^{K} \mathrm{C}_l' + \sigma^2 \mathrm{I}_{ML}$.

3.6 Proposed Method

The performance and complexity of channel estimation algorithms are two key issues in CF M-MIMO systems. The proposed method takes the diagonal of the MMSE matrix i.e. element-wise the MMSE estimator and applies QR decomposition to it to find the matrix inversion, then applied it to the estimation process. Since the UE is multi-antenna equipment a precoding matrix is used at the user side to manage the interference. The estimator is phase-aware because it takes into consideration the received signal's phase information, which is crucial for correctly predicting the channel in a system with many antennas. The estimator estimates the medium coefficients for every element of the channel separately, making it element-wise as well. The received signal's phase information is taken into account during the estimating process in the phase-aware version of the estimator, which might increase the channel estimation's precision. EW-MMSE is a computationally effective method that calculates the channel coefficients of each antenna individually while taking the correlation between several antennas into account. The MMSE estimator may be more successful in capturing this correlation in CF M-MIMO with multi-antenna user equipment since the channel may be highly correlated across antennas. On the other hand, element-wise MMSE may perform better if the channel correlation is minimal by making use of the antennas' independence. The channel estimator for element-wise estimator $\hat{\mathrm{h}}_{mk}^{ew}$ is defined by,

$$\hat{\mathrm{h}}_{mk}^{ew} = \mathrm{vec}\left(\hat{\mathrm{H}}_{mk}\right) = \bar{\mathrm{h}}_{mk} e^{j\varphi_{mk}} + \mathrm{R}_{mk} \tilde{\mathrm{F}}_k \Psi_{mk}^{-1} \mathrm{vec}\left(\mathrm{Y}_{mk}^p\right) \tag{3.18}$$

Where, R_{mk} and Ψ_{mk}^{-1} are diagonal matrices defined in (3.4) and (3.8), respectively.

3.6.1 Precoding matrix

To improve the SE performance, the UL precoding can be implemented at the UE side in the scenario with multi-antenna UEs. Inspired by (Li et al., 2010), for CF M-MIMO, the UL precoding scheme can be based on the correlation feature $\mathrm{U}_{mk,\mathrm{t}}$ at the UE side as,

$$\mathrm{F}_k = \sqrt{p_k}\left\|\sum_{m=1}^{M} \mathrm{U}_{mk,\mathrm{t}}\right\|_{\mathrm{F}}^{-1}\left(\sum_{m=1}^{M} \mathrm{U}_{mk,\mathrm{t}}\right) \tag{3.19}$$

The correlation feature $\mathrm{U}_{mk,\mathrm{t}}$ represents the correlation between the channel vectors at the UE side and can be used to design efficient precoding schemes that take advantage of the spatial diversity of the wireless channel.

The flowchart shows the EW MMSE with QR decomposition and precoding matrix at the UE side channel estimation process in a CF M-MIMO system. This flowchart outlines the EW-MMSE channel estimation process in a CF M-MIMO system with multi-antenna UE under rician fading channel conditions. It includes the steps of transmitting pilot signals, receiving and measuring pilot signals, initializing the channel estimation variables, performing QR decomposition on the channel matrix, computing the precoding matrix at the UE side, calculating MMSE weights, performing channel estimation for each element in the channel estimate matrix, and finally sending the estimated channel coefficients back to the central processor.

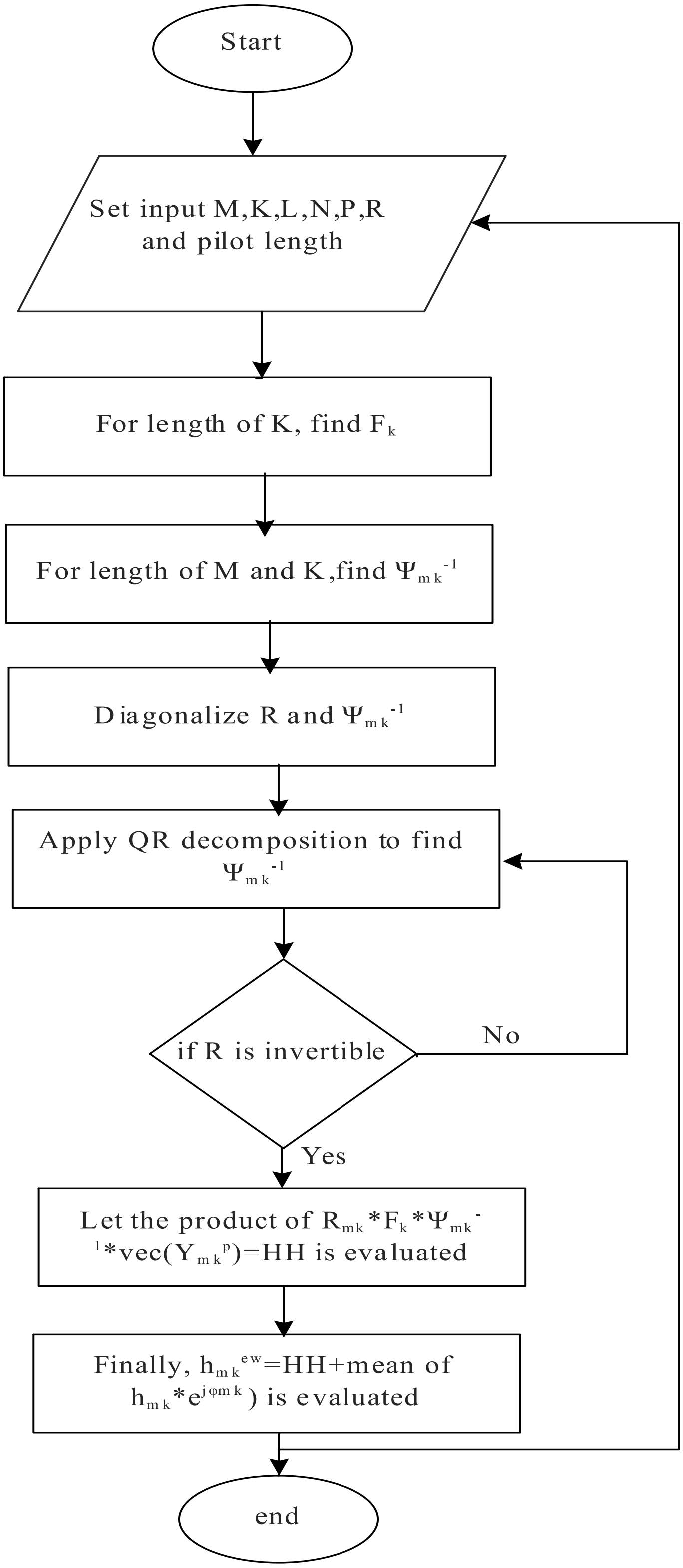

Figure 3.4: Flow chart of the proposed channel estimator based on elementwise MMSE and QR decomposition with precoding matrix at UE side.

3.6.2 Computational complexity

To achieve great SE and trustworthy communication in CF M-MIMO, channel estimation is essential. The MMSE channel estimator offers the best estimate of the channel by reducing the mean square error (MSE) between the estimated and the genuine medium. It necessitates estimating the channel covariance matrix, which entails estimating the channel's second-order statistics (Amadid, Belhabib, Khabba, et al., 2022). Channel covariance matrix estimation and matrix multiplications are the two main computational processes involved in the MMSE channel estimator. Matrix inversions, which have a computational complexity of $O(N^3)$, are often needed for channel covariance matrix estimation. The MMSE estimator requires many matrix multiplications, each of which has an $O(N^3)$ complexity for square matrices. The EW-MMSE channel estimator makes the uncorrelated assumption that the channels between various antennas and users do not exist. Rather than calculating the entire channel covariance matrix, it individually calculates each channel coefficient. Compared to the MMSE estimator, this simplification lessens the computational complexity. EW-MMSE is a computationally effective method that calculates the channel coefficients of each antenna individually while taking the correlation between several antennas into account. The MMSE estimator may be more successful in capturing this correlation in CF M-MIMO with multi-antenna user equipment since the channel may be highly correlated across antennas. However, if the channel correlation is minimal, EW-MMSE may perform better by making use of the antennas' independence.

$$\mathrm{CC}_{\mathrm{MMSE}} = \left(\mathrm{L} * \tau_p + \mathrm{L}^2\right) * \mathrm{M} * \mathrm{K} * \mathrm{N} \tag{3.20}$$

$$\mathrm{CC}_{\mathrm{EW-MMSE}} = \left(\mathrm{L} * \tau_p + \mathrm{L}\right) * \mathrm{M} * \mathrm{K} * \mathrm{N} \tag{3.21}$$

Where, $\mathrm{CC}_{\mathrm{MMSE}}$ and $\mathrm{CC}_{\mathrm{EW-MMSE}}$ are the computational complexity of MMSE and EW-MMSE channel estimator, M, L, K, and N defined in 3.4 and τ_p in (3.1)

3.7 Performance Metrix of the System

3.7.1 Area throughput

The data transmission rate per square meter in a wireless network is known as area throughput. Ordinarily, it is expressed in bits per second per square meter (bps/m^2). It serves as a gauge for how many users a network can accommodate at once in a specific location.

$$\mathrm{Throughput} = \mathrm{B} * \mathrm{SE} * \mathrm{D} \tag{3.22}$$

Where, SE is the amount of data that can be sent per unit of the spectrum, measured in bits per second per Hertz (bps/Hz) which is evaluated by in (3.16), B is the total amount of spectrum available for transmission, measured in Hertz (Hz) and D is the number of APs deployed per unit area, measured in number of APs per square meter (APs/m^2).

3.7.2 Energy efficiency

EE is the capacity of the system to send and receive wireless signals at high data rates while consuming the least amount of energy possible. EE is a crucial factor to take into account when designing wireless communication systems, particularly in the case of M-MIMO, which deploys a lot of antennas to serve several user devices. It can be evaluated as,

$$EE = B * SE / P \tag{3.23}$$

Where, EE energy efficiency (bit/joule), B bandwidth of the system, SE spectral efficiency (bit/s/Hz), and P power required to transmit the signal (W). The EE is evaluated from the SE discussed in equation (3.16).

3.7.3 Spectral efficiency

The amount of data that can be conveyed per spectrum unit, or Hz of bandwidth, is known as SE. It quantifies the system's ability to utilize the available frequency spectrum efficiently to carry data. It is typically expressed in bits per second per hertz (bps/Hz). It can be evaluated as in equation (3.16).

CHAPTER FOUR

4. RESULT AND DISCUSSION

This section describes the simulation outcomes for achieving the study's specific goal. The simulation results and discussions on how the proposed channel estimator performs in comparison to the current estimate for the CF M-MIMO UL system based on the SE, EE, and area throughput parameters under the Weichselberger rician fading channel are provided. Additionally, a comparison of the proposed estimator's complexity with an existing estimator based on the number complex of multiplications is provided. The table below is a list of the simulation parameters that are used in this thesis to compare the proposed channel estimator's performance and complexity to the previous work channel estimator for a CF M-MIMO UL system.

Table 4.1: Simulation parameter

No.	Simulation parameter	Type and value
1	Pilot reuse factor (w)	1,2,5
2	Uplink transmitter power(p)	200mW
3	Number of access points (M)	10,20,40,80, and for computational complexity 20 to 200
4	Number of antennae per UE (N)	1,2,3,4,5,6 and for computational complexity 1 to 10
5	Number of antennae per APs (L)	2,4,9, and for computational complexity 10 to 90
6	Number of user equipment (K)	8,10,15,20 and for computational complexity 10 to 100
7	Coherence block	200 to 800
8	Bandwidth (B)	1MHz
9	Coverage area	1km by 1km

4.1 Spectral Efficiency Comparison

To simulate the system's performance, the transmission channel is modeled as a Weichselberger rician fading channel, the noise is additive Gaussian white noise i.e. IID, and the UL combining scheme is set to MMSE combiner. The number of antenna per UE is set from 1 to 6 and the number of access points is set to 10, 20, 40, and 80. The UL transmitter power is set to 200mW and the pilot reuse factor is set to one for none reuse pilots whereas set to 2 or 5 when considering pilot reuse. The outcome of the simulation is used to compare the effectiveness of the proposed channel estimator with that of the recently introduced CF M-MIMO UL channel estimator. The performance is discussed in terms of SE versus the number of antenna per user of the equipment and SE versus the number of AP. MATLAB software is used to generate simulation results.

The pilot length can be evaluated by $\tau_p = \frac{\mathrm{K} * \mathrm{N}}{\mathrm{w}}$, where w is the reuse factor.

4.1.1 The effect of number of users and antennas per access point on spectral efficiency

The simulation findings and feedback concentrate on the impact of the number of users and antennae per AP on spectral efficiency by maintaining the coherence time and pilot reuse factor, τ_c=200, and w=1. The results demonstrate the performance in various aspects such as SE to the number of antenna used by each user of the equipment and SE to the number of AP.

Figure 4.1 depicts the UL SE for the fully centralized processing with the number of antennae per user equipment (N) and the MMSE combining at different numbers of access points (M). It shows the comparison of the proposed estimator with the phase-aware MMSE estimator. The proposed method outperforms the existing one as the number of antenna per user of equipment increases. For the smaller number of antenna per user equipment, the proposed estimator and the existing estimator have a closer performance. For example, when M=10 and N=1, the average UL SE achieved by the proposed estimator 12.66bit/s/Hz which is the same as UL SE achieved by the existing method. This shows the proposed method is not effective for single antenna UE and a smaller number of AP. When N increased to 2 for the same value of M=10, the average UL SE attained by existing and proposed estimators is 20.38bit/s/Hz and 21bit/s/Hz, respectively that is the performance enhanced by 3% compared to the existing estimator. When N=6 and M=80, the average UL SE achieved by the proposed and existing estimator are 54.17bit/s/Hz and 49.8bit/s/Hz, respectively, that is the proposed estimator outperforms by 8.777%. The performance of the UL SE is enhanced as M increases by allowing each UE to have more antenna. Furthermore, the computational complexity required to optimize the system is tolerable since the UEs in actual networks typically have a few antenna. The pilot length can be $\tau_p = \frac{\mathrm{K} * \mathrm{N}}{\mathrm{w}}$, for N=6, K=8, and w=1, then the pilot length becomes 48. The pilot reuse factor, w=1 shows for every user we assign a unique pilot sequence i.e., no pilot reuse which is practically impossible due to a constrained quantity of pilot resources.

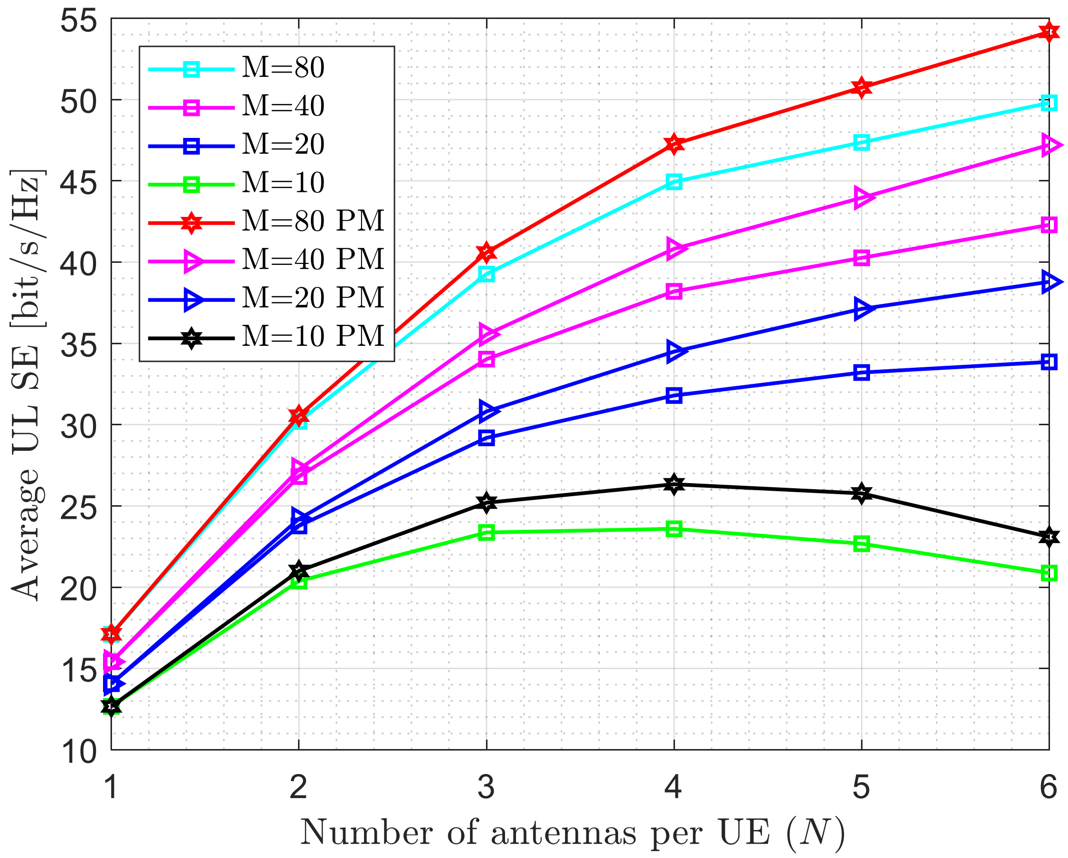

Figure 4.1: The spectral efficiency versus the number of antennas per UE for the fully centralized processing with the MMSE combiner at K = 8, L = 4, τ_c =200, and w=1.

The comparison of the proposed estimator's performance with the existing estimator is presented in Table 4.2 for various values of M and N. As we observed from the table the performance of the proposed estimator is better than that of the existing one. The maximum average UL SE achieved by the proposed estimator is 54.17 bits/s/Hz. This value is obtained when N=6 and M=80. The table also shows the average UL SE achieved by the proposed and existing nearly the same performance for single antenna UE. The table below indicates the tabular form of Figure 4.1 by considering some value of N.

Table 4. 2: The spectral efficiency versus the number of antennas per UE for the fully centralized processing with the MMSE combiner at K = 8, L = 4, τ_c =200, and w=1.

Average UL SE (bit/s/Hz)					Average UL SE (bit/s/Hz) for the proposed estimator			
No. antenna per UE (N)	M=10	M=20	M=40	M=80	M=10	M=20	M=40	M=80
1	12.66	14.06	15.41	17.1	12.66	14.06	15.41	17.1
2	20.38	24.2	27.24	30.55	21	24.2	27.24	30.55
3	23.37	29.19	34.03	39.27	23.2	30.81	35.55	40.59
4	23.59	31.79	38.2	44.94	26.33	34.49	40.82	47.26
5	22.68	33.21	40.26	47.37	25.77	37.12	43.96	50.74
6	20.87	33.86	42.29	49.8	23.09	38.79	47.21	54.17

Figure 4.2 demonstrates the comparison of the proposed estimator with the existing estimator when the number of UE increase from K= 8 to K= 10. As the number of user equipment increased the performance for both the proposed and existing estimator decreased compared to Figure 4.1. For instance, for N=3 and M =40, the average UL SE for the existing estimator decreased 34.03bit/s/Hz to 31.72bit/s/Hz, as the K increased from 8 to 10. Similarly, the average UL SE for the proposed estimator decreased 35.55bit/s/Hz to 33.09bit/s/Hz, as the K increased from 8 to 10. For M=10, the average UL SE raised to N=3 and then diminished as N increased. This is due to the number of AP being low compared to another number of AP so that the chance of interference happens between the user antenna and the access point antenna is high. But, still, the proposed estimator has better performance than the existing estimator. The proposed estimator obtained the average UL SE= 49.1bit/s/Hz at N=5 and M=80, whereas the MMSE estimator reached the average UL SE= 42.72bit/s/Hz i.e., the proposed outperformed by 14.93%. The pilot length becomes τ_p =60 i.e. the pilot length increases as the number of users increases.

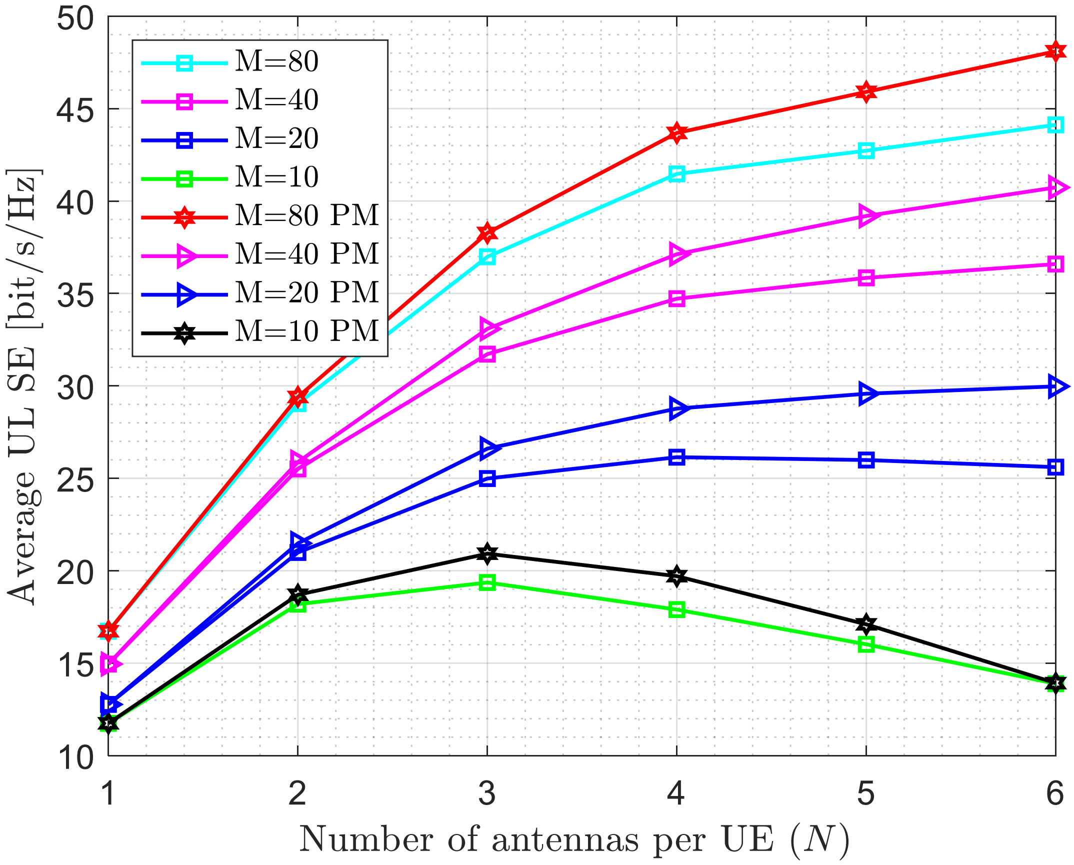

Figure 4.2: The spectral efficiency versus the number of antennas per UE for the fully centralized processing with the MMSE combiner at K = 10, L = 4, τ_c =200, and w=1.

Table 4.3: The spectral efficiency versus the number of antennas per UE for the fully centralized processing with the MMSE combiner at K = 10, L = 4, τ_c =200, and w=1.

Average UL SE (bit/s/Hz)					Average UL SE (bit/s/Hz) for proposed			
No. antenna per UE (N)	M=10	M=20	M=40	M=80	M=10	M=20	M=40	M=80
1	11.5	12.77	14.95	16.73	11.75	12.77	14.95	16.73
2	18.19	21.48	25.88	29.4	18.7	21.48	25.88	29.4
3	19.36	24.99	31.72	36.98	20.92	26.61	33.09	38.27
4	17.9	26.14	34.72	41.47	19.71	28.77	37.12	43.68
5	16.02	25.99	35.84	42.72	17.1	29.58	39.19	45.9
6	13.92	25.6	36.59	44.12	13.92	29.97	40.74	48.1

In Figure 4.3, the proposed estimator is compared to the current estimate when the number of antennae per AP increases from L=4 to L=9. Performance for both the proposed and existing estimators increased as the antenna per AP rose. As the L grows from 4 to 9, the average UL SE for the current estimator for N=6 and M=80 is enhanced from 44.12bit/s/Hz to 49.1bit/s/Hz. Similar to this, the average UL SE for the proposed estimator rose from 48.1bit/s/Hz to 53.23bit/s/Hz when the L raised from 4 to 9. As the number of antennae per AP increased the average UL SE also enhanced and the proposed estimator outperforms the current estimator. The maximum average UL SE achieved by the proposed estimator is 53.23bit/s/Hz and obtained at N=6 and M=80. The proposed estimator obtained the average UL SE= 50.34bit/s/Hz at N=5 and M=80, whereas the MMSE estimator reached the average UL SE= 47.15bit/s/Hz i.e. the proposed outperformed by 6.766%. The pilot length not changing i.e. τ_p =60 because the user keeps the same as the previous value.

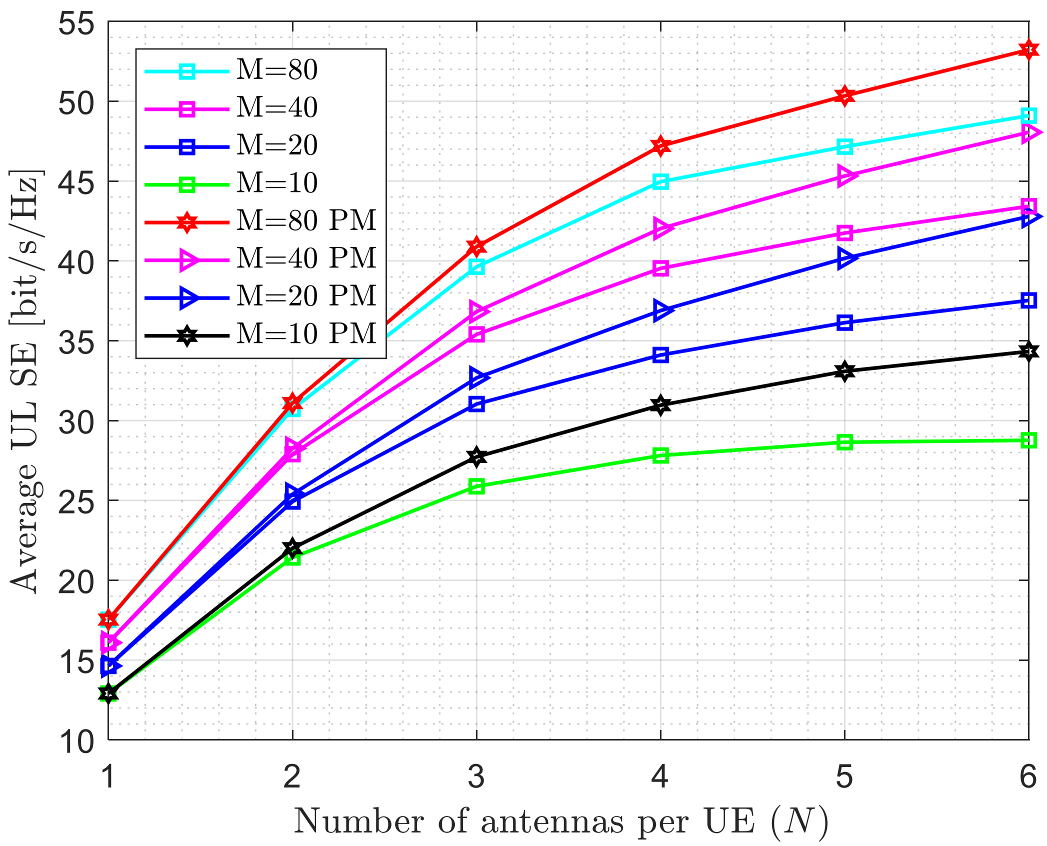

Figure 4.3: The spectral efficiency versus the number of antennas per UE for the fully centralized processing with the MMSE combiner at K = 10, L = 9, τ_c =200, and w=1.

Figure 4.4 shows the effect of both the number of users and the number of antennae per AP on average UL SE, as both parameters increase. The proposed estimator obtained the average UL SE= 42.81bit/s/Hz at N=6 and M=80, whereas the MMSE estimator reached the average UL SE= 39.38bit/s/Hz i.e., the proposed outperformed by 8.71%. The pilot length τ_p =90, due to the increment in the number of users.

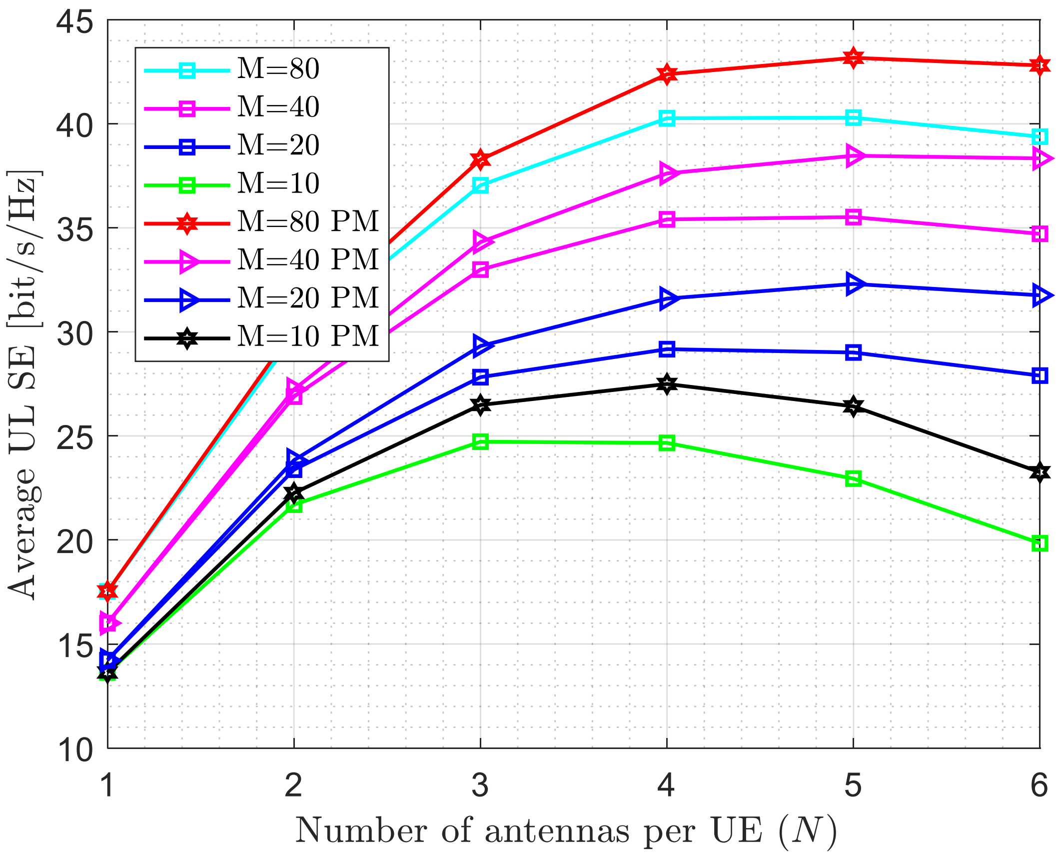

Figure 4.4: The spectral efficiency versus the number of antennas per UE for the fully centralized processing with the MMSE combiner at K = 15, L = 9, τ_c =200, and w=1.

Figure 4.5 shows the average UL SE as a function of AP with different numbers of the antenna of UE. As the number of AP and number of antenna per UE increased the average UL SE is increased for both proposed and current estimators. The proposed estimator enhanced the average UL SE when the number of AP increased. For N=1 i.e. single antenna UE, initially, the average UL SE is increased up to M=20 for both the proposed and current estimator. This is due to with more APs, the available resources and spatial diversity increase, which allows for better signal quality and potentially higher data rates. As the AP increases beyond M=20, the average UL SE is diminished for both the proposed and existing method. This is due to several factors, with more APs, the probability of pilot contamination also increases, the potential for inter-AP interference rises, and with a single-antenna UE, there is a limit to the number of spatial degrees of freedom that can be exploited. Adding more APs beyond a certain point may not significantly increase the spatial diversity gain and, therefore, the spectral efficiency. The maximum average UL SE achieved by the proposed and existing method at N=4 is 44.91bit/s/Hz and 42.73bit/s/Hz respectively i.e., the proposed method outperforms by 5.1% that of the existing estimator. For the low number of AP, the performance of the proposed estimator and existing estimator are almost similar. The pilot length τ_p is 40 since the K=10, N=4, and w=1.

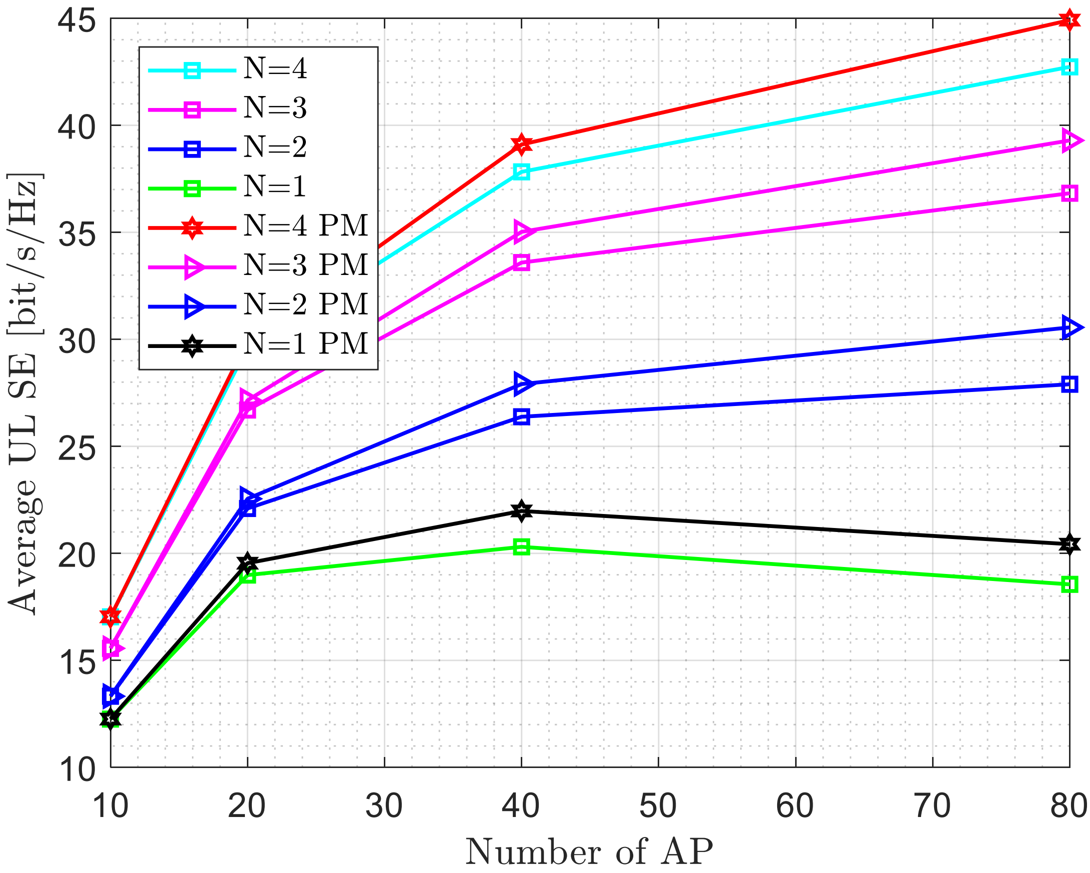

Figure 4.5: The spectral efficiency versus the number of access points for the fully centralized processing with the MMSE combiner at K = 10, L = 4 τ_c=200, and w=1.

Table 4.4: The spectral efficiency versus the number of access points for the fully centralized processing with the MMSE combiner at K = 10, L = 4, τ_c =200, and w=1.

Average UL SE (bit/s/Hz)					Average UL SE (bit/s/Hz) for proposed			
No. AP(M)	N=1	N=2	N=3	N=4	N=1	N=2	N=3	N=4
10	12.26	13.32	15.56	17.04	12.26	13.32	15.56	17.04
20	19.54	22.1	27.15		19.54	27.15	27.15	
40	20.3	26.38	33.59	37.82	21.98	21.98	35.02	39.1
80	18.55	27.9	36.82	42.73	20.43	20.43	39.29	44.91

Figure 4.6 shows the comparison of average UL SE for completely centralized processing as a function of the number of AP (M), with the MMSE combining over varied numbers of a number of antennae per user equipment (N). When the number of users increases to K=20, the maximum average UL SE achieved by the proposed method is 30.14bit/s/Hz. For the single antenna user especially, the performance is diminished highly from 10.26bit/s/Hz to 4.408bit/s/Hz for the existing estimator and 15.07bit/s/Hz to 30.14bit/s/Hz for the proposed estimator. This shows the proposed estimator is not effective for the single antenna user equipment for a large number of users. The proposed estimator obtained the average UL SE= 30.14bit/s/Hz at N=4 and M=80, whereas the MMSE estimator reached the average UL SE= 28.55bit/s/Hz i.e., the proposed outperformed by 5.57%. The pilot length is 80 since K=20 and N=4.

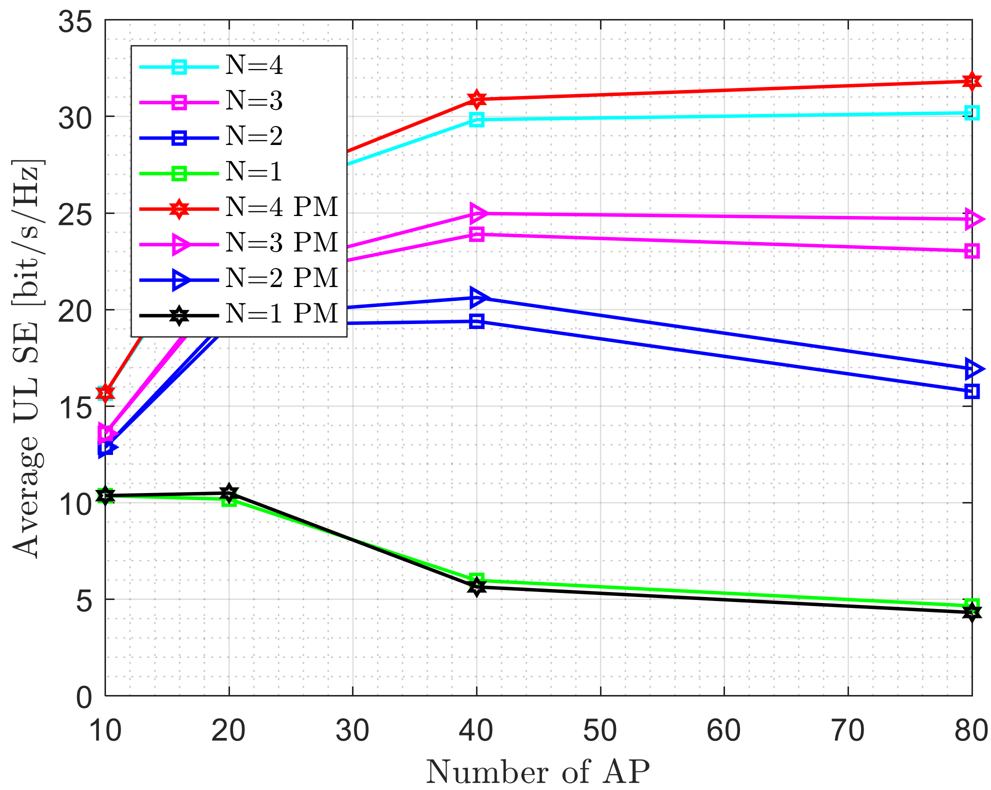

Figure 4.6: The spectral efficiency versus the number of access points for the fully centralized processing with the MMSE combiner at K = 20, L = 4, τ_c =200, and w=1.

Figure 4.7 describes the effect of the number of antennae per AP on the average UL SE when increased from L=4 to L=9. As the number of antennae per AP increases, the average UL SE is increased. This is because as the number of antennae per AP increases, spatial processing, spatial diversity, interference management, and channel estimate accuracy all improve. The proposed estimator obtained the average UL SE= 48.11bit/s/Hz at N=4 and M=80, whereas the MMSE estimator reached the average UL SE= 45.79bit/s/Hz i.e., the proposed outperformed by 5.1%. The pilot length is 40 since K=10 and N=4. The average UL SE is achieved by the proposed and existing estimator for single antenna UE at M=80, N=4 is 31.62bit/s/Hz and 28.4bit/s/Hz, respectively. The pilot length is 40 since K=10, N=4, and w=1.

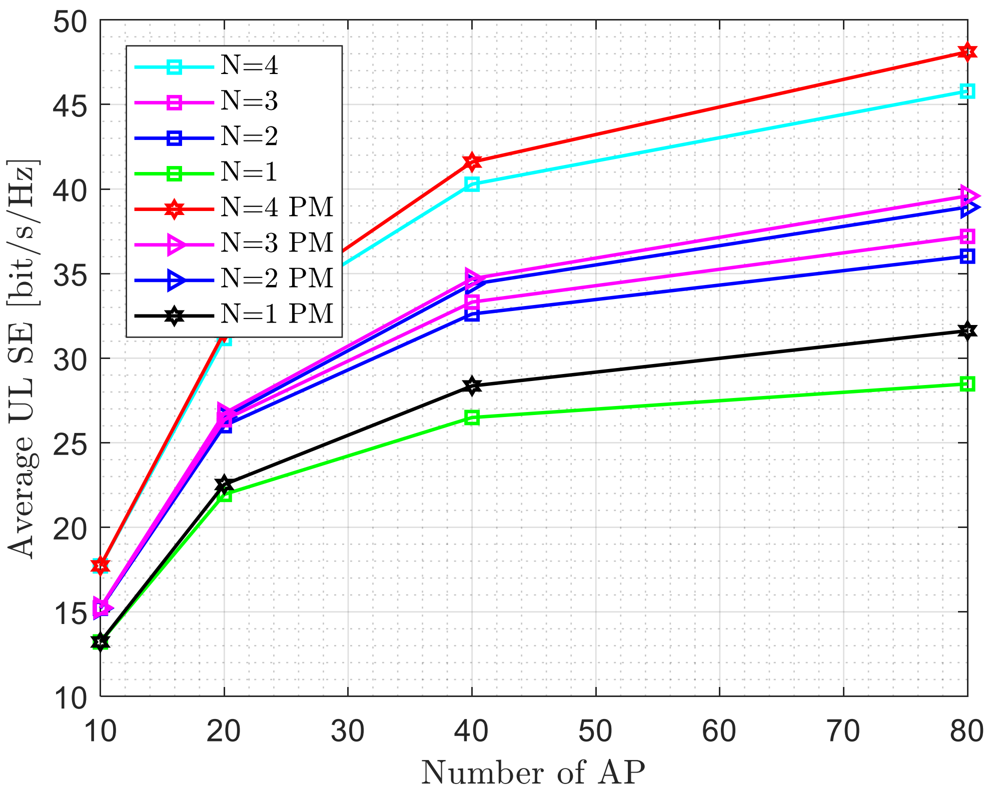

Figure 4.7: The spectral efficiency versus the number of access points for the fully centralized processing with the MMSE combiner at K = 10, L = 9, τ_c =200, and w=1.

4.1.2 The effect of coherence time and pilot reuse factor on spectral efficiency

The simulation findings concentrate on the impact of the coherence time and pilot reuse factor on spectral efficiency by maintaining the number of users and number of antennae per AP, K=10, and L=4, respectively. Performance is shown in terms of spectral efficiency with the number of antennae used by each user of the equipment and spectral efficiency with the number of AP.

The effect of coherence time on the SE is demonstrated in Figure 4.8. As the coherence time increases, so does the average UL SE. The longer coherence time allows for better utilization of temporal correlation which is leading to increased diversity gain. The proposed estimator obtained the average UL SE= 58.41bit/s/Hz at N=6 and M=80, whereas the MMSE estimator reached the average UL SE= 53.82bit/s/Hz i.e., the proposed outperformed by 8.53%. And also, the proposed estimator obtained the average UL SE= 15.12bit/s/Hz at N=6 and M=10. The pilot length is 60 since K=10, N=6, and w=1.

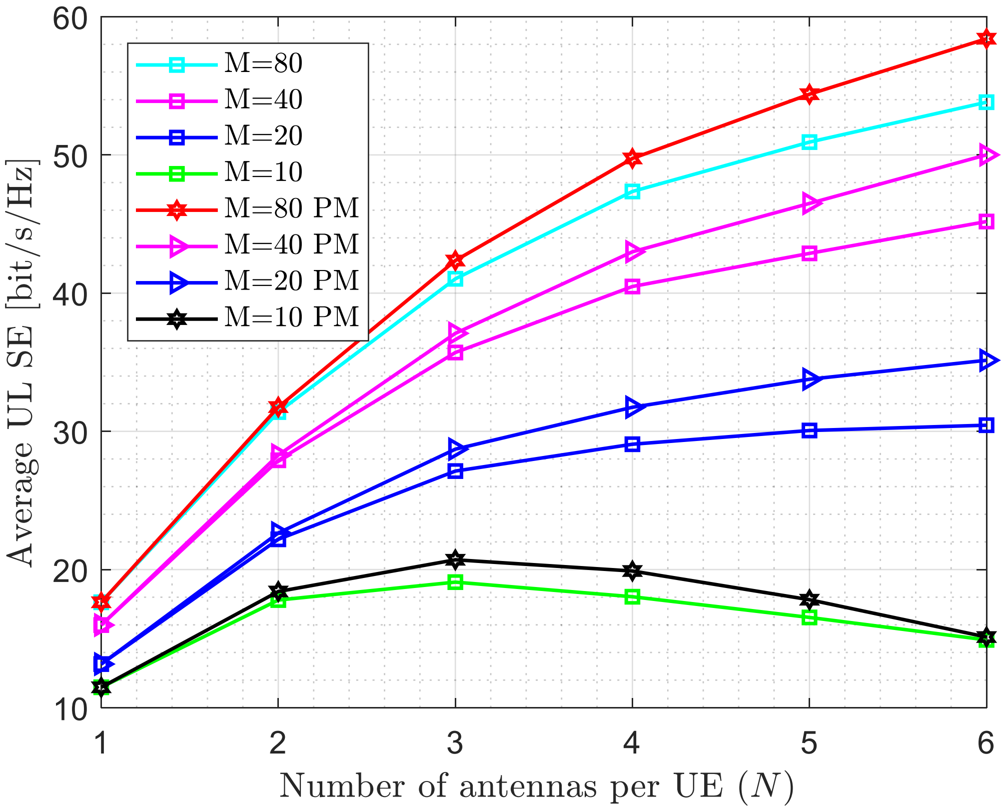

Figure 4.8: The spectral efficiency versus the number of antennas per UE for the fully centralized processing with the MMSE combiner at K = 10, L = 4, τ_c =300, and w=1.

Figure 4.9 emphasizes the impact of the pilot reuse factor on the SE for different numbers of AP varied across the number of antennae per UE. The proposed estimator obtained the average UL SE= 17.268bit/s/Hz at N=6 and M=80, whereas the MMSE estimator reached the average UL SE= 15.894bit/s/Hz i.e., the proposed outperformed by 8.53%. The increment of the pilot reuses factor results in a decrease in average UL SE. The proposed estimator has better performance as compared to the existing estimator when the number of antennae per UE for different numbers of AP. The pilot length is 30 since w=2, K=1=and N=6. The pilot length is decreased due to the pilot reuse factor i.e., as the pilot reuse factor increases the pilot length decreases. The maximum average UL SE achieved for the proposed method is 18.228bit/s/Hz at N=4 and M=80, whereas for the existing one is 17.69bit/s/Hz.

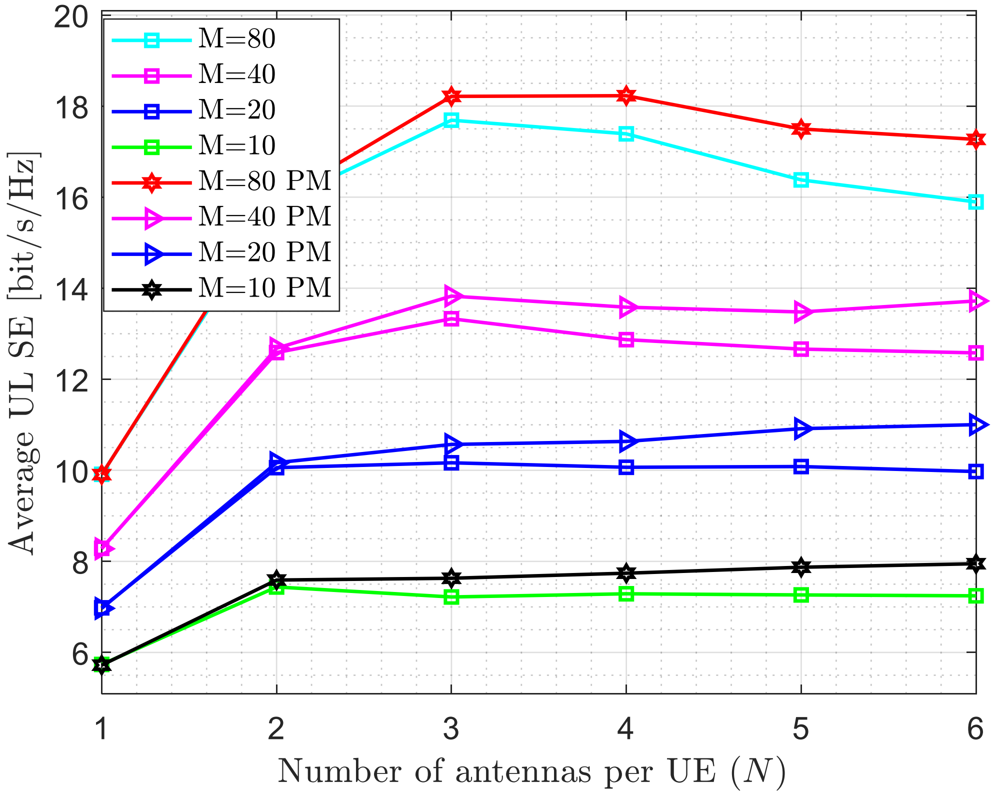

Figure 4.9: The spectral efficiency versus the number of antennas per UE for the fully centralized processing with the MMSE combiner at K = 10, L = 4, τ_c =200, and w=2.

Figure 4.10 depicts the impact of the pilot reuse factor on the SE for different numbers of AP varied across the number of antennae per UE as the pilot reuse factor increases to 5. The proposed estimator obtained the average UL SE= 11.9bit/s/Hz at N=6 and M=80, whereas the MMSE estimator reached the average UL SE= 11.54bit/s/Hz i.e., the proposed outperformed by 3.11%. The increment of the pilot reuses factor results in a decrease in average UL SE. The proposed estimator has better performance as compared to the existing estimator when the number of antennae per UE is increased for different numbers of AP. The pilot length is 12 since w=5, K=10, and N=6. The pilot length is decrease more when compared to pilot reuse 2 by keeping another parameter the same i.e., the pilot reuse factor and pilot length are inversely proportional. The maximum average UL SE achieved for the proposed method is 14.342bit/s/Hz at N=3 and M =80, whereas for the existing one is 14.055bit/s/Hz at N=3 and M =80.

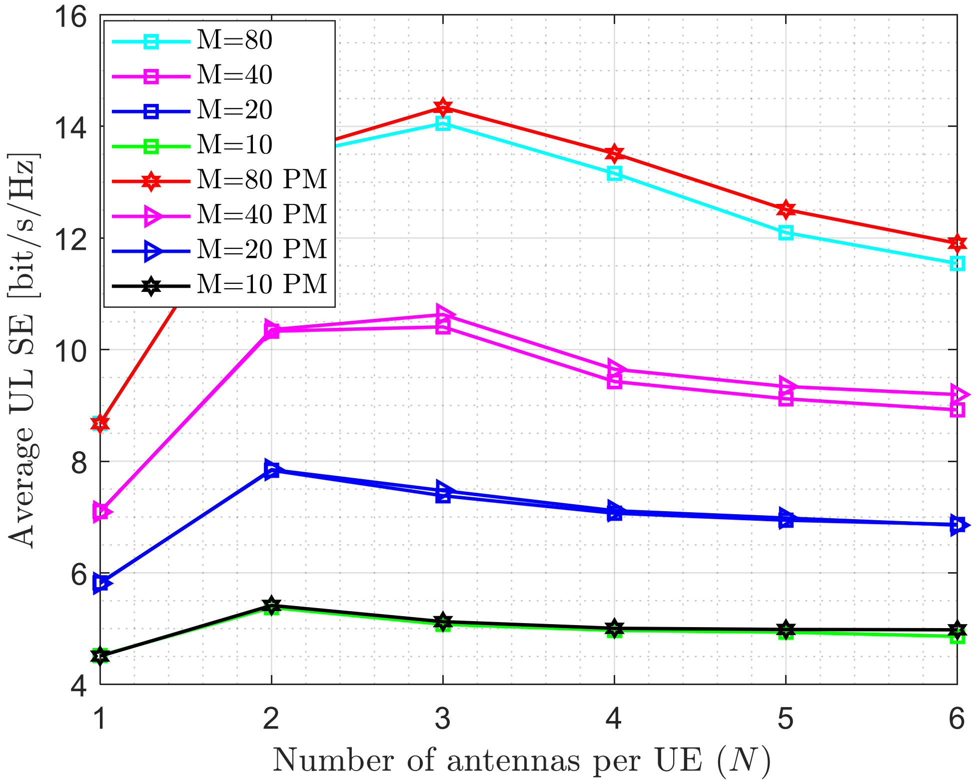

Figure 4.10: The spectral efficiency versus the number of antennas per UE for the fully centralized processing with the MMSE combiner at K = 10, L = 4, τ_c=200, and w=5.

Figure 4.11 illustrates the average UL SE versus AP with different N and τ_c=300. The average UL SE is increased when the coherence time increase from τ_c=200 to τ_c=300. For single antenna UE (N), the average UL SE is not enhanced more compared to other values of N. This is due to the ability to exploit spatial diversity or multiplexing gains being inherently limited in single antenna UE. The maximum average UL SE achieved for the current and proposed estimator are 18.26bit/s/Hz and 20.11bit/s/Hz at N=1 and M=80 respectively i.e., the proposed method enhances the UL SE by 9.2%. For the single antenna UE keeping other parameter constant and increasing τ_c leads to a reduction of average UL SE. The maximum average UL SE achieved for the current and proposed estimator at N=4 and M=80 is 46.43bit/s/Hz and 48.87bit/s/Hz respectively, the proposed outperform by 5.25%. The average UL SE for the proposed method at M=80, N=1 is 20.11bit/s/Hz, and M=80, N=4 is 48.87bit/s/Hz i.e., increased by 143%. This due to multiple antennas enables spatial multiplexing, beamforming, and diversity techniques that can be leveraged to increase the SE. The pilot length is 40 since the w=1, K=10, and N=4.

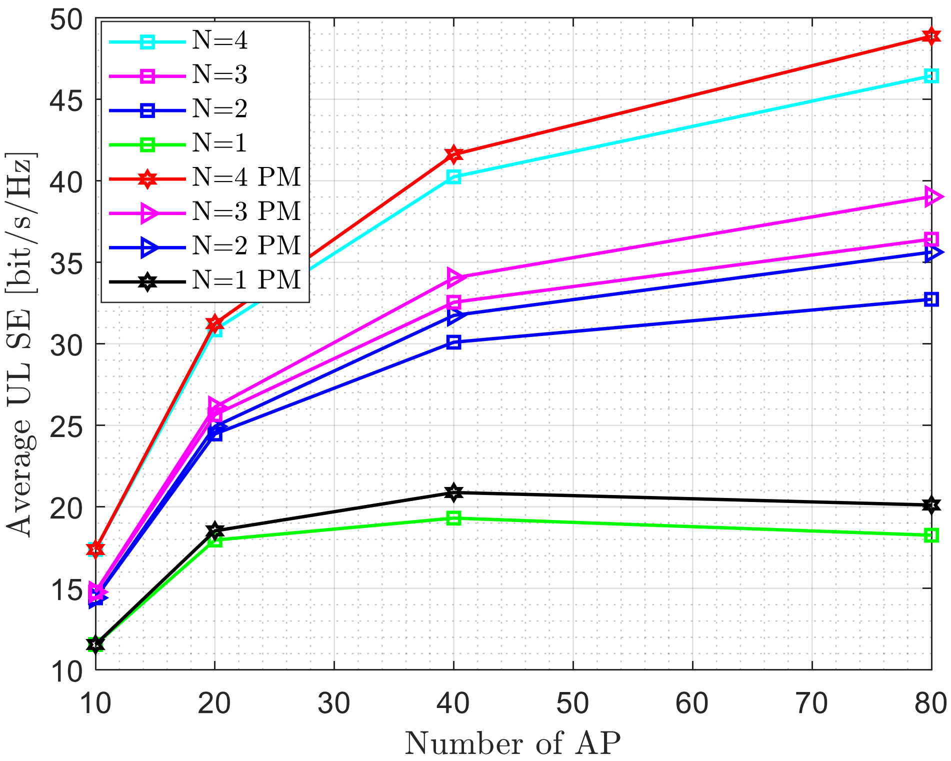

Figure 4.11: The spectral efficiency versus the number of access points for the fully centralized processing with the MMSE combiner at K = 10, L = 4, τ_c=300, and w=1.

Table 4.5: The spectral efficiency versus the number of access points for the fully centralized processing with the MMSE combiner at K = 10, L = 4, τ_c=300, and w=1.

Average UL SE (bit/s/Hz)					Average UL SE (bit/s/Hz) for proposed			
No. AP(M)	N=1	N=2	N=3	N=4	N=1	N=2	N=3	N=4
10	11.56	14.78	14.78	17.38	11.56	14.78	14.78	17.38
20	18.53	24.47	26.12	31.24	18.53	25.55	26.12	31.21
40	19.31	30.1	32.55	40.24	20.88	32.55	34.04	41.61
80	18.26	32.73	36.41	46.43	20.11	35.62	39.03	48.87

Figure 4.12 describes the impact of the pilot reuse factor on the SE for a different number of UE antenna varied across a number of AP as the pilot reuse factor increases to 2. The proposed estimator obtained the average UL SE= 17.87bit/s/Hz at N=4 and M=80, whereas the MMSE estimator reached the average UL SE= 16.977bit/s/Hz i.e., the proposed outperformed by 5.27%. The increment of the pilot reuses factor results in a decrease in average UL SE for both existing and proposed estimators. The proposed estimator has better

performance as compared to the existing estimator when the number of AP is increased for different numbers of UE. The pilot length is 20 since w=2, K=10=and N=6. The maximum average UL SE achieved for the proposed method is 17.88bit/s/Hz at N=4 and M =40, whereas for the existing one is 17.35bit/s/Hz at N=4 and M =80.

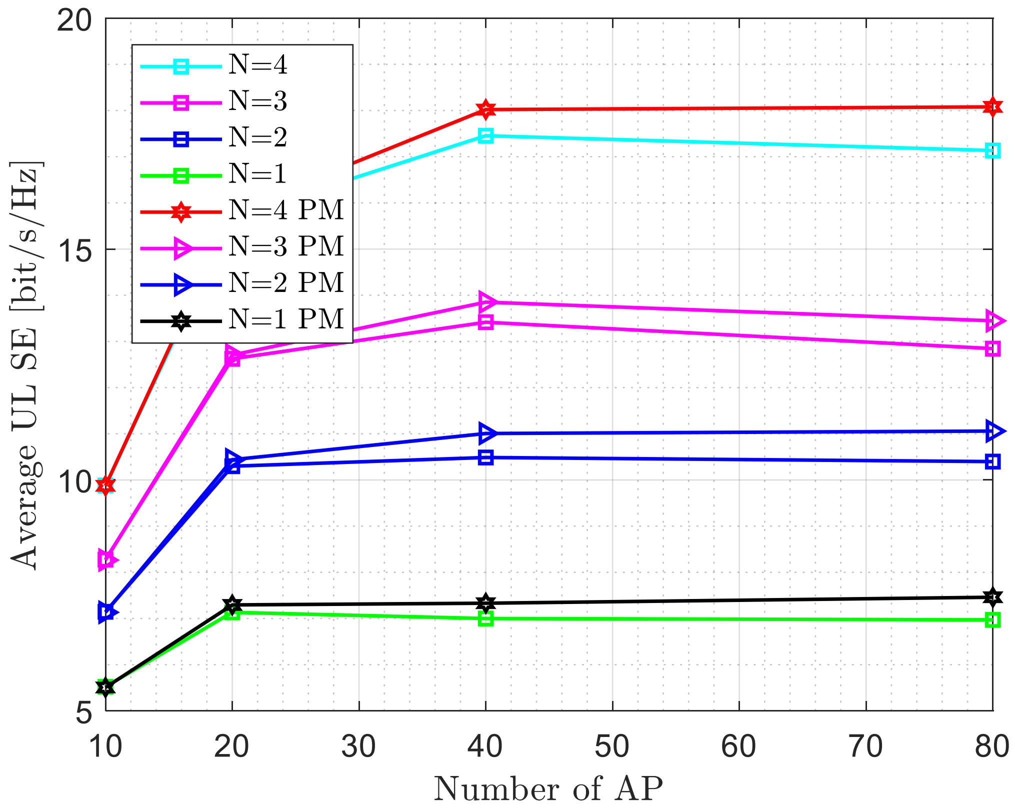

Figure 4.12: The spectral efficiency versus the number of access points for the fully centralized processing with the MMSE combiner at K = 10, L = 4, τ_c =200, and w=2.

The effect of the pilot reuse factor on the SE for different numbers of UE antenna varied over various numbers of AP is shown in Figure 4.1 as it approaches 5. The MMSE estimator reached the average UL SE= 10.628bit/s/Hz at N=4 and M=40, whereas the proposed estimator obtained the average UL SE= 10.867bit/s/Hz. As the pilot reuse factor increased the gap between the proposed and existing estimator narrows and decreased. When the number of AP is raised for various numbers of UE, the suggested estimate outperforms the present estimator in terms of performance. Since w=5, K=10, and N=6, the pilot length is 12. The maximum average UL SE at N=4 and M=80 is 14bit/s/Hz. As the number of antennae per UE increases the improvement gap between the proposed and existing estimator increases. For the small number of antennae per UE i.e., N=1 and N=2, the performance of the proposed and current estimators is almost the same.

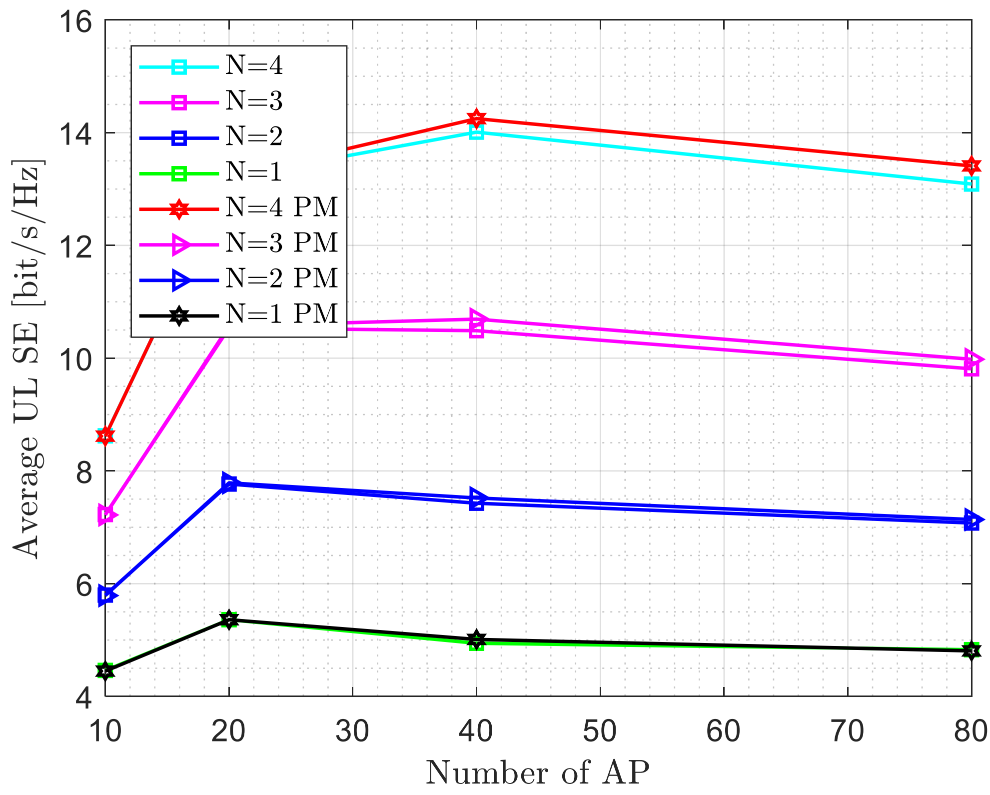

Figure 4.13: The spectral efficiency versus the number of access points for the fully centralized processing with the MMSE combiner at K = 10, L = 4, τ_c=200, and w=5.

4.2 Energy Efficiency Comparison

4.2.1 The effect of the number of users and antennas per user access point on energy efficiency

The simulation findings concentrate on the impact of the number of users and antennae per AP on energy efficiency by maintaining the coherence time and pilot reuse factor, τ_c=200, and w=1. Performance is shown in terms of energy efficiency with the number of antennae used by each user of the equipment and energy efficiency with the number of AP.

Figure 4.14 shows the comparison of the proposed estimator with the existing estimator using the parameter average UL EE with the number of antennae per UE. The simulation result implies as the number of antennae per UE increases the EE increases for a large value of the number of AP, whereas for a small value of M initially rises and then diminishes as N increases. The MMSE estimator reached the maximum of average UL EE= 214.2Mbit/joule at N=6 and M=80, whereas the proposed estimator obtained the average UL EE= 234.5Mbit/joule i.e. the proposed outperformed by 9.77% at this point. The maximum EE achieved by the proposed estimator for M=10 is at N=3 which is

122.8Mbit/joule, whereas for the existing estimator is 114.3Mbit/joule. The pilot length is 60 since w=1, N=6, and K=10.

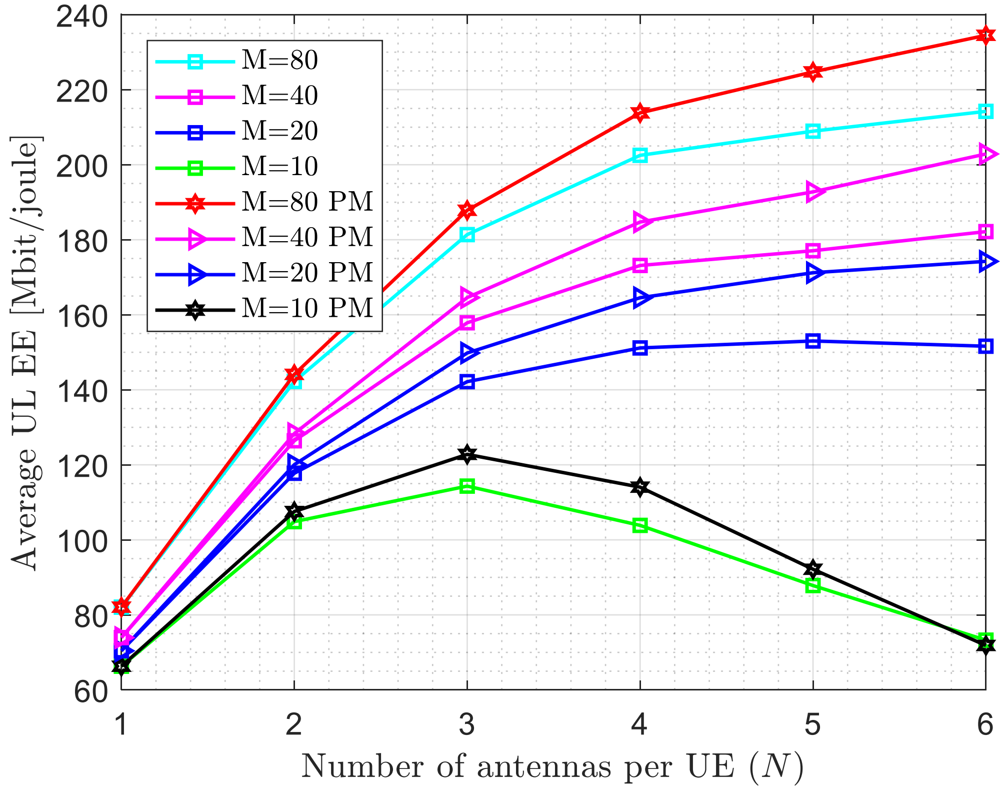

Figure 4.14: The energy efficiency versus the number of antennas per UE for the fully centralized processing with the MMSE combining at K = 10, L = 4, τ_c=200, and w=1.

Table 4.6: The energy efficiency versus the number of antennas per UE for the fully centralized processing with the MMSE combining at K = 10, L = 4, τ_c=200, and w=1.

Average UL EE(Mbit/joule)					Average UL SE(Mbit/joule) for proposed			
No. antenna per UE (N)	M=10	M=20	M=40	M=80	M=10	M=20	M=40	M=80
1	66.31	120	14.95	16.73	11.75	12.77	14.95	16.73
2	104.9	142.2	25.88	29.4	18.7	21.48	25.88	29.4
3	114.3	151.2	31.72	36.98	20.92	26.61	33.09	38.27
4	103.9	153	34.72	41.47	19.71	28.77	37.12	43.68
5	87.82	25.99	35.84	42.72	17.1	29.58	39.19	45.9
6	71.85	25.6	36.59	44.12	13.92	29.97	40.74	48.1

Figure 4.15 demonstrates the impact of users on energy efficiency with the number of antennae per UE. As the number of users increased, the energy efficiency decreased. The average UL EE achieved by the proposed estimator at N=6 and M=80 is 178.4Mbit/joule, whereas for the existing estimator the average UL EE achieved is 163.4Mbit/joule at the same point i.e., the proposed still enhanced by 9.2% from the existing estimator. The maximum average UL EE reached by the proposed method at N=4 and M=80 is 183Mbit/joule, whereas for the existing estimator is 173.5Mbit/joule i.e., the proposed enhanced by 5.47% from the MMSE channel estimator. This shows even if the number of user increments decreases the performance of the system, still the proposed better performance than the existing one. The performance proposed performs badly when the number of user increase for a small number of AP. The pilot length is 120 since K=20, N=6, and w=1.

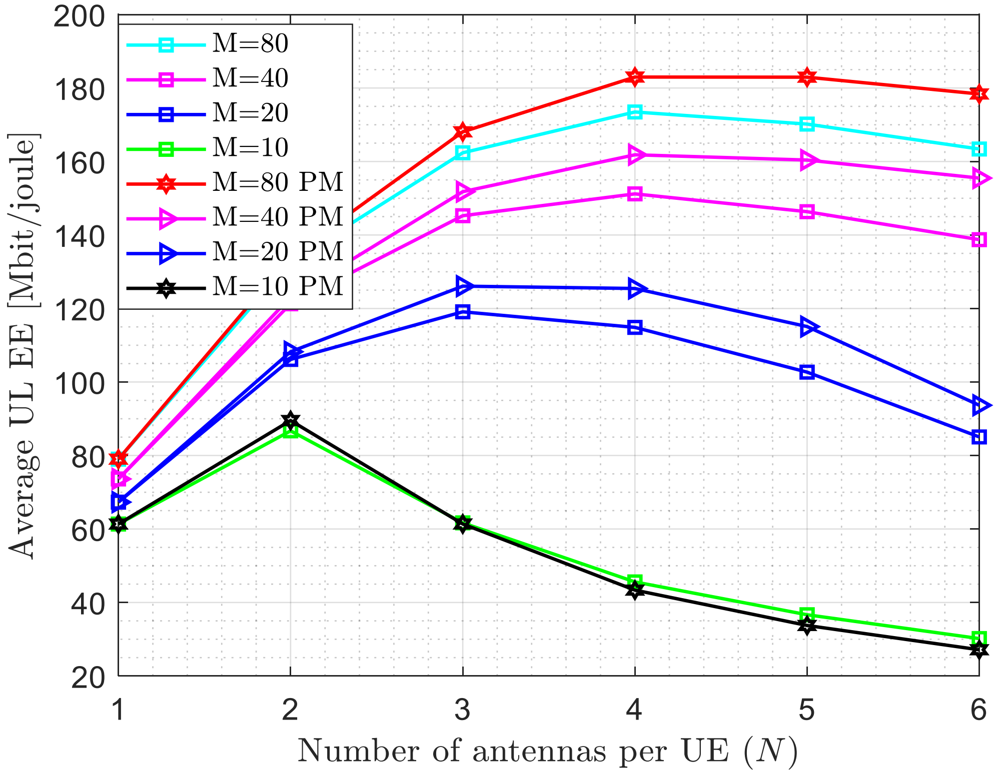

Figure 4.15: The energy efficiency versus the number of antennas per UE for the fully centralized processing with the MMSE combining at K = 20, L = 4, τ_c =200, and w=1.

Figure 4.16 shows the effect of antenna per AP on the energy efficiency with the number of antennae per UE. As the number of antenna per AP increased, the energy efficiency also increased. The average UL EE achieved by the proposed estimator at N=6 and M=80 is 273.21Mbit/joule, whereas for the existing estimator the average UL EE achieved is

252.3Mbit/joule at the same point i.e., the proposed enhanced by 8.29% from the existing estimator. The average UL EE reached by the proposed at N=4 and M=40 is 219.1Mbit/joule, whereas for the existing estimator is 206.1Mbit/joule. This shows the increment of the number of antenna per AP has a positive effect on energy efficiency. The performance of the proposed estimator for the single antenna user i.e. N<2 is closer to the existing estimator. With more antennas per AP, the system can achieve higher spatial resolution, increased spatial degrees of freedom, and enhanced spatial multiplexing gain allowing for better spatial channel estimation and interference suppression. This can lead to more accurate beamforming and reduced interference, resulting in improved energy efficiency. The pilot length is 60 since K=60, N=6, and w=1.

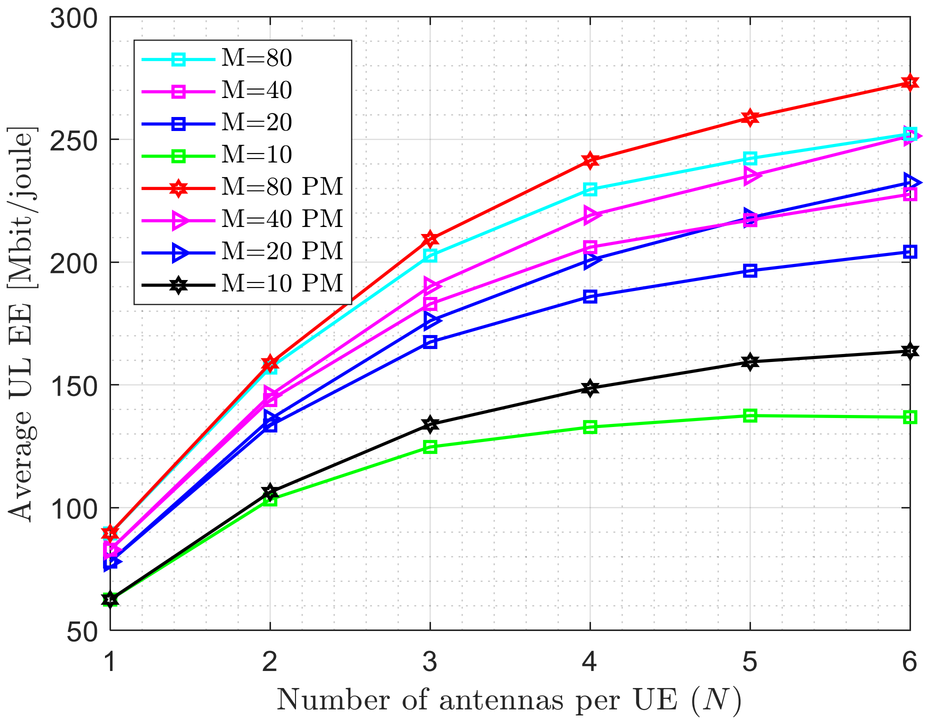

Figure 4.16: The energy efficiency versus the number of antennas per UE for the fully centralized processing with the MMSE combining at K = 10, L = 9, τ_c =200, and w=1.

Figure 4.17 shows that the comparison of the proposed estimator with the existing estimator based on energy efficiency varied across the number of AP at different numbers of antenna per UE. The proposed estimator achieved energy efficiency EE =213.695Mbit/joule at N=4 and M=80, whereas for the existing estimator the EE =203.299Mbit/joule at N=4 and M=80. At N=3 and M =40, the energy efficiency achieved by the existing and proposed estimator became 169.435Mbit/joule and 176.33Mbit/joule, respectively. The pilot length became 40 since K=10, N=4, and w=1. The proposed estimator achieved better performance than the existing one as the number of antenna per AP increased.

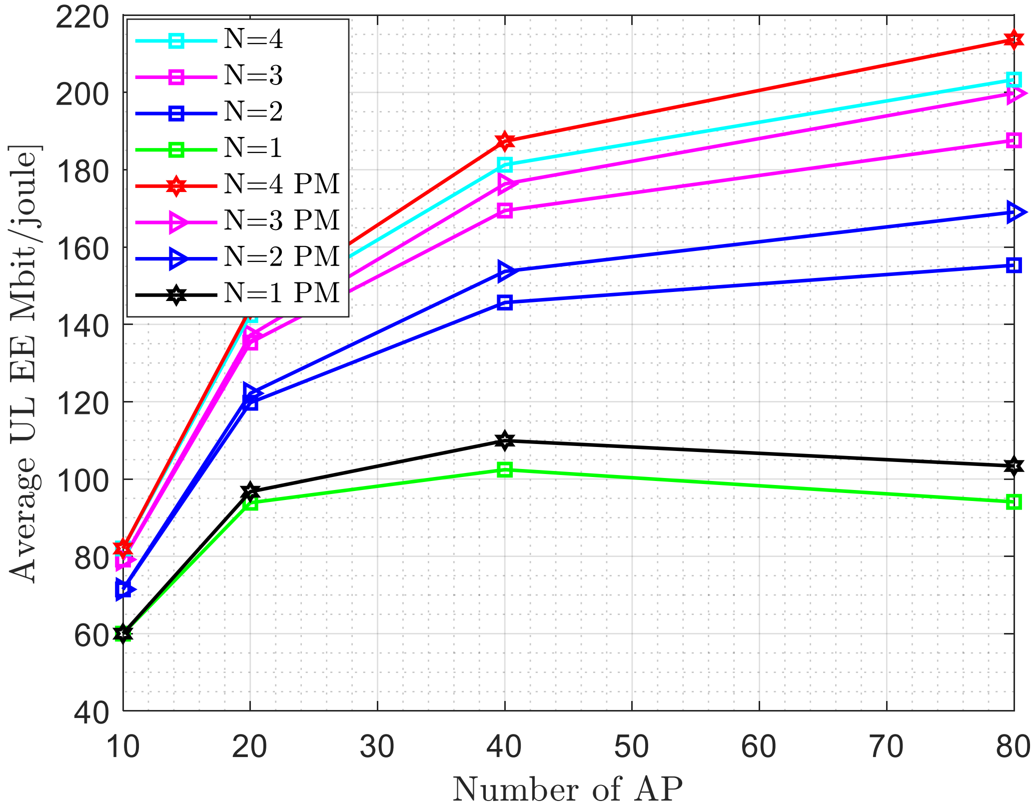

Figure 4.17: The energy efficiency versus the number of access points for the fully centralized processing with the MMSE combining at K = 10, L = 4, τ_c=200, and w=1.

Figure 4.18 shows the effect of users on energy efficiency with a varied number of AP and at different numbers of antennae per UE. The proposed estimator achieved energy efficiency EE=175.249Mbit/joule at N=4 and M=80, whereas for the existing estimator, the EE=165.704Mbit/joule at N=4 and M=80 i.e the proposed estimator outperform by 5.76% than existing at this point. At N=3 and M =40, the energy efficiency achieved by the existing and proposed estimator became 138.755Mbit/joule and 144.847Mbit/joule, respectively. At N=2 and M=20, the energy efficiency achieved by the existing and proposed estimator became 98.932Mbit/joule and 98.932Mbit/joule, respectively. This indicates that as the number of users increased the energy efficiency decreased. The pilot length is 60 since K=15, N=4, and w=1. The pilot length depends on the number of users, the number of antennae per UE, and the pilot reuse factor i.e. as the number of users increased, the pilot length also increased.

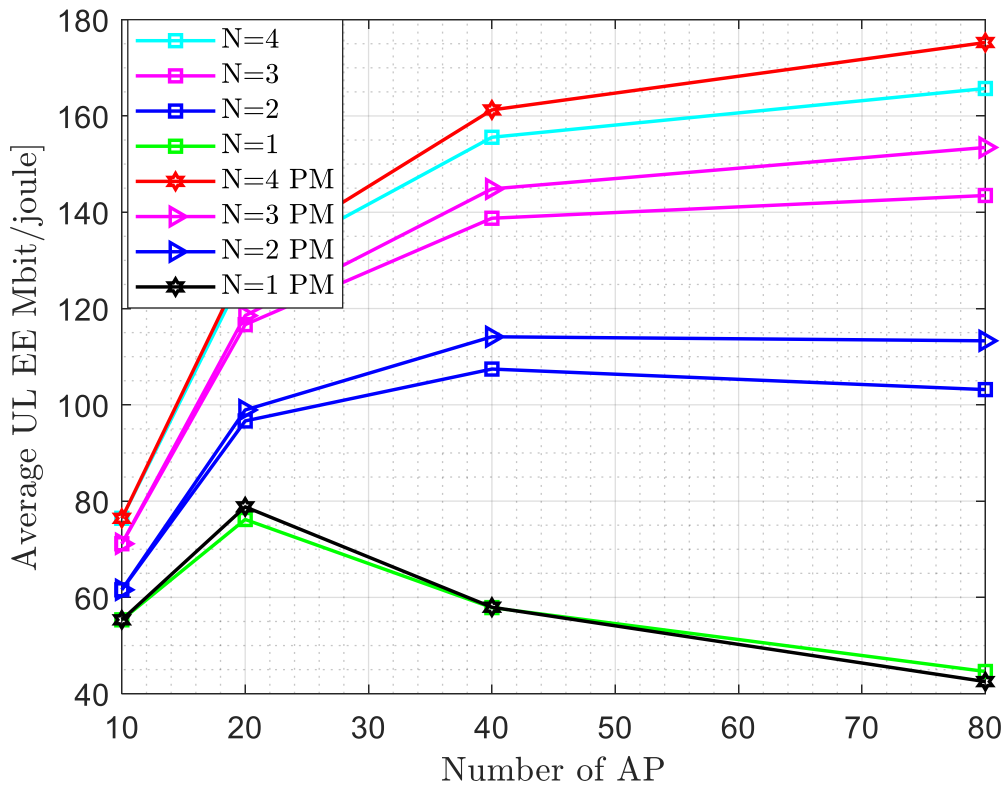

Figure 4.18: The energy efficiency versus the number of access points for the fully centralized processing with the MMSE combining at K = 15, L = 4, τ_c=200, and w=1.

Figure 4.19 shows the impact of the number of antennae per AP on the energy efficiency with a varied number of AP and at a different number of antennae per UE. The proposed estimator achieved energy efficiency EE=240.6Mbit/joule at N=4 and M=80, whereas for the existing estimator the EE=228.9Mbit/joule at N=4 and M=80. The proposed improves the performance by 5.11% at this point. At N=1 and M=80, the energy efficiency achieved by the existing and proposed estimator became 142.4Mbit/joule and 158.1Mbit/joule, respectively. As the number of antenna per AP increased, then the energy efficiency improved more. The pilot length became 40 since K=10, N=4, and w=1.

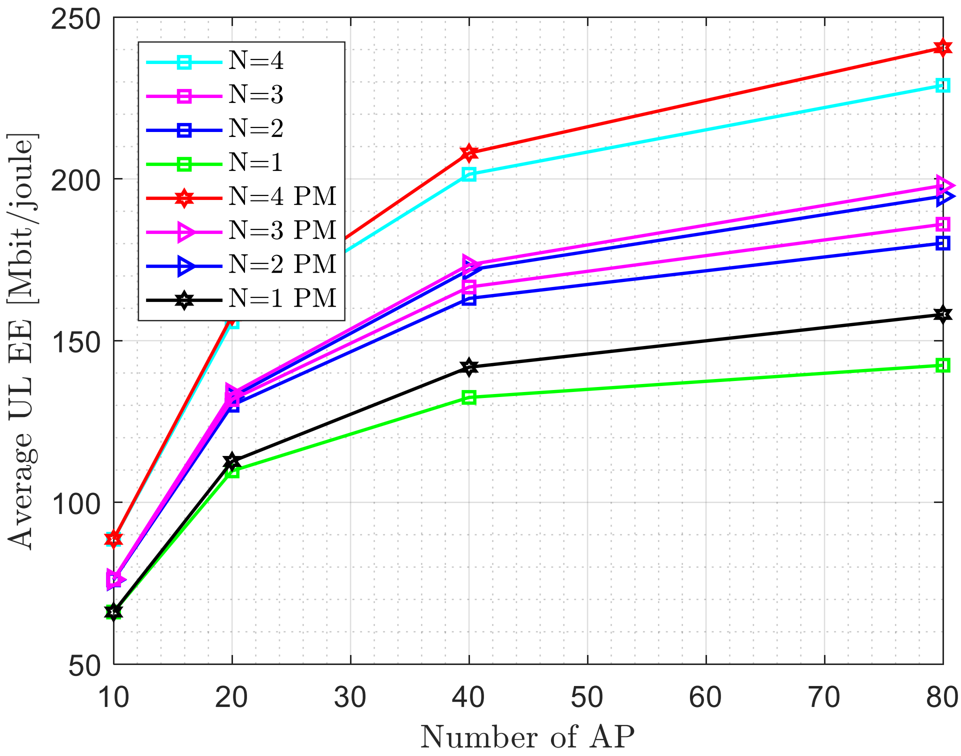

Figure 4.19: The energy efficiency versus the number of access points for the fully centralized processing with the MMSE combining at K = 10, L = 9, τ_c =200, and w=1.

4.2.2 The effect of coherence time and pilot reuse factor on energy efficiency

The simulation findings and feedback concentrate on the impact of the coherence time and pilot reuse factor on energy efficiency by maintaining the number of users and number of antennae per AP, K=10, and L=4, respectively. Performance is shown in terms of energy efficiency concerning the number of antennae used by each user of the equipment and spectral efficiency concerning the number of AP.

Figure 4.20 depicts the effect of coherence time on the energy efficiency varied across the number of antennae per UE at different numbers of AP. The proposed estimator achieved energy efficiency EE=292Mbit/joule at N=6 and M=80, whereas for the existing estimator the energy efficiency EE =267.9Mbit/joule at N=6 and M=80. The proposed improves the performance by 8.99% at this point. At N=5 and M=40, the area throughput achieved by the existing and proposed estimator became 209.1Mbit/joule and 228.6Mbit/joule, respectively. At N=3 and M =10, the energy efficiency achieved by the existing and proposed estimators became 99.37Mbit/km^2 and 107.3Mbit/km^2 respectively. The pilot length became 60 since K=10, N=6, and w=1. when the number of coherence time slots increases in combination with a varied number of antennas per UE and a different number of Aps, it can enhance the system's energy efficiency. This is due to improved channel estimation accuracy, increased spatial resolution, better interference management, and higher spatial multiplexing gains.

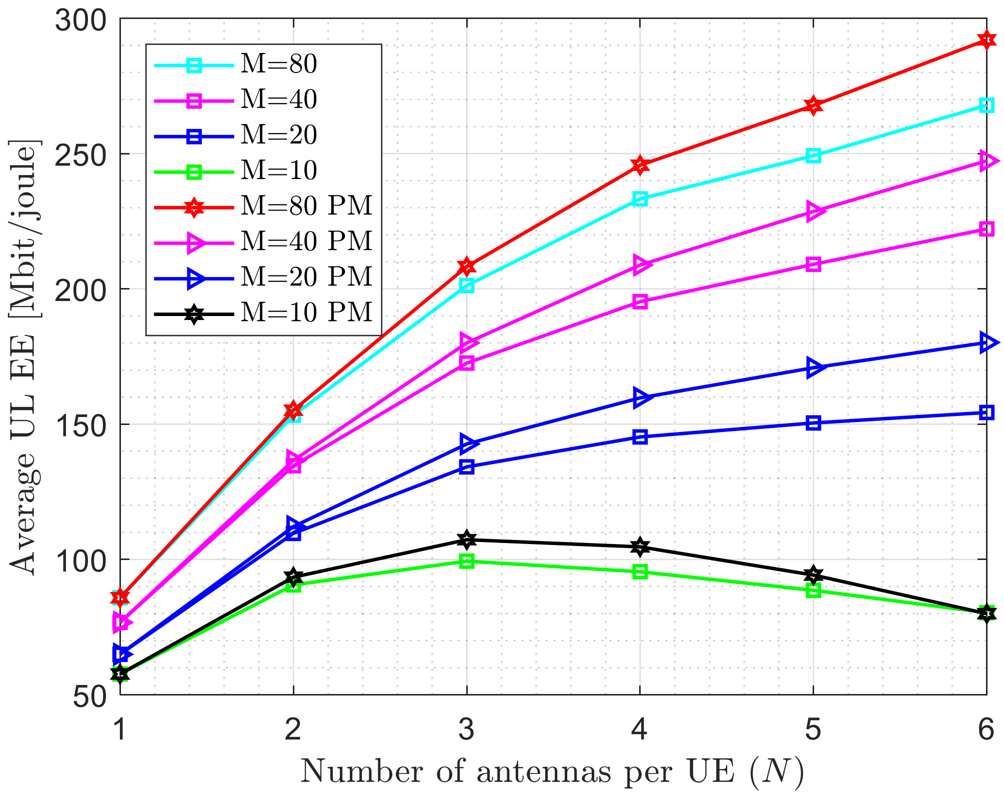

Figure 4.20: The energy efficiency versus the number of antennas per UE for the fully centralized processing with the MMSE combining at K = 10, L = 4, τ_c=400, and w=1.

Figure 4.21 shows that the effect of the pilot reuse factor on the energy efficiency varied across the number of antennae per UE at different numbers of AP when the pilot reuse factor was raised to 2. The proposed estimator achieved energy efficiency EE=176.7bit/joule at N=6 and M=80, whereas for the existing estimator the EE=162.2Mbit/joule at N=6 and M=80. The proposed improves the performance by 8.94% at this point. At N=6 and M=20, the energy efficiency achieved by the existing and proposed estimator became 97.04Mbit/joule and 108.2Mbit/joule, respectively. The maximum energy efficiency reached by the proposed estimator occurred at N=4 i.e.184.2Mbit/joule, whereas for existing 178.2Mbit/joule at N=3. As the pilot reuse factor increased from w=1 to w=2, then the energy efficiency initially increased and then decreased as the number of antenna per UE increased. The pilot length became 30 since K=10, N=6, and w=2 which means the pilot length decreased as the pilot reuse factor increased.

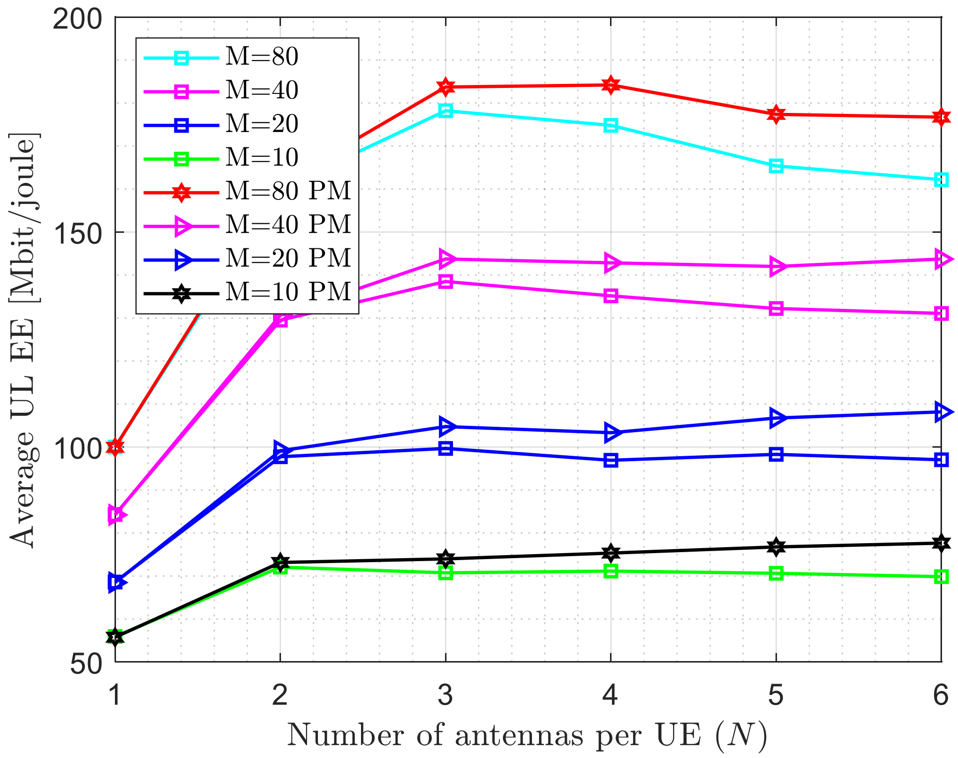

Figure 4.21: The energy efficiency versus the number of antennas per UE for the fully centralized processing with the MMSE combining at K = 10, L = 4, τ_c =200, and w=2.

Figure 4.22 shows that the effect of the pilot reuse factor on the energy efficiency varied across the number of antennae per UE at different numbers of AP when the pilot reuse factor was raised to 5. The proposed estimator achieved energy efficiency EE=60.23bit/joule at N=6 and M=80, whereas for the existing estimator the EE=58.12Mbit/joule at N=6 and M=80. The proposed improves the performance by 3.63% at this point. The maximum energy efficiency reached by the proposed estimator occurred at N=4 i.e.73.11Mbit/joule, whereas for existing 71.9Mbit/joule at the same point. As the pilot reuse factor increased from w=1 to w=5, then the energy efficiency initially increased and then decreased as the number of antenna per UE increased. The pilot length became 12 since K=10, N=6, and w=5 which means the pilot length decreased as the pilot reuse factor increased.

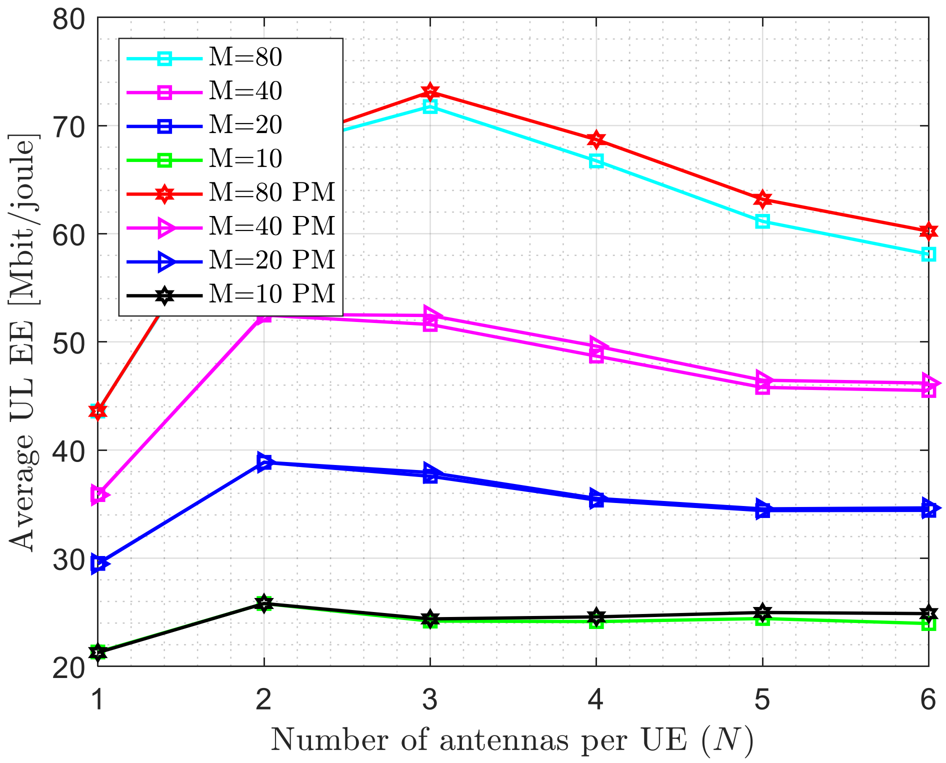

Figure 4.22: The energy efficiency versus the number of antennas per UE for the fully centralized processing with the MMSE combining at K = 10, L = 4, τ_c =200, and w=5.

Figure 4.23 shows that the effect of coherence time on the energy efficiency varied across the number of AP at different numbers of antenna per UE. The proposed estimator achieved energy efficiency EE=243.3Mbit/joule at N=4 and M=80, whereas for the existing estimator the area throughput =230.9Mbit/joule at N=4 and M=80. The proposed improves the performance by 5.4% at this point. At N=3 and M =40, the energy efficiency achieved by the existing and proposed estimators became 166.5Mbit/joule and 174.2Mbit/joule, respectively. At N=2 and M=20, the area throughput achieved by the existing and proposed estimator became 121.8Mbit/joule i.e., at this point the performance of the two estimators achieved the same value. The energy efficiency attained by the proposed and existing estimators for N<2 has a nearly closer value i.e. the proposed estimator is not efficient for single antenna UE. The pilot length became 40 since K=10, N=4, and w=1.

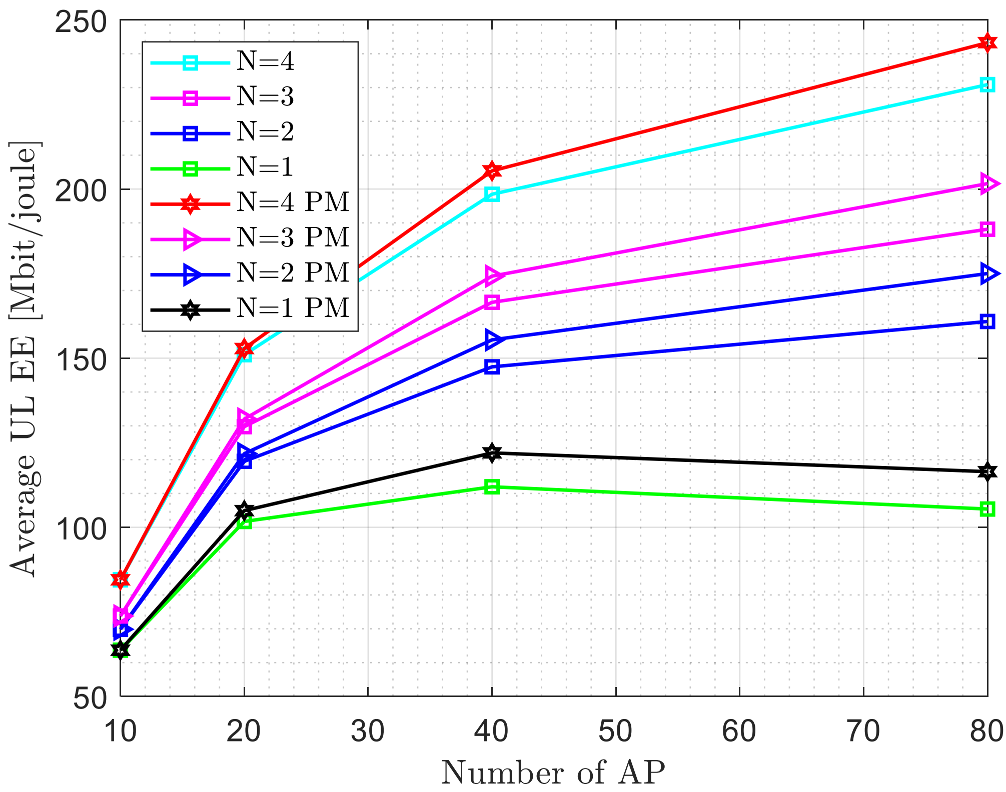

Figure 4.23: The energy efficiency versus the number of access points for the fully centralized processing with the MMSE combining at K = 10, L = 4, τ_c =400, and w=1.

Figure 4.24 describes the effect of the pilot reuse factor on the energy efficiency varied across the number of antennae per AP at different numbers of UE when the pilot reuse factor was raised to 2. The proposed estimator achieved energy efficiency EE =87.67Mbit/joule at N=4 and M=80, whereas for the existing estimator the energy efficiency EE=83.25Mbit/joule at N=4 and M=80. The proposed improves the performance by 8.94% at this point. At N=3 and M =40, the energy efficiency achieved by the existing and proposed estimator became 65.97Mbit/joule and 68.45Mbit/joule, respectively. At N=2 and M=20, the energy efficiency achieved by the existing and proposed estimator became 49.46Mbit/joule and 50.03Mbit/joule, respectively. The energy efficiency attained by the proposed and existing estimator for N<2 have nearly the same value. As the pilot reuse factor increased from w=1 to w=2, then the energy efficiency decreased. When the number of AP increased with the increased pilot reuse factor, the area throughput increased up to some point and diminished after a certain point. The pilot length became 20 since K=10, N=4, and w=2 which means the pilot length decreased as the pilot reuse factor increased.

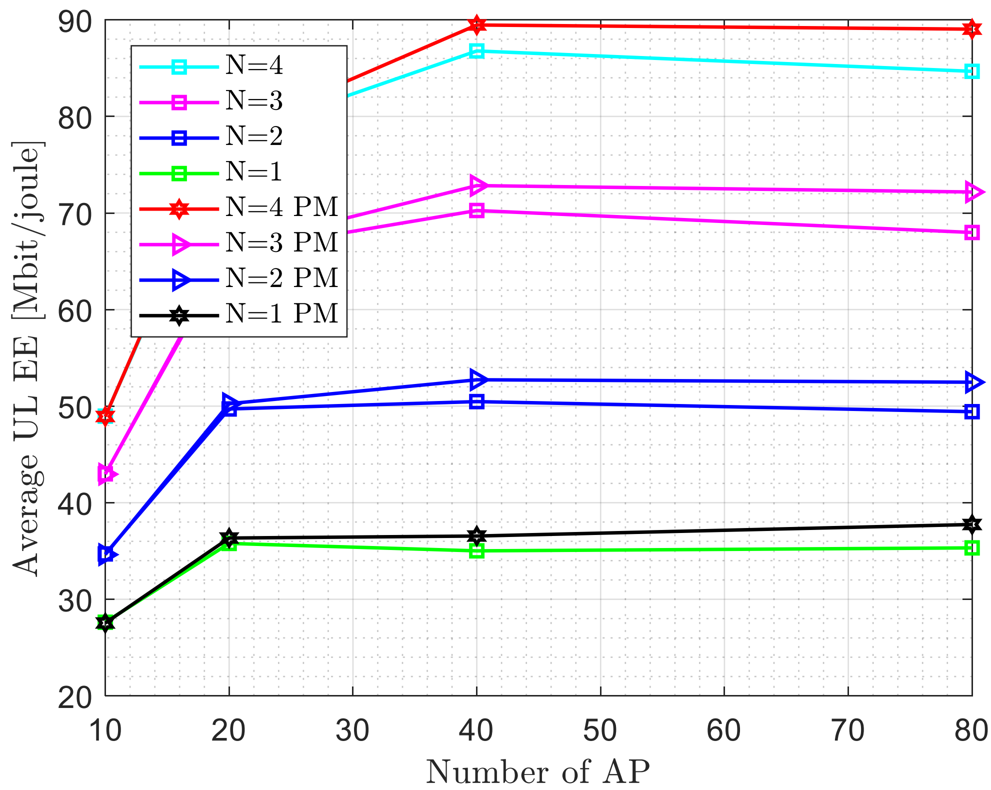

Figure 4.24: The energy efficiency versus the number of access points for the fully centralized processing with the MMSE combining at K = 10, L = 4, τ_c =200, and w=2.

Figure 4.25 depicts the impact of the pilot reuse factor on the energy efficiency varied across the number of AP at the different numbers of antenna per UE when the pilot reuse factor was raised to 5. The proposed estimator achieved energy efficiency EE =66.04Mbit/joule at N=4 and M=80, whereas the existing estimator EE=64.79Mbit/joule at N=4 and M=80. The proposed improves the performance by 3.08% at this point. At N=2 and M=40, the energy efficiency achieved by the existing and proposed estimator becomes 37.34Mbit/joule i.e., at this point, the performance of the two estimators has the same value. The energy efficiency attained by the proposed and existing estimator for N=1 has nearly the same value. As the pilot reuse factor increased from w=1 to w=5, then the energy efficiency decreased. When the number of AP increased with the increased pilot reuse factor, then the energy efficiency increased up to some point and diminished after a certain point. The pilot length became 8 since K=10, N=4, and w=5 which means the pilot length decreased as the pilot reuse factor increased.

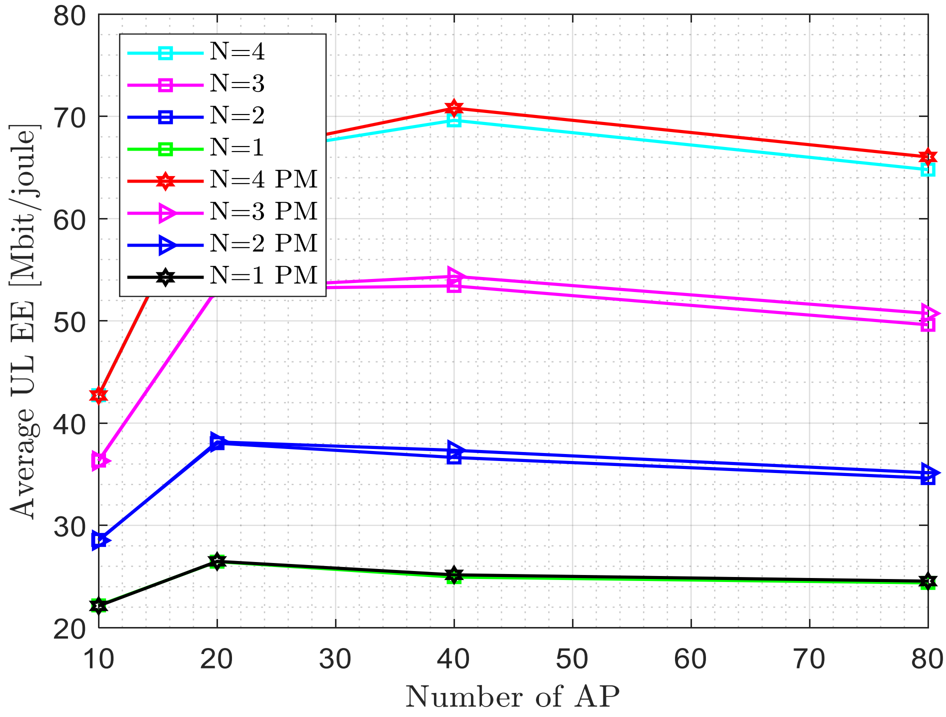

Figure 4.25: The energy efficiency versus the number of access points for the fully centralized processing with the MMSE combining at K = 10, L = 4, τ_c =200, and w=5.

4.3 Area Throughput Comparison

4.3.1 The impact of number of users and antennas per access point on area throughput

The simulation findings show the impact of the number of users and antenna per AP on area throughput by maintaining the coherence time and pilot reuse factor, τ_c =200, and w=1. Performance is shown in terms of area throughput with the number of antenn used by each user of the equipment and area throughput with the number of AP.

The comparison between the proposed estimator and the existing estimate utilizing the parameter area throughput with the number of antenna per UE is shown in Figure 4.26. The area throughput increased as the number of antennae per UE increased for M values 20,40, and 80, however for M values 10 the area throughput initially increased and then it decreased. The suggested estimate attained area throughput AT=3792Mbit/s/km^2 at N=6 and M=80, whereas the existing attained AT =3467Mbit/s/km^2 at N=6 and M=80. The proposed estimator enhanced the performance by 9.374% at this point. For M=10, the proposed estimator and existing estimator maximumly reached the area throughput at N=3, which are 1612Mbit/s/km^2 and 1491Mbit/s/km^2, respectively. The length of the pilot is 60 since w=1, N=6, and K=10.

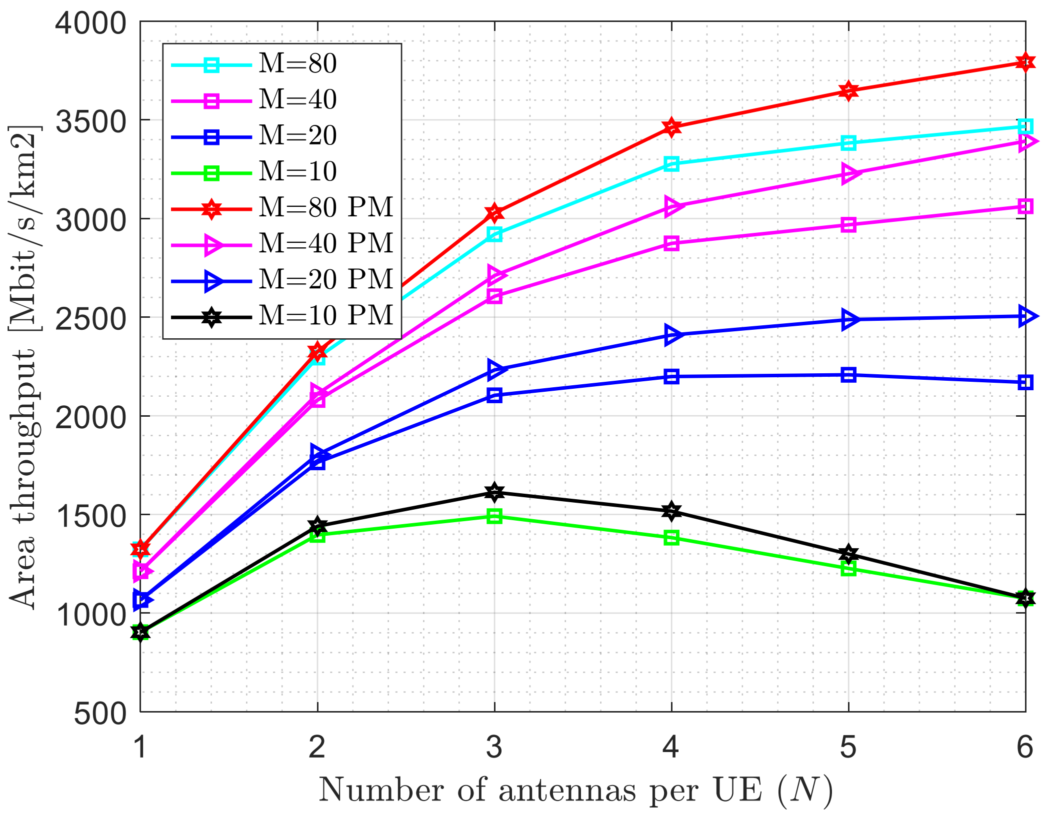

Figure 4.26: The area throughput versus the number of antenna per UE for the fully centralized processing with the MMSE combining at K = 10, L = 4, τ_c=200, and w=1.

In Figure 4.27, the new estimator and the existing estimate are compared using the parameter area throughput with the number of antennae per UE and the effect of the number of users on area throughput. For M=10 the area throughput raised to N=2 and falls as the number of users increased from K= 10 to K=15 and the number of antennae per UE increased. The achieved throughput became 1216Mbit/km^2 and 1254Mbit/km^2 at N=2, M=10 for existing and proposed estimators respectively. The area throughput for the suggested estimate became 2892 Mbit/s/km^2 at N=6 and M=80, while the area throughput for the current estimator became 2652Mbit/km^2. At this stage, the performance has been improved by 9.05% using the suggested estimator. At N=5, M=80, the proposed reached maximum area throughput 2958Mbit/km^2 and for the existing estimator maximumly reached area throughput 2802Mbit/km^2 at N=4, M=80. This shows that as the number of UE increased, the area throughput diminished. The proposed estimator for the smaller number of AP performs badly as the number of users increases and the number of antennae per UE increased parallelly. The pilot length became 60 and this showed that as the number of users increased the pilot length also increased.

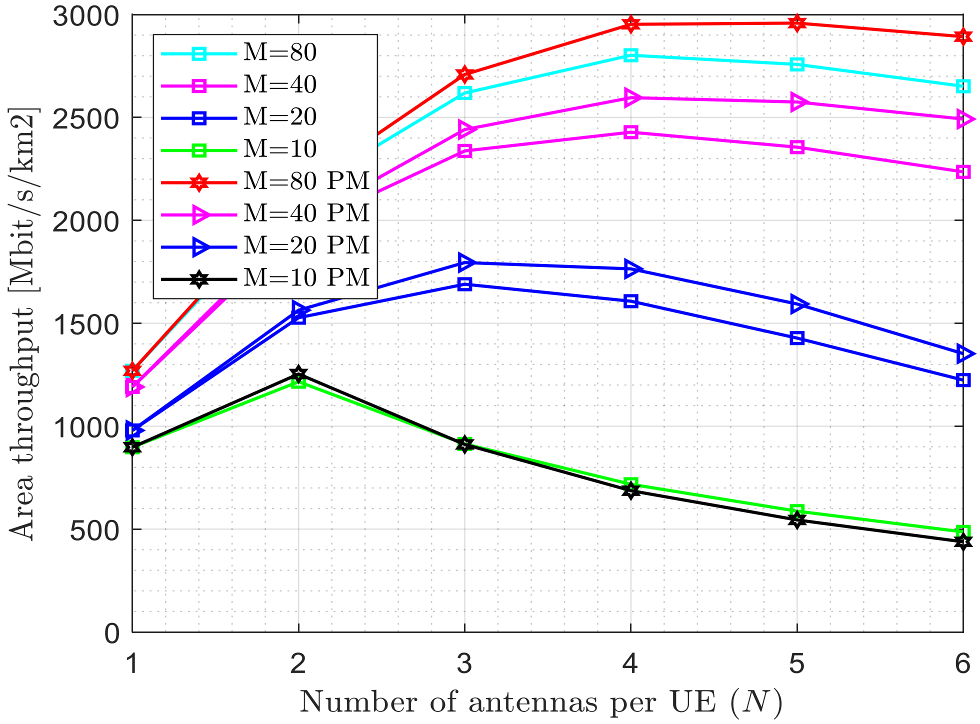

Figure 4.27: The area throughput versus the number of antennae per UE for the fully centralized processing with the MMSE combining at K = 15, L = 4, τ_c=200, and w=1.

Figure 4.28 shows the impact of the number of antennae per UE on the area throughput with varied numbers of antennae per UE and at different numbers of AP. The proposed estimator achieved area throughput =4076Mbit/km^2 at N=6 and M=80, whereas for the existing estimator the area throughput =3753Mbit/km^2 at N=6 and M=80. The proposed improves the performance by 8.61% at this point. As the number of antennae per AP increased the throughput also increased. At N=5 and M=40, the area throughput achieved by the existing and proposed estimators became 3015Mbit/km^2 and 3297Mbit/km^2, respectively. At N=4 and M=20, the area throughput achieved by the existing and proposed estimators became 2462Mbit/km^2 and 2691Mbit/km^2, respectively. The area throughput attained by the proposed and existing estimator for N<2 has a nearly closer value. The pilot length became 60 since K=10, N=6, and w=1. The pilot length depends on the number of users, the number of antennae per UE, and the pilot reuse factor i.e., the number of antennae per AP does not affect pilot length.

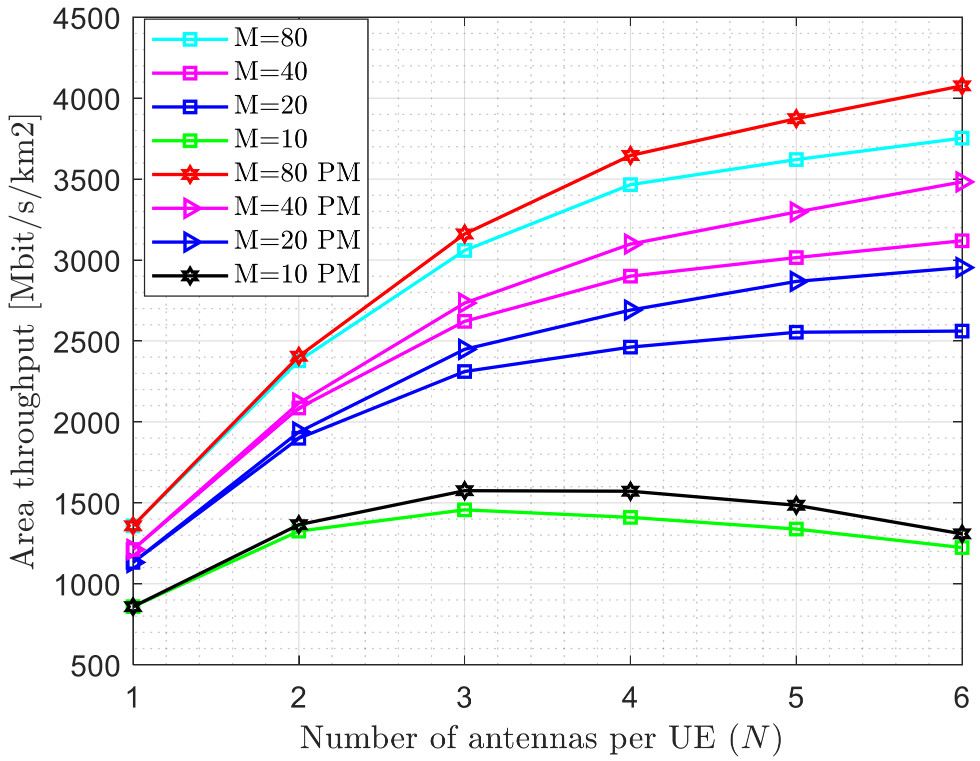

Figure 4.28: The area throughput versus the number of antennae per UE for the fully centralized processing with the MMSE combining at K = 10, L = 9, τ_c =200 and w=1

Figure 4.29 shows the effect of users on the area throughput with varied numbers of AP and at different numbers of antennae per UE. When the number of users increased the area throughput reduced. The proposed estimator achieved area throughput =3051.17Mbit/km^2 at N=4 and M=80, whereas for the existing estimator the area throughput =2895.84Mbit/km^2 at N=4 and M=80. As the number of AP increased the throughput also increased. At N=3 and M =40, the area throughput achieved by the existing and proposed estimators became 2405.29Mbit/km^2 and 2511.62Mbit/km^2, respectively. At N=4 and M=20, the area throughput achieved by existing and proposed estimators became 2226.1Mbit/km^2 and 2226.7Mbit/km^2, respectively. The area throughput attained by the proposed and existing estimator for M<20 has a nearly closer value. The pilot length became 60 since K=15, N=4, and w=1. The pilot length depends on the number of users, the number of antennae per UE, and the pilot reuse factor i.e., as the number of users increased, the pilot length also increased.

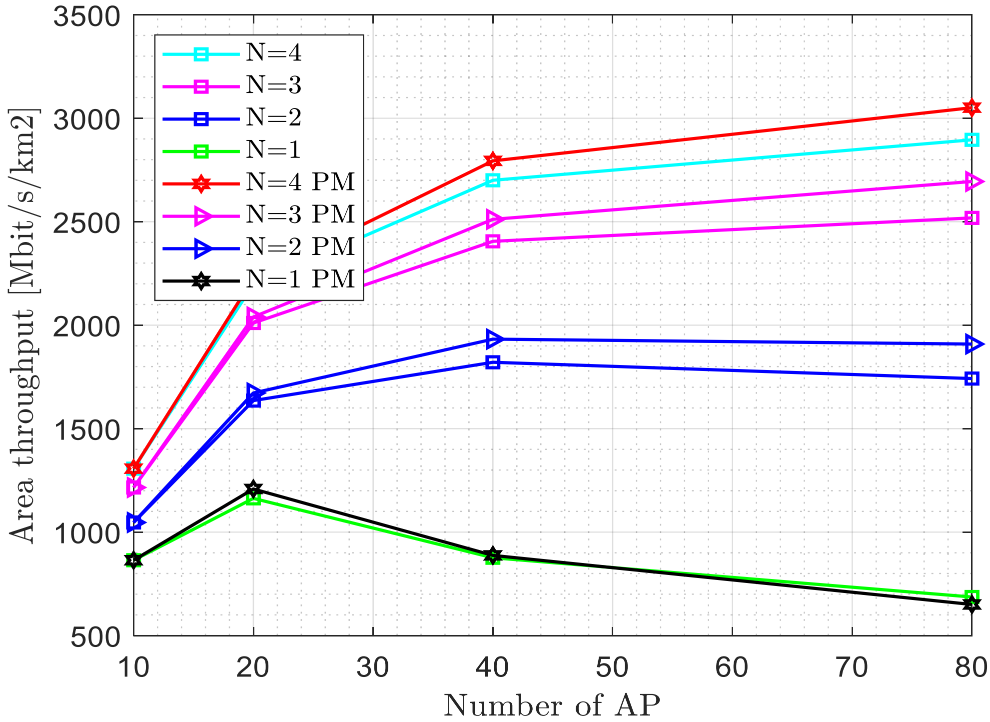

Figure 4.29: The area throughput versus the number of access points for the fully centralized processing with the MMSE combining at K = 15, L = 4, τ_c =200, and w=1.

Figure 4.30 shows the impact of several antennae per AP on the area throughput with varied numbers of AP and at different numbers of antennae per UE. The proposed estimator achieved area throughput =3909Mbit/km^2 at N=4 and M=80, whereas for the existing estimator the area throughput =3730Mbit/km^2 at N=4 and M=80. The proposed improves the performance by 4.79% at this point. As the number of antennae per AP increased the throughput also increased. At N=3 and M =40, the area throughput achieved by the existing and proposed estimators became 2859Mbit/km^2 and 2980Mbit/km^2, respectively. At N=2 and M=20, the area throughput achieved by the existing and proposed estimators became 2102Mbit/km^2 and 2142Mbit/km^2, respectively. The area throughput attained by the proposed and existing estimator for N<2 has a nearly closer value. The pilot length became 40 since K=10, N=4, and w=1.

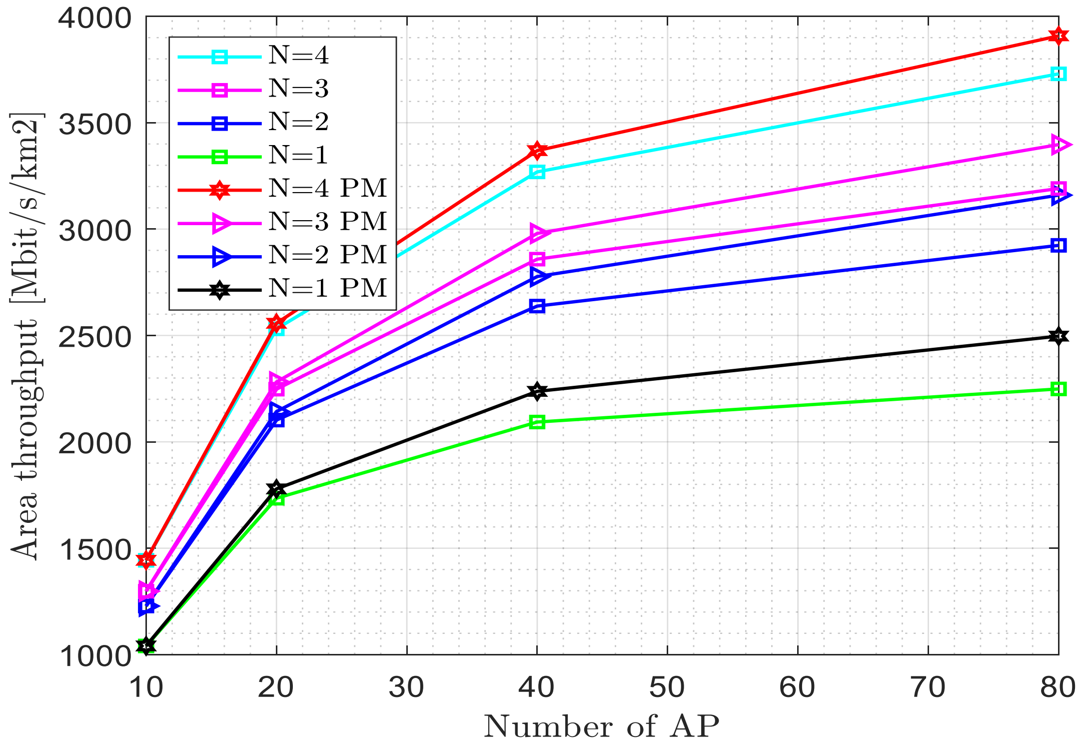

Figure 4.30: The area throughput versus the number of access points for the fully centralized processing with the MMSE combining at K = 10, L = 9, τ_c=200, and w=1.

4.3.2 The impact of coherence time and pilot reuse factor on area throughput

The simulation results focus on the effects of the coherence time and pilot reuse factor on area throughput by keeping K=10 and L=4 for the number of users and antennae per AP, respectively. Performance is displayed as area throughput relative to the number of antenna utilized by each equipment user as well as area throughput relative to the number of AP.

Figure 4.31 shows that the effect of coherence time on the area throughput varied across the number of antennae per UE at different numbers of AP. The proposed estimator achieved area throughput =4673Mbit/km^2 at N=6 and M=80, whereas for the existing estimator the area throughput =4286Mbit/km^2 at N=4 and M=80. The proposed improves the performance by 9.03% at this point. At N=5 and M=40, the area throughput achieved by the existing and proposed estimators became 3345Mbit/km^2 and 3658Mbit/km^2, respectively. At N=3 and M =20, the area throughput achieved by the existing and proposed estimators became 2147Mbit/km^2 and 2283Mbit/km^2 respectively. The area throughput attained by the proposed and existing estimator for N<2 has a nearly closer value. The pilot length became 40 since K=10, N=4, and w=1. When the coherence time is increased, it allows for longer periods of reliable channel estimation and coherent data transmission. This can result in more efficient resource allocation and scheduling, leading to improved area throughput.

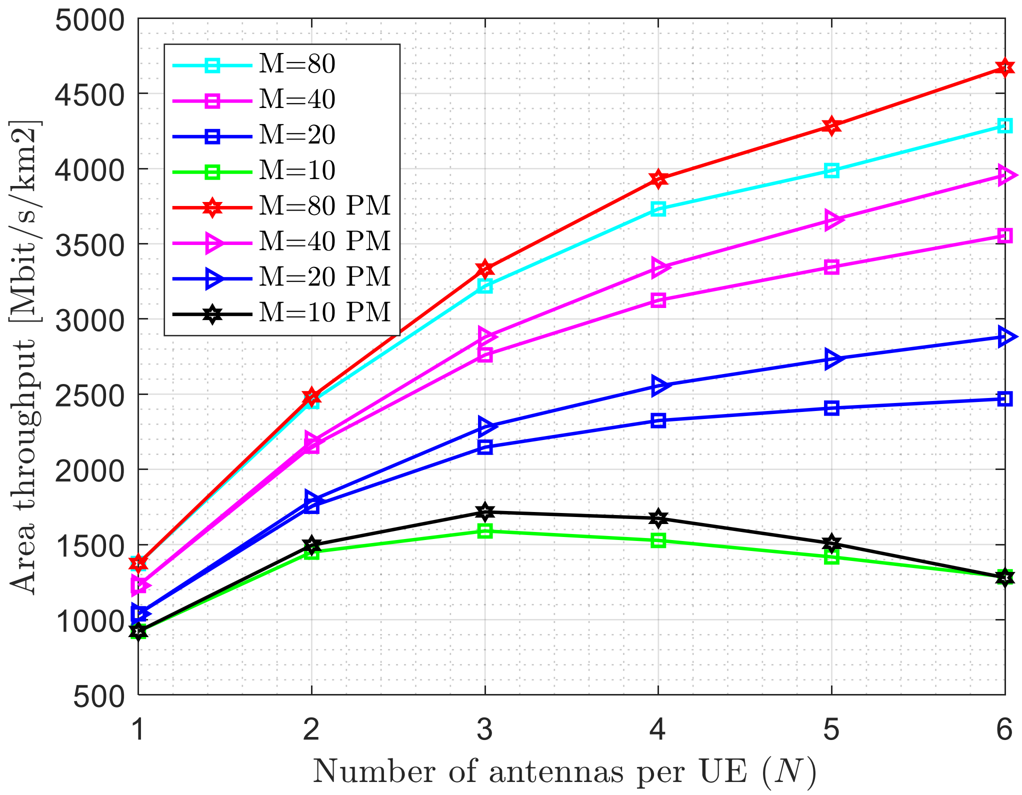

Figure 4.31: The area throughput versus the number of antenna per UE for the fully centralized processing with the MMSE combining at K = 10, L = 4, τ_c=400, and w=1.

Figure 4.32 shows that the effect of the pilot reuse factor on the area throughput varied across the number of antennae per UE at different numbers of AP when the pilot reuse factor was raised to 2. The proposed estimator achieved area throughput =1325bit/km^2 at N=6 and M=80, whereas for the existing estimator the area throughput =1200Mbit/km^2 at N=6 and M=80. The proposed improves the performance by 10.42% at this point. At N=4 and M=40, the area throughput achieved by the existing and proposed estimator became 1050Mbit/km^2 and 1150Mbit/km^2. The area throughput attained by the proposed and existing estimator for N<2 has a nearly closer value. The maximum area throughput reached by the proposed estimator occurred at N=3 i.e.,1400 Mbit/km^2, whereas for the existing 1350 Mbit/km^2 As the pilot reuse factor increased from w=1 to w=2, then the area throughput decreased. As a result, the gap between the proposed and existing estimator also decreased. The pilot length became 30 since K=10, N=6, and w=2 which means the pilot length decreased as the pilot reuse factor increased.

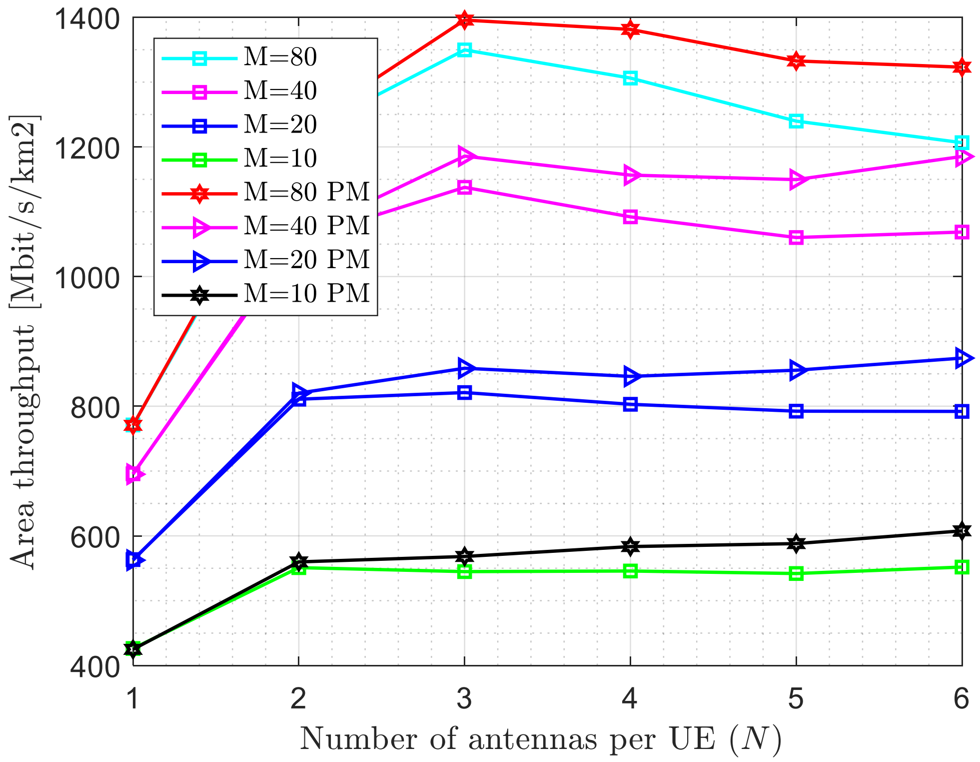

Figure 4.32: The area throughput versus the number of antenna per UE for the fully centralized processing with the MMSE combining at K = 10, L = 4, τ_c =200, and w=2.

Figure 4.33 shows that the effect of the pilot reuse factor on the area throughput varied across the number of antennae per UE at different numbers of AP when the pilot reuse factor was raised to 5. The proposed estimator achieved area throughput =922.98bit/km^2 at N=6 and M=80, whereas for the existing estimator the area throughput =896.667Mbit/km^2 at N=6 and M=80. The proposed improves the performance by 2.93% at this point. At N=4 and M=40, the area throughput achieved by the existing and proposed estimator became 785.959Mbit/km^2 i.e., at this point the performance of the two estimators is the same. At N=5 and M=20, the area throughput achieved by the existing and proposed estimator became 554.302Mbit/km^2 and 560.327Mbit/km^2. The area throughput attained by the proposed and existing estimator for N<2 has a nearly closer value. As the pilot reuse factor increased from w=1 to w=5, then the area throughput decreased. As a result, the gap between the proposed and existing estimator also decreased. When the number of antenna per UE increased with the increased pilot reuse factor, the area throughput increased up to some point and diminished after a certain point. The pilot length became 12 since K=10, N=6, and w=5 which means the pilot length decreased as the pilot reuse factor increased.

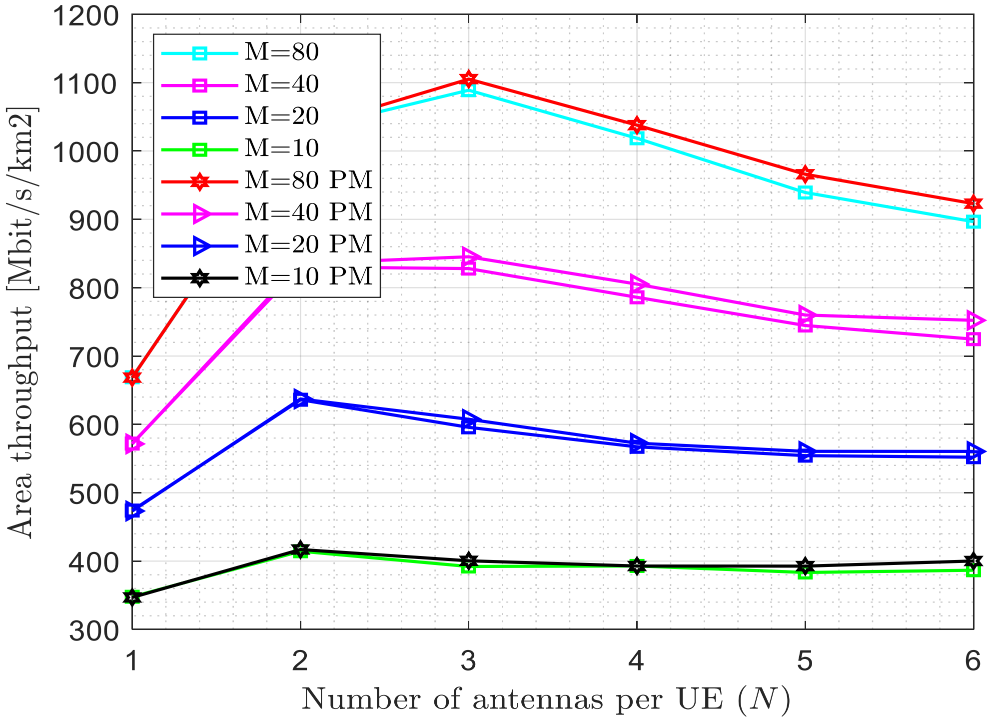

Figure 4.33: The area throughput versus the number of antenna per UE for the fully centralized processing with the MMSE combining at K = 10, L = 4, τ_c =200, and w=5.

Figure 4.34 shows that the comparison of the proposed estimator with the existing estimator varied across the number of AP at different numbers of antenna per UE. The proposed estimator achieved area throughput =3358.01Mbit/km^2 at N=4 and M=80, whereas for the existing estimator the area throughput =3186.56Mbit/km^2 at N=4 and M=80. At N=3 and M =40, the area throughput achieved by the existing and proposed estimators became 2559.57Mbit/km^2 and 2669.91Mbit/km^2, respectively. The pilot length became 40 since K=10, N=4, and w=1.

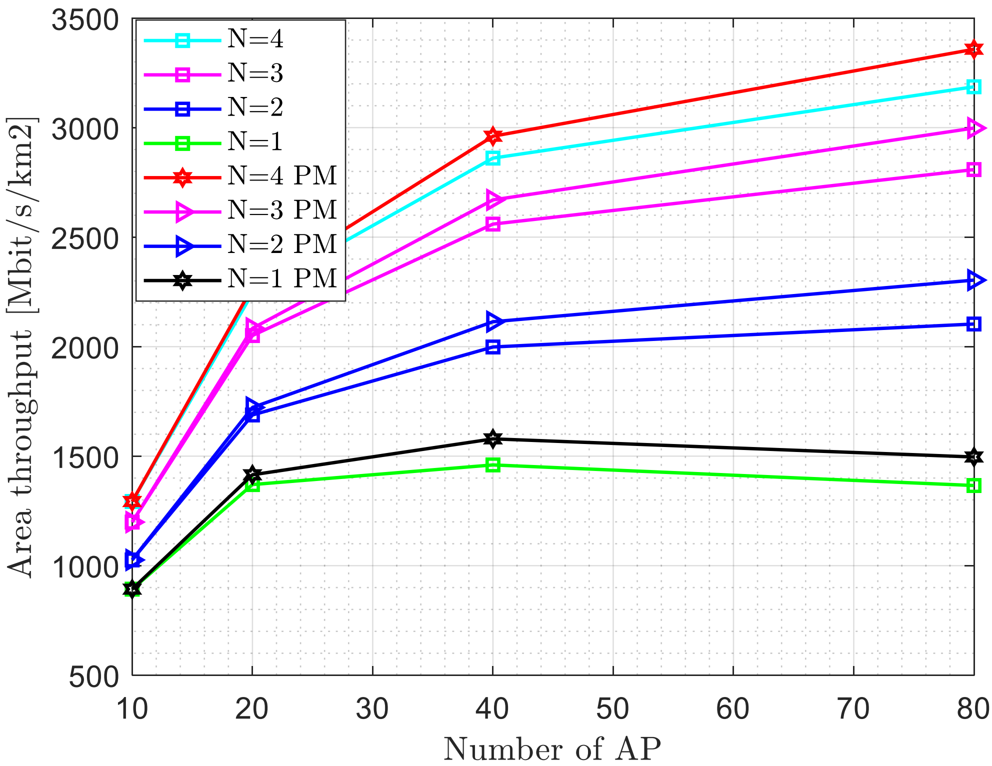

Figure 4.34: The area throughput versus the number of access points for the fully centralized processing with the MMSE combining at K = 10, L = 4, τ_c =200, and w=1.

Figure 4.36 shows that the effect of coherence time on the area throughput varied across the number of AP at different numbers of antenna per UE. The proposed estimator achieved area throughput =4082Mbit/km^2 at N=4 and M=80, whereas for the existing estimator the area throughput =3817Mbit/km^2 at N=4 and M=80. The proposed improves the performance by 6.94% at this point. At N=3 and M =40, the area throughput achieved by the existing and proposed estimator became 2686Mbit/km^2 and 2812Mbit/km^2, respectively. At N=2 and M=20, the area throughput achieved by the existing and proposed estimator became 1825Mbit/km^2 i.e., at this point the performance of the two estimators is the same. The area throughput attained by the proposed and existing estimator for N<2 has a nearly closer value. The pilot length became 40 since K=10, N=4, and w=1. When the coherence time is increased, it allows for longer periods of reliable channel estimation and coherent data transmission. This can result in more efficient resource allocation and scheduling, leading to improved area throughput.

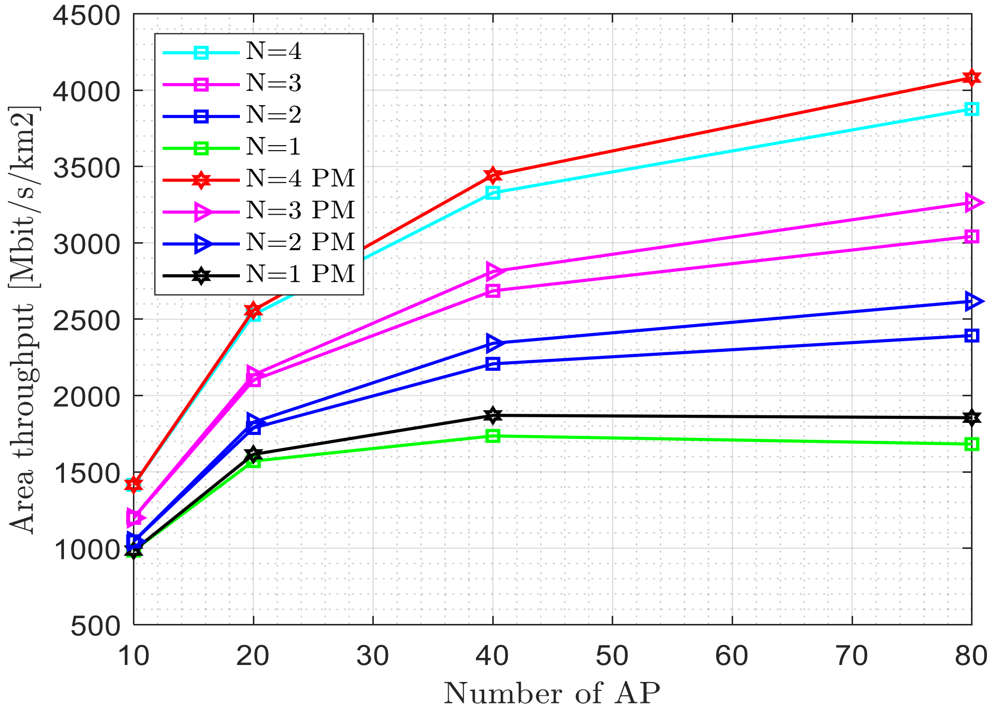

Figure 4.35: The area throughput versus the number of access points for the fully centralized processing with the MMSE combining at K = 10, L = 4, τ_c =400, and w=1.

Figure 4.36 shows that the effect of the pilot reuse factor on the area throughput varied across the number of antennae per AP at different numbers of UE when the pilot reuse factor was raised to 2. The proposed estimator achieved area throughput =1476Mbit/km^2 at N=4 and M=80, whereas for the existing estimator the area throughput =1399Mbit/km^2 at N=4 and M=80. The proposed improves the performance by 5.50% at this point. At N=3 and M =40, the area throughput achieved by the existing and proposed estimator became 1100Mbit/km^2 and 1142Mbit/km^2, respectively. At N=2 and M=20, the area throughput achieved by the existing and proposed estimator became 837.3Mbit/km^2 i.e., at this point the performance of the two estimators is the same. The area throughput attained by the proposed and existing estimator for N<2 has a nearly closer value. As the pilot reuse factor increased from w=1 to w=2, then the area throughput decreased. When the number of AP increased with the increased pilot reuse factor, the area throughput increased up to some point and diminished after a certain point. The pilot length became 20 since K=10, N=4, and w=2 which means the pilot length decreased as the pilot reuse factor increased.

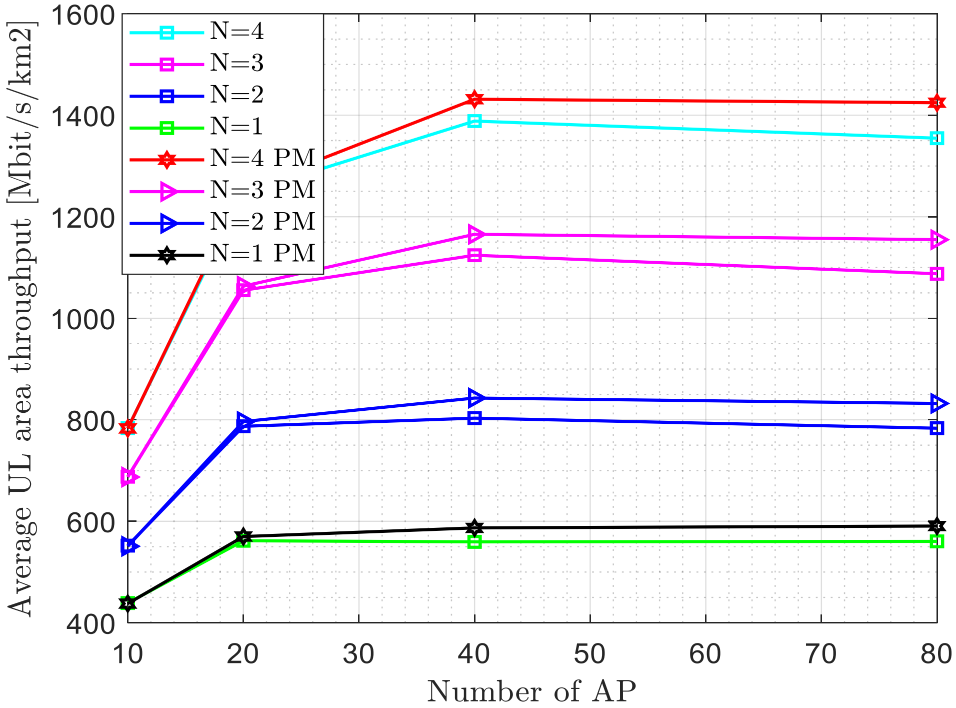

Figure 4.36: The area throughput versus the number of access points for the fully centralized processing with the MMSE combining at K = 10, L = 4, τ_c=200, and w=2.

Figure 4.37 shows that the effect of the pilot reuse factor on the area throughput varied across the number of AP at different numbers of antenna per UE when the pilot reuse factor was raised to 5. The proposed estimator achieved area throughput =1071Mbit/km^2 at N=4 and M=80, whereas for the existing estimator the area throughput =1039Mbit/km^2 at N=4 and M=80. The proposed improves the performance by 3.08% at this point. At N=3 and M =40, the area throughput achieved by the existing and proposed estimators became 854.5Mbit/km^2 and 867.7Mbit/km^2, respectively. At N=2 and M=20, the area throughput achieved by the existing and proposed estimator became 624.3Mbit/km^2 i.e., at this point the performance of the two estimators is the same. The area throughput attained by the proposed and existing estimator for N<2 has a nearly closer value. As the pilot reuse factor increased from w=1 to w=5, then the area throughput decreased. When the number of AP increased with the increased pilot reuse factor, the area throughput increased up to some point and diminished after a certain point. The pilot length became 8 since K=10, N=4, and w=5 which means the pilot length decreased as the pilot reuse factor increased.

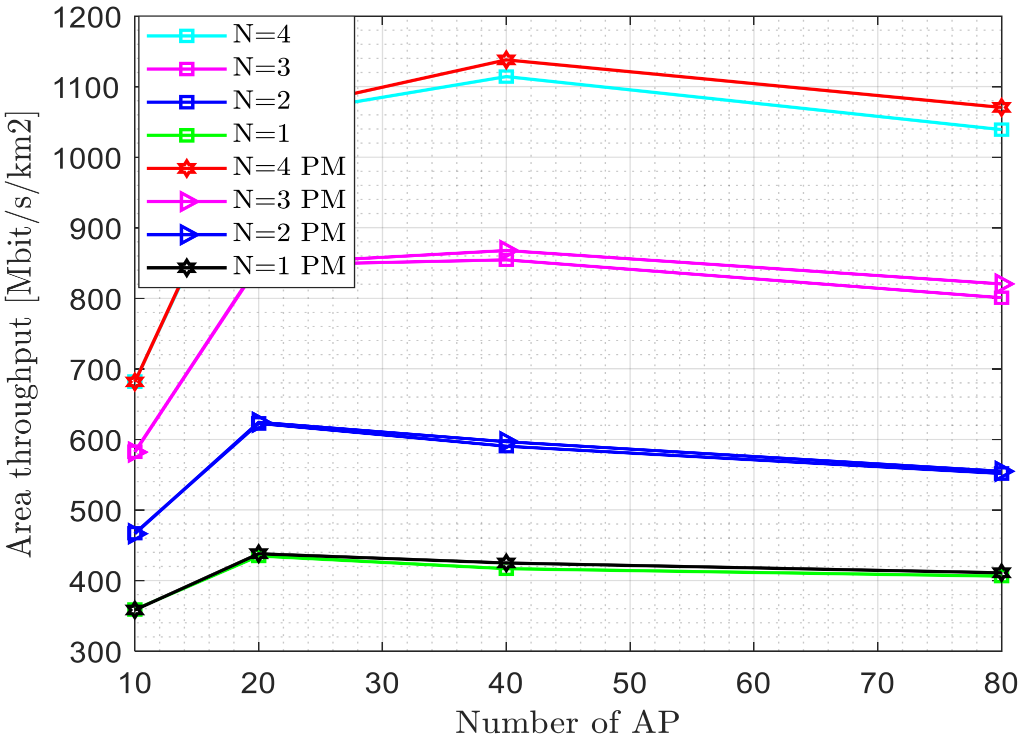

Figure 4.37: The area throughput versus the number of access points for the fully centralized processing with the MMSE combining at K = 10, L = 4, τ_c =200, and w=5.

4.4 Computational Complexity Comparison

The simulation findings concentrate on the impact of the number of users, the number of antennae per UE, the number of antennae per AP, and the number of AP on computational complexity. The comparison is shown in terms of the number of complex multiplications with the number of antennae used by each user of the equipment and complex multiplication with the number of AP.

Figure 4.38 shows the comparison of the proposed channel estimator with the current estimator based on the number of complex multiplications with the number of users for the value N=6, M=40, L=30,and τ_p =30. The proposed estimator had a $4.464*10^6$ number of complex multiplications at K=20, whereas the existing estimator is $8.64*10^6$. At K=60, the proposed attained $1.339*10^7$ and for the existing estimator is $2.592*10^7$. For both proposed and existing estimators, the number of complex multiplications rises as the number of user equipment does. Comparing the proposed estimator to the phase-aware MMSE estimator, fewer complex multiplications are accomplished.

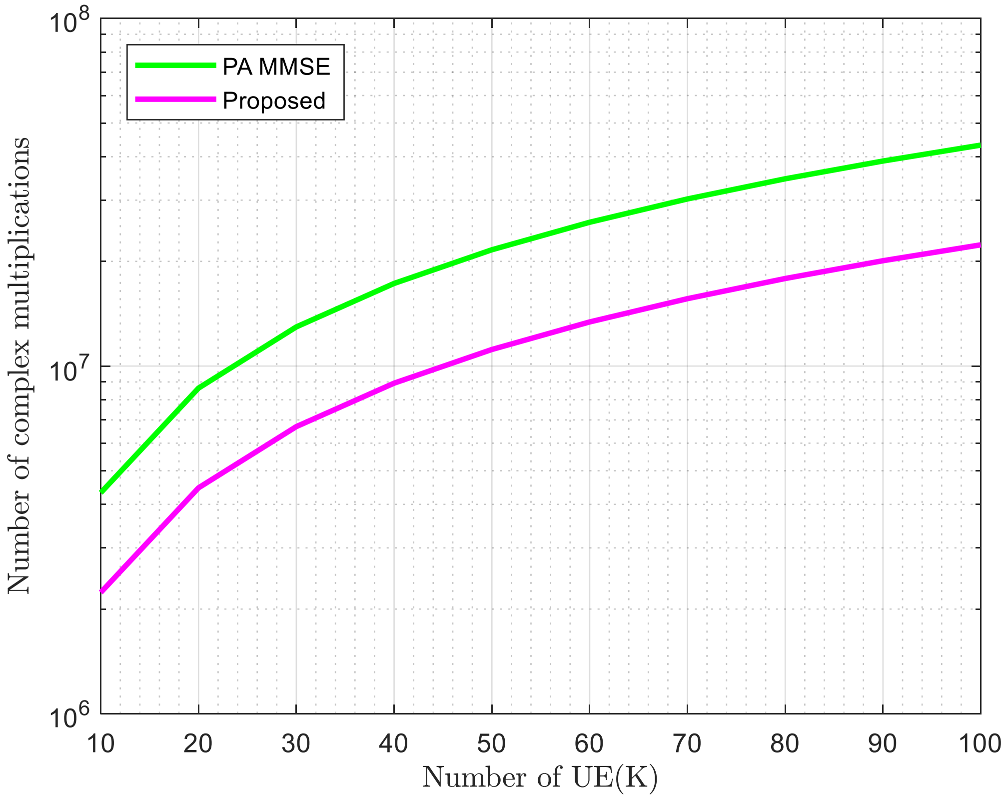

Figure 4.38: The number of complex multiplications versus the number of users at N=6, M=40, L=30, and τ_p =30.

Figure 4.39 compares the proposed channel estimator with the existing estimate based on the quantity of complex multiplication and the number of antennae per AP with K=20, N=6, M=40, and τ_p =30. The proposed estimator had a $2.976*10^6$ number of complex multiplications at L=20, whereas the existing estimator is $4.8*10^6$ at the same number of antennae per AP. At L=70, the proposed attained $1.042*10^{7,}$ and for the existing estimator the number of complex multiplications is $3.36*10^7$. This shows that as the number of antennae per AP increased the number of the complex multiplication increased for both proposed and existing estimator. At L=90, the proposed attained $1.339*10^7$ and for the existing estimator the number of complex multiplications is $5.184*10^7$ i.e., as the number of antennae per AP increases more, the suggested estimate completes fewer complex multiplications than the phase-aware MMSE estimator.

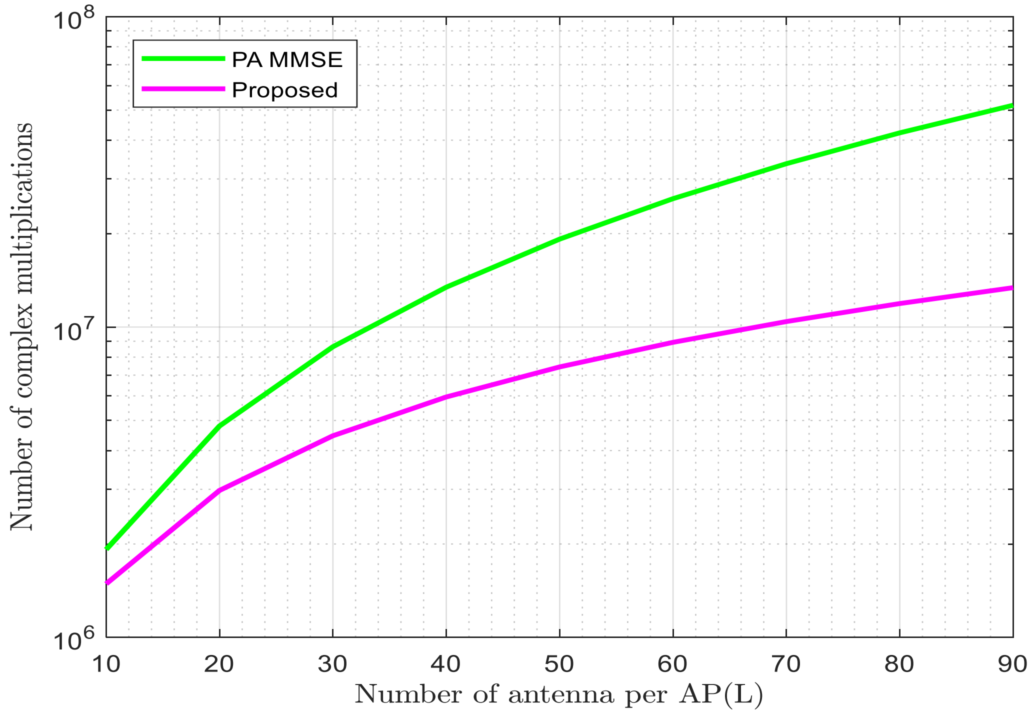

Figure 4.39: The number of complex multiplications versus the number of antenna per AP at K=20, N=6, M=40, and τ_p =30.

The existing estimate based on the quantity of complex multiplication and the number of antennae per AP with K=20, N=6, M=40, and τ_p =30 is contrasted with the proposed channel estimator in Figure 4.40. The proposed estimator had a $4.46*10^6$ number of complex multiplications at M=40, whereas the existing estimator is $8.64*10^6$ at the same number of AP. At M=40, the proposed attained $1.562*10^{7,}$ and for the existing estimator the number of complex multiplications is $3.024*10^7$. This shows that as the number of AP increased the number of the complex multiplication increased for both proposed and existing estimator.

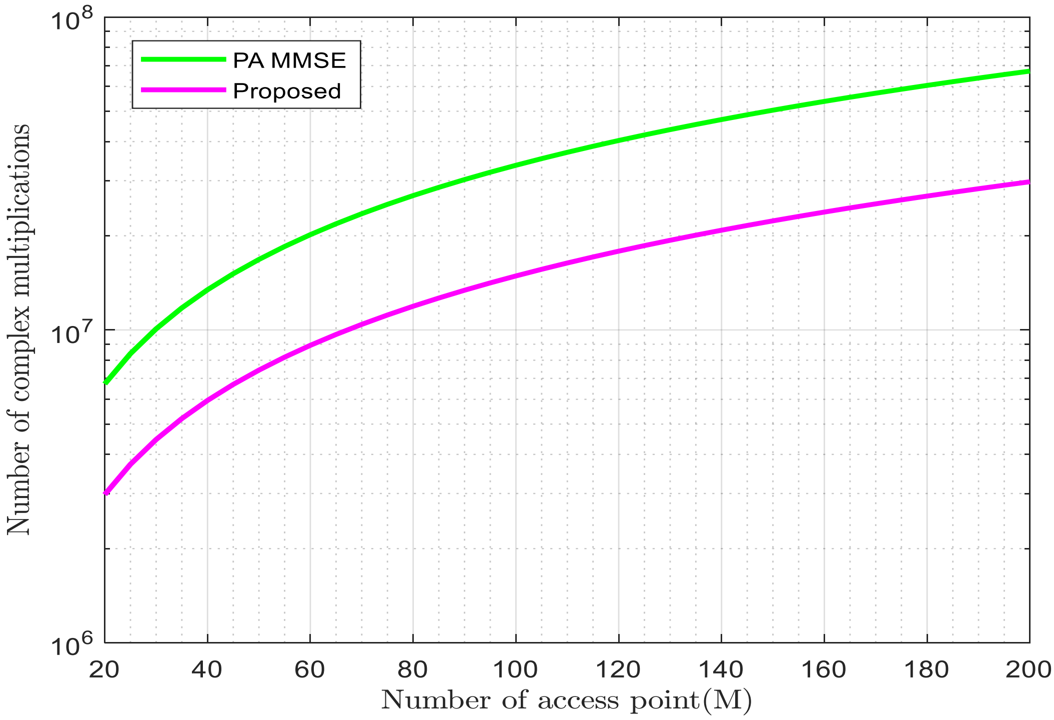

Figure 4.40: The number of complex multiplications versus the number of access points at K=20, N=6, L=40, and τ_p =30.

The proposed channel estimator and the current estimator based on the number of complex multiplications with the number of AP are compared in Figure 4.40 for the values K=20, N=6, L=40, and τ_p =30. The proposed estimator attained a 3.968*106 number of complex multiplications at N=2, whereas for the existing estimator, the number of complex multiplications is 8.96*106. At N=8, the proposed had 1.587*107 complex multiplication, whereas the existing estimator is 3.584*107. Both the proposed and the existing estimators experience an increase in complex multiplication as the number of antennae per UE rises. In comparison to the phase-aware MMSE estimator, the suggested estimate completes less complicated multiplications.

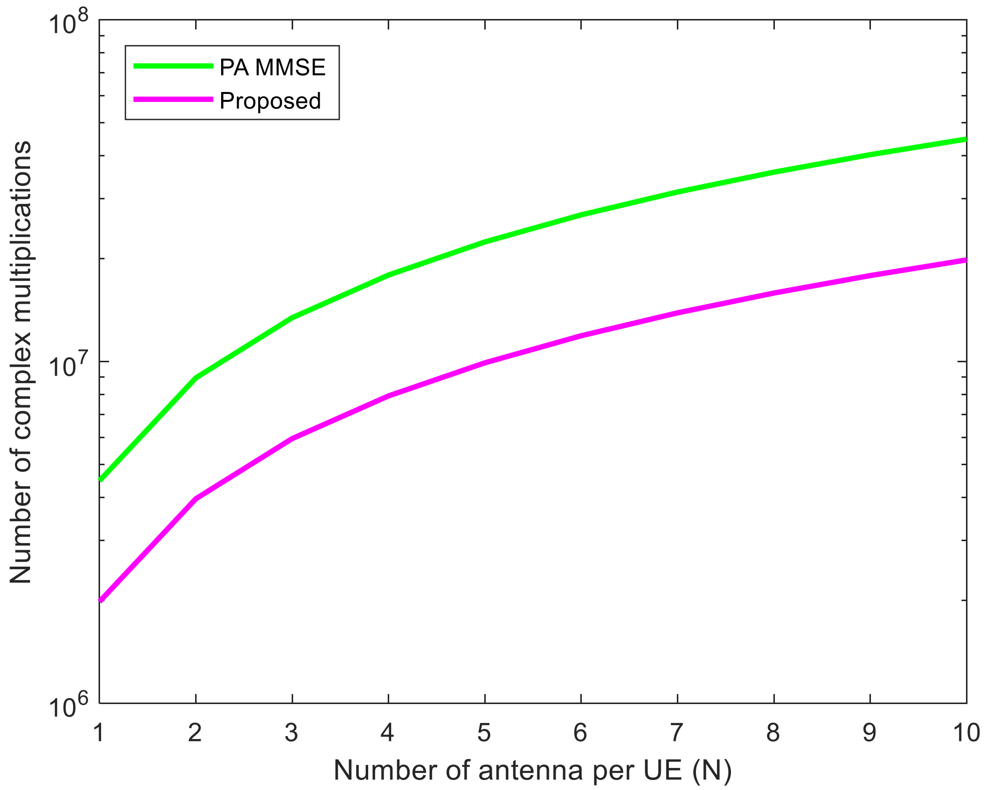

Figure 4.41: The number of complex multiplications versus the number of antenna per UE at K=20, L=40, M=80, and τ_p=30.

5. CONCLUSION AND RECOMMENDATION

5.1 Conclusion

CF M-MIMO is one of the promising technologies in the future wireless communication network due to its high spectral efficiency, high energy efficiency, high data rate, and delivering uniform data rate to UEs. However, the deployment of CF M-MIMO systems faces many challenges. One of the major challenges in the deployment of CF M-MIMO systems is estimating the channel between the UEs and APs. To solve this problem, several channel estimator algorithms have been studied. The performance and complexity are the major issues in the channel estimation process. A channel estimator with low complexity and high performance is needed. A low complexity and better performance phase aware element-wise minimum mean square error with QR decomposition and user precoding matrix is proposed in this thesis.

In this thesis, we studied the performance evaluation of the UL CF M-MIMO network under Weichselberger rician fading channels. This thesis analyses the average UL SE, EE, and area throughput for multiple antenna AP and multiple antenna UE. As shown in the simulation results, the performance of the proposed estimator is evaluated based on the SE, EE, and area throughput with multi-antenna AP and multi-antenna UE. The fully centralized processing scheme is considered. The performance of the proposed estimator is high, when the number of access points and the number of antennae per UE are increased. As the pilot reuse factor increased the SE, EE and area throughput are reduced and the pilot length also decreased due to pilot contamination. The number of antennae per AP, the number of AP, and coherence time have positive effects on the EE, SE, and area throughput i.e. when those parameters increased the EE, SE, and area throughput raised. For small the number of antennae per UE i.e., $N<2$, the SE, EE, and area throughput under different numbers of AP for the proposed and existing estimator are overlapped i.e., the performance of the proposed estimator is not effective for the single antenna user equipment's and the performance is reduced as the number of antennae per UE and number of AP raised due to interference. The computational complexity of the proposed estimator is lower as compared to phase aware MMSE channel estimator.

5.2 Recommendation

In this thesis, the proposed channel estimator performance is only evaluated at the simulation level and the scalability of the estimator is not considered. In the future scope of this thesis, the performance of the proposed estimator with a scalable scheme can also be investigated by applying dynamic cooperation clustering (DCC). In the future, this work can be further improved by a machine learning-based and deep learning-based channel estimator channel such as FFDNet and CBDNet channel estimators.

6. REFERENCES

Abdul Kadir, E., Shubair, R., abdul rahim, S., Himdi, M., Kamarudin, M., & Rosa, S. (2021). *B5G and 6G: Next Generation Wireless Communications Technologies, Demand and Challenges*. 1–6.

Amadid, J., Belhabib, A., Khabba, A., Zeroual, A., & Hassani, M. M. (2022). On channel estimation and spectral efficiency for cell-free massive MIMO with multi-antenna access points considering spatially correlated channels. *Transactions on Emerging Telecommunications Technologies*, *33*(5), e4438.

Amadid, J., Belhabib, A., & Zeroual, A. (2022). On channel estimation in cell-free massive MIMO for spatially correlated channels with correlated shadowing under Rician fading. *International Journal of Communication Systems*, *35*(1), e5011.

Ammar, H. A., Adve, R., Shahbazpanahi, S., Boudreau, G., & Srinivas, K. V. (2022). User-Centric Cell-Free Massive MIMO Networks: A Survey of Opportunities, Challenges and Solutions. *IEEE Communications Surveys & Tutorials*, *24*(1), 611–652.

Bashar, M., Cumanan, K., Burr, A., Debbah, mérouane, & Ngo, H. (2018, April 22). *Enhanced Max-Min SINR for Uplink Cell-Free Massive MIMO Systems*.

Björnson, E., Hoydis, J., & Sanguinetti, L. (2017). Massive MIMO Networks: Spectral, Energy, and Hardware Efficiency. *Foundations and Trends® in Signal Processing*, *11*(3–4), 154–655.

Björnson, E., & Sanguinetti, L. (2019a). Cell-Free versus Cellular Massive MIMO: What Processing is Needed for Cell-Free to Win? *2019 IEEE 20th International Workshop on Signal Processing Advances in Wireless Communications (SPAWC)*, 1–5.

Björnson, E., & Sanguinetti, L. (2019b). *Making Cell-Free Massive MIMO Competitive With MMSE Processing and Centralized Implementation* (arXiv:1903.10611). arXiv.

Björnson, E., Zakhour, R., Gesbert, D., & Ottersten, B. (2010). Cooperative Multicell Precoding: Rate Region Characterization and Distributed Strategies With Instantaneous and Statistical CSI. *IEEE Transactions on Signal Processing*, *58*(8), 4298–4310.

Chataut, R., & Akl, R. (2020a). Massive MIMO Systems for 5G and beyond Networks—Overview, Recent Trends, Challenges, and Future Research Direction. *Sensors*, *20*(10), Article 10.

Chataut, R., & Akl, R. (2020b). Massive MIMO Systems for 5G and beyond Networks—Overview, Recent Trends, Challenges, and Future Research Direction. *Sensors*, *20*(10), Article 10.

Chen, S., Zhang, J., Zhang, J., Björnson, E., & Ai, B. (2022a). A survey on user-centric cell-free massive MIMO systems. *Digital Communications and Networks*, *8*(5), 695–719.

Chen, S., Zhang, J., Zhang, J., Björnson, E., & Ai, B. (2022b). A survey on user-centric cell-free massive MIMO systems. *Digital Communications and Networks*, *8*(5), 695–719.

Demir, Ö. T., Björnson, E., & Sanguinetti, L. (2021). Foundations of User-Centric Cell-Free Massive MIMO. *Foundations and Trends® in Signal Processing*, *14*(3–4), 162–472.

Elhoushy, S., Ibrahim, M., & Hamouda, W. (2022). Cell-Free Massive MIMO: A Survey. *IEEE Communications Surveys & Tutorials*, *24*(1), 492–523.

Foschini, G. J., Karakayali, K., & Valenzuela, R. A. (2006). Coordinating multiple antenna cellular networks to achieve enormous spectral efficiency. *IEE Proceedings - Communications*, *153*(4), 548–555.

Gashtasbi, A., da Silva, M. M., & Dinis, R. (2022). IRS, LIS, and Radio Stripes-Aided Wireless Communications: A Tutorial. *Applied Sciences*, *12*(24), Article 24.

Hu, S., Rusek, F., & Edfors, O. (2018). Beyond Massive MIMO: The Potential of Data Transmission With Large Intelligent Surfaces. *IEEE Transactions on Signal Processing*, *66*(10), 2746–2758.

Huang, S., Ye, Y., Xiao, M., Poor, H. V., & Skoglund, M. (2021). Decentralized Beamforming Design for Intelligent Reflecting Surface-Enhanced Cell-Free Networks. *IEEE Wireless Communications Letters*, *10*(3), 673–677.

Interdonato, G., Björnson, E., Quoc Ngo, H., Frenger, P., & Larsson, E. G. (2019). Ubiquitous cell-free Massive MIMO communications. *EURASIP Journal on Wireless Communications and Networking*, *2019*(1), 197.

Interdonato, G., Frenger, P., & Larsson, E. G. (2019). Scalability Aspects of Cell-Free Massive MIMO. *ICC 2019 - 2019 IEEE International Conference on Communications (ICC)*, 1–6.

Kassam, J., Castanheira, D., Silva, A., Dinis, R., & Gameiro, A. (2023). A Review on Cell-Free Massive MIMO Systems. *Electronics*, *12*(4), Article 4.

Li, X., Jin, S., Gao, X., & McKay, M. R. (2010). Capacity Bounds and Low Complexity Transceiver Design for Double-Scattering MIMO Multiple Access Channels. *IEEE Transactions on Signal Processing*, *58*(5), 2809–2822.

Li, X., Zhang, J., Wang, Z., Ai, B., & Ng, D. W. K. (2022). *Cell-Free Massive MIMO with Multi-Antenna Users over Weichselberger Rician Channels* (arXiv:2207.10891). arXiv.

Liu, Y., Liu, X., Mu, X., Hou, T., Xu, J., Di Renzo, M., & Al-Dhahir, N. (2021). Reconfigurable Intelligent Surfaces: Principles and Opportunities. *IEEE Communications Surveys & Tutorials*, *23*(3), 1546–1577.

Mai, T. C., Ngo, H. Q., & Duong, T. Q. (2020). Downlink Spectral Efficiency of Cell-Free Massive MIMO Systems With Multi-Antenna Users. *IEEE Transactions on Communications*, *68*(8), 4803–4815.

Ngo, H. Q., Ashikhmin, A., Yang, H., Larsson, E. G., & Marzetta, T. L. (2017). *Cell-Free Massive MIMO versus Small Cells* (arXiv:1602.08232). arXiv.

Obakhena, H. I., Imoize, A. L., Anyasi, F. I., & Kavitha, K. V. N. (2021). Application of cell-free massive MIMO in 5G and beyond 5G wireless networks: A survey. *Journal of Engineering and Applied Science*, *68*(1), 13.

Özdogan, Ö., Björnson, E., & Zhang, J. (2019). Performance of Cell-Free Massive MIMO With Rician Fading and Phase Shifts. *IEEE Transactions on Wireless Communications*, *18*(11), 5299–5315. https://doi.org/10.1109/TWC.2019.2935434

Pereira, A., Rusek, F., Gomes, M., & Dinis, R. (2022). Deployment Strategies for Large Intelligent Surfaces. *IEEE Access*, *10*, 61753–61768.

Shaik, Z. H. (2022). *Cell-Free Massive MIMO: Distributed Signal Processing and Energy Efficiency*.

Shaik, Z. H., Björnson, E., & Larsson, E. G. (2020). Cell-Free Massive MIMO with Radio Stripes and Sequential Uplink Processing. *2020 IEEE International Conference on Communications Workshops (ICC Workshops)*, 1–6.

Ueoka, T., Souza, D., Freitas, M., Cavalcante, A., & Costa, J. (2022, September 28). *Performance of Cell-Free Massive MIMO Networks under Rayleigh and Rician fading*.

Wang, Z., Zhang, J., Ai, B., Yuen, C., & Debbah, M. (2022). Uplink Performance of Cell-Free Massive MIMO With Multi-Antenna Users Over Jointly-Correlated Rayleigh Fading Channels. *IEEE Transactions on Wireless Communications*, *21*(9), 7391–7406.

Wang, Z., Zhang, J., Björnson, E., & Ai, B. (2021a). Uplink Performance of Cell-Free Massive MIMO Over Spatially Correlated Rician Fading Channels. *IEEE Communications Letters*, *25*(4), 1348–1352.

Wang, Z., Zhang, J., Björnson, E., & Ai, B. (2021b). Uplink Performance of Cell-Free Massive MIMO Over Spatially Correlated Rician Fading Channels. *IEEE Communications Letters*, *25*(4), 1348–1352.

Wang, Z., Zhang, J., Ngo, H. Q., Ai, B., & Debbah, M. (2023). Uplink Precoding Design for Cell-Free Massive MIMO With Iteratively Weighted MMSE. *IEEE Transactions on Communications*, *71*(3), 1646–1664.

Weichselberger, W., Herdin, M., Ozcelik, H., & Bonek, E. (2006). A stochastic MIMO channel model with joint correlation of both link ends. *IEEE Transactions on Wireless Communications*, *5*(1), 90–100.

Yadav, R., Tripathi, A., Pathak, S., & Gill, H. S. (2022). 5G and Beyond Networks for 3D MIMO Using Artificial Intelligence in 5G Network. *Journal of Physics: Conference Series*, *2273*(1), 012007.

Ye, F., Li, J., Zhu, P., Wang, D., Wu, H., & You, X. (2022). Spectral Efficiency Analysis of Cell-Free Distributed Massive MIMO Systems With Imperfect Covariance Matrix. *IEEE Systems Journal*, *16*(4), 5402–5412.

Yetis, C. M., Björnson, E., & Giselsson, P. (2021). Joint Analog Beam Selection and Digital Beamforming in Millimeter Wave Cell-Free Massive MIMO Systems. *IEEE Open Journal of the Communications Society*, *2*, 1647–1662.

Zhang, C., Ueng, Y.-L., Studer, C., & Burg, A. (2020). Artificial Intelligence for 5G and Beyond 5G: Implementations, Algorithms, and Optimizations. *IEEE Journal on Emerging and Selected Topics in Circuits and Systems*, *10*(2), 149–163.

Zhang, J., Chen, S., Lin, Y., Zheng, J., Ai, B., & Hanzo, L. (2019). Cell-Free Massive MIMO: A New Next-Generation Paradigm. *IEEE Access*, *7*, 99878–99888.